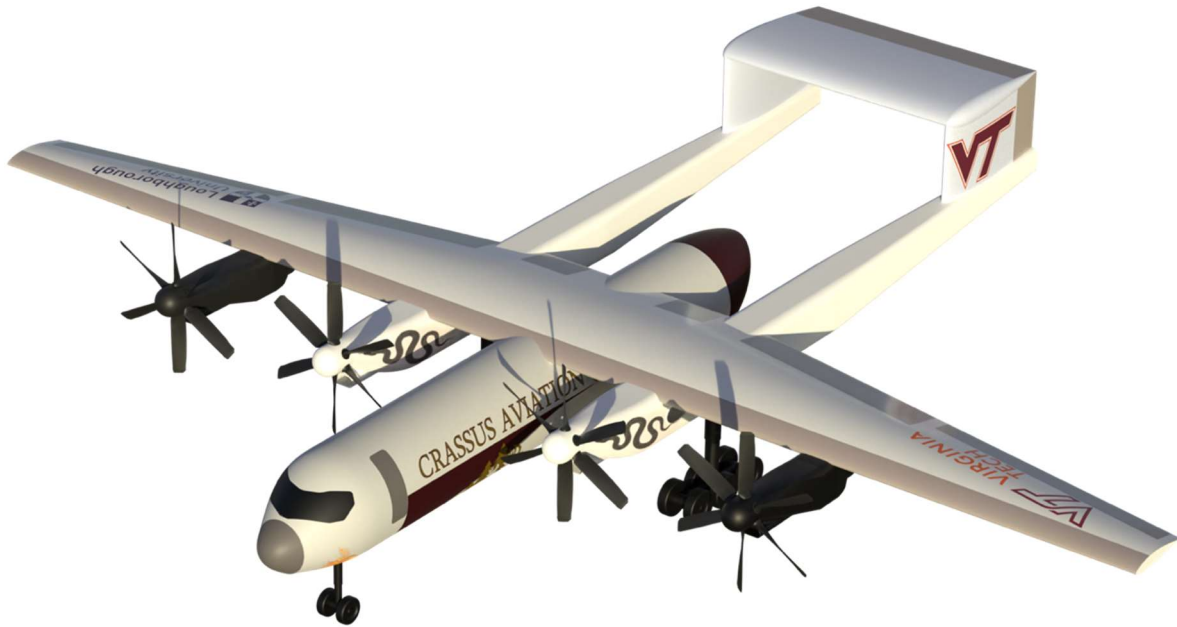


21TTD009: Final Report

Nerodia: Fire Fighting Aircraft

Loughborough University & Virginia Tech



OMEGA
Firefighting Solutions



VT
COLLEGE OF ENGINEERING
KEVIN T. CROFTON DEPARTMENT OF
AEROSPACE AND OCEAN ENGINEERING
VIRGINIA TECH™



Loughborough
University

Loughborough University Members



Peter Cassidy

Team Lead
Propulsion



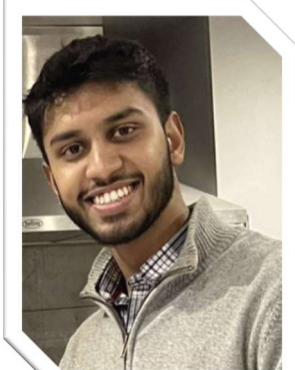
Duncan Livingstone

Chief Engineer
Structures & Payload



Pip Thorpe-Morgan

Stability & Performance
Payload



Kritish Gopi

Business Operations
Payload



Matt McCarney

Subsystems



Jeswin Roy

Payload
Risk & Reliability



Nish Selvakumar

Payload
Cost & Manufacturing



Sam Markert

Aerodynamics

Virginia Tech Members



Brian Kelly

Team Lead
Aerodynamics



Letian Leng

Chief Engineer
CAD & Mass



Kevin Yarnall

Propulsion Integration



Taylor Ordile

Structures & Materials



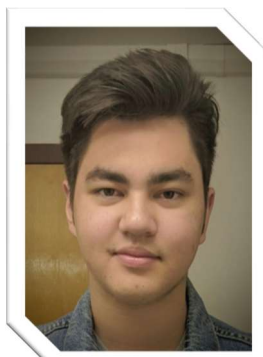
Jimmy Murray

Cost & Manufacturing



Criostoir Neal

Handling & Flight Control



Michael Sharp

Vehicle Subsystems

Summary

Crassus Aviation and Omega Firefighting Solutions are proud to present Nerodia, a purpose-built firefighting aircraft (FFA) capable of carrying and deploying a 6,000 US-gallon payload of fire retardant. The rapidly increasing occurrence & size of wildfires combined with retiring existing FFA emboldens the necessity for new, technologically advanced solutions. Crassus and Omega's Nerodia is a large-air-tanker style FFA weighing 67 tonnes, aimed at entry into the market by 2030. Of the current firefighting methodologies, the indirect attack method is used – whereby streaks of retardant are dropped as boundaries to the propagating wildfire, all within a 750km design mission radius.

Nerodia specifically is capable of a variable drop rate to service continuous lengths of retardant, with a maximum payload dispersal rate of 6869 l/s from its bespoke-designed anti-slosh payload tank and pintle nozzle. To future-proof the design and flex the muscles of innovation, Nerodia incorporates middle-to-low technology readiness level (TRL) systems for payload planning and deployment, alongside current technologies including fully autonomous and night flying instruments.

The entire program is estimated to cost \$8.9 b by 2030 (accounting for inflation), with a production run of 85 aircraft for service – each costing \$119.9 m. Nerodia can perform 5 of the design missions a day dropping a total of 30,000 US-g of retardant whilst still costing less than the daily operating cost of the 747 Supertanker making only one drop.



Contents

<i>Nomenclature</i>	vii
<i>Table of Figures</i>	viii
<i>Table of Tables</i>	xi
1. Introduction	1
2. Mission Profile	2
2.1 Regular Mission.....	2
2.2 Aborted Drop Mission	3
2.3 Ferry Mission.....	3
3. Design Summary	4
4. Performance Statement	7
5. Payload Design	8
6. Aerodynamic Design	10
7. Drag Breakdown	11
8. Propulsion Design	11
9. Systems Breakdown	12
10. Structures	14
11. Mass Breakdown	16
12. Project Viability	17
12. Conclusion	18
1 Design Brief and User Requirement	20
1.1 Operational Environment And FFA Regulations	20
1.2 Key Technologies.....	20
1.3 QFD	21
1.4 Requirement Statement	21
2 Competitor Benchmarking	22
3 Concept Generation	24
3.1 Initial Concepts.....	24
3.2 Down Selection.....	24
3.3 VT-LU Merger And Evolution.....	26
4 Mission Performance	28
5 Aerodynamics	30
5.1 Requirements And Initial Sizing.....	30
5.2 Main Wing	30
5.3 High-Lift Devices.....	34

5.4	Stall.....	36
5.5	Drag Breakdown	40
6	<i>Performance, Stability and Control.....</i>	41
6.1	Empennage Configuration And Sizing.....	41
6.1.1	Tail Disposition	41
6.1.2	Horizontal Stabiliser.....	41
6.1.3	Vertical Stabiliser	43
6.2	Ailerons, Rudders, And Elevator Sizing	44
6.2.1	Aileron Sizing.....	45
6.2.2	Rudder Sizing	46
6.2.3	Elevator Sizing	46
6.3	Static Stability And Centre-Of-Gravity Envelope	47
6.4	Dynamic Stability Derivatives.....	49
7	<i>Payload.....</i>	51
7.1	Mission Requirement	51
7.2	Baffle & Tank Design.....	52
7.2.1	Outlet Pipe Sizing.....	53
7.2.2	One-Way Valve Sizing	54
7.2.3	Payload Tank Baffle Sizing	54
7.2.4	Optimisation	55
7.3	Pressurisation	56
7.3.1	Bleed Air Pipe & Slot Gap Calculations	57
7.4	Pintle Nozzle (Dispersal System).....	57
7.5	Payload Stability.....	58
7.6	Refill	61
7.7	Maintenance.....	61
8	<i>Structures.....</i>	62
8.1	Load Definition.....	62
8.2	Material Selection.....	64
8.3	Initial Wing Sizing.....	65
8.4	Reinforcement Optimisation With LS-DYNA FEA-FEM.....	66
8.5	Deformable Boom.....	68
8.6	Landing Gear Loading.....	69
8.7	Tank Construction	69
8.8	Tank Mounting.....	71
9	<i>Propulsion and Power</i>	72
9.1	Functional Analysis And Design Requirement.....	72

9.2	Engine Down Selection.....	73
9.2.1	Engine Type.....	73
9.2.2	Engine Selection.....	73
9.2.3	Engine Placement And Configuration	74
9.3	Propulsion Performance.....	75
9.4	Propeller Design	76
9.5	Airframe Integration.....	79
10	<i>Avionics and Systems.....</i>	81
10.1	Avionics And Flight Deck	81
10.2	Autonomous Operation.....	84
10.3	Power Systems	86
10.4	Fuel	88
10.5	Landing Gear.....	89
10.6	Actuation.....	90
10.7	De-Icing	91
11	<i>Cost and Manufacturing</i>	92
11.1	Production Rates	92
11.2	Rtd&E Cost.....	92
11.3	Flyaway Cost.....	93
11.4	Direct Operating Costs	94
11.5	Ffa Cost Comparison	94
11.6	Loan & Lease Schemes	95
12	<i>Business Operations</i>	97
12.1	Business Operations Plan	97
12.2	Stage 1: Design Phase.....	97
12.3	Stage 2: Marketing Phase	98
12.4	Stage 3: Manufacturing Phase	98
12.5	Stage 4: Sales Phase.....	99
13	<i>Risk and Reliability.....</i>	101
14	<i>Conclusion</i>	103
14.1	Viability	103
14.2	Future Work	103
References.....		104
Appendix		108
Public Engagement.....		108
Meeting Minutes.....		114

Nomenclature

Symbol/ Acronym	Definition	Symbol/ Acronym	Definition
C_{L_p}	Propeller lift coefficient	FEA	Finite Element Analysis
C_{d0}	Zero-lift drag coefficient	FEM	Finite Element Method
D_p	Propeller diameter	FFA	Fire Fighting Aircraft
K_{np}	Blade correction factor	FLIR	Forward-Looking InfraRed
t_b	Baffle Thickness	HLD	High-Lift Devices
η_p	Propeller efficiency	HPC	High Pressure Compressor
A/C	Aircraft	LU	Loughborough University
AF	Activity factor	MAC	Mean Aerodynamic Chord
AGL	Above Ground Level	MAFFS	Modular Airborne Fire Fighting System
AoA	Angle of Attack	MEA	More-Electric Aircraft
APU	Auxiliary Power Unit	MFR	Mass Flow Rate
AR	Aspect Ratio	MTOW	Maximum Take Off Weight
BDUBS	Buffalo Wild Wings™	NASA	National Aeronautics and Space Administration
BEMT	Blade Element Momentum Theory	NRV	Non-Return Valve
BFL	Balanced Field Length	OEM	Original Equip. Manufacturer
CA	Crassus Aviation	OEW	Operational Empty Weight
CAD	Computer Aided Design	PSC	Proposed System Concept
CFD	Computational Fluid Dynamics	QFD	Quality Functional Deployment
CFR	Code and Federal Regulations	RADS	Retardant Aerial Delivery System
CoG	Centre of Gravity	RAT	Ram-Air Turbine
DOC	Direct Operating Costs	RFP	Request For Proposal
EFVS	Enhanced Flight Visibility System	RTD&E	Research Testing Development and Evaluation
EHA	Electro-Hydrostatic Actuation	TRL	Technology Readiness Level
EMA	Electro-Mechanical Actuation	VLM	Vortex Lattice Method
FADEC	Full Authority Digital Engine Control	VT	Virginia Tech

Table of Figures

Figure 1: Mission profile showing 3 possible mission: standard aerial firefighting, ferry, and no-drop	2
Figure 2: Illustrated design radius.....	3
Figure 3: Nerodia's configuration (underside view). N.B. Fuselage is depicted as wireframe to illustrate payload location and size, all other internals omitted.	4
Figure 4: Nerodia's configuration (front view).	4
Figure 5: Internal payload configuration of Nerodia.....	8
Figure 6: Baffle and One-way valve design.....	8
Figure 7: Pintle nozzle design. N.B. diagram not to scale.	9
Figure 8: Main wing planform.	10
Figure 9: High-Lift Devices.	10
Figure 10: Engines and propellers on Nerodia's port side. Wireframe view showing engine inside nacelle, air intake, and exhaust port (wireframe not representative of actual nacelle).....	11
Figure 11: Subsystems layout of Nerodia.	13
Figure 12: Combined gust and V-N diagram.	14
Figure 13: Examples of FEM analysis carried out in supporting information.	15
Figure 14: Quality Function Deployment for firefighting aircraft.	21
Figure 15: Payload capacities of varying FFA, with Nerodia's design goal highlighted.	23
Figure 16: Crassus' initial concepts.....	24
Figure 17: LU and VT shortlisted and ultimately selected concepts.....	27
Figure 18: LU and VT merged and evolved concept: Nerodia	27
Figure 19: Turn rate diagram.	29
Figure 20: Constraints Diagram.	30
Figure 21: Induced Drag vs Wing Taper Ratio [14].	31
Figure 22: Main wing aerofoil profile NACA 63(2)-615.....	32
Figure 23. Cl/Cd plot of NACA 63(2)-615 from XFLR5.	33
Figure 24. Balanced Field Length.	34
<i>Figure 25. High Lift Device Placement and Sizing.</i>	35
Figure 26. Single-Slotted Flap and Slat.	35
Figure 27. XFLR5 Cl vs Alpha Main Wing.....	36
Figure 28. Wind Tunnel Testing Flow Separation.	37
Figure 29. Flow Separation due to the nacelles (Isosurface of Q-Criterion).....	37
Figure 30. Engine Strakes of CFD model.	38
Figure 31. Strakes effect on flow separation.....	38
Figure 32. CFD simulation done as part of the HiLift-2 Prediction Workshop [18].	39

Figure 33. Left: Blown Flaps [19] , Right: Propeller Wake Influence [20].	39
Figure 34. CFD model to be separated by patch.	40
Figure 35: Horizontal tail volume coefficient scissor plot.	42
Figure 36: Control surface efficiency plot.	45
Figure 37: Bank angle against time at approach speed and max aileron deflection.	45
Figure 38: CG Excursion envelope.	48
Figure 39: Lift curve vs moment curve.	49
Figure 40: Early Baffle Concepts.	52
Figure 41: Baffle with one-way valves.	54
Figure 42: Optimisation at single state (left), full baffle range results (right).	55
Figure 43: Payload system schematic.	56
Figure 44: Baffle slot gap.	57
Figure 45: Payload slosh CFD time-history for un-baffled, baffled and baffled (NRV).	59
Figure 46: Payload CFD CG shift.	60
Figure 47: Structural X-Ray rendering of Nerodia.	62
Figure 48: V-N / Gust Diagram.	63
Figure 49: Wing loading distribution. N.B. Point loads not to scale.	63
Figure 50: Model loading configuration for wing bending.	66
Figure 51: 40% Load displacement map (mm).	66
Figure 52: Wing Von Mises strain, internal and external at peak load (MPa).	67
Figure 53: Structure overall stress strain.	68
Figure 54: Amplified boom displacement (mm).	68
Figure 55: Boom reinforcement (front view).	68
Figure 56: Acetyl baffle positioned in tank slot.	69
Figure 57: Baffle hinge locations.	70
Figure 58: Baffle layup seen through split casing.	70
Figure 59: NRV in situ.	70
Figure 60: Bolt-double shear mounting technique.	71
Figure 61: Mounting force representation (N).	71
Figure 62: Propulsion system design process, adapted from Sadraey [35].	72
Figure 63: Required power curves for mission flight conditions varied with velocity. Operating points signified with dots.	76
Figure 64: Bespoke-designed propeller performance versus NACA propellers.	78
Figure 65: Radial variation of chord length, coefficient of lift, and twist of Nerodia's propeller blades.	79
Figure 66: Simplified heat exchanger temperature profile.	80

Figure 67: Internal layout of boom fore section, showing engine position, air intake & passages, and bleed air tapping	80
Figure 68: Avionics and cockpit cross section.....	81
Figure 69: Rockwell Collins Pro Line Fusion avionics flight deck.	83
Figure 70: Payload Targeting System view (left) and Rockwell Collins Enhanced Synthetic Vision System integrated into the heads-up display (right).....	83
Figure 71: Cockpit layout.....	83
Figure 72: Windscreen geometry.	84
Figure 73: Autonomous flight system diagram.....	85
Figure 74: Aircraft power schematic.....	87
Figure 75: Aircraft fuel tank layout.....	88
Figure 76: Aircraft landing gear angles.....	89
Figure 77: Aircraft actuator locations.	91
Figure 78: Aircraft De-icing locations.	91
Figure 79: RDT&E cost breakdown of the Nerodia program.	93
Figure 80: Production break even graph used to identify the production breakeven point.....	93
Figure 81: Operational cost breakdown of Nerodia for private entities.	94
Figure 82: Cost/drop comparison of 1 US-g of existing FFA with Nerodia.	95
Figure 83: Project timeline and EIS.	97
Figure 84: Poster for public engagement and awareness.	98
Figure 85: Crassus Aviation's manufacturing & maintenance facility.....	99

Table of Tables

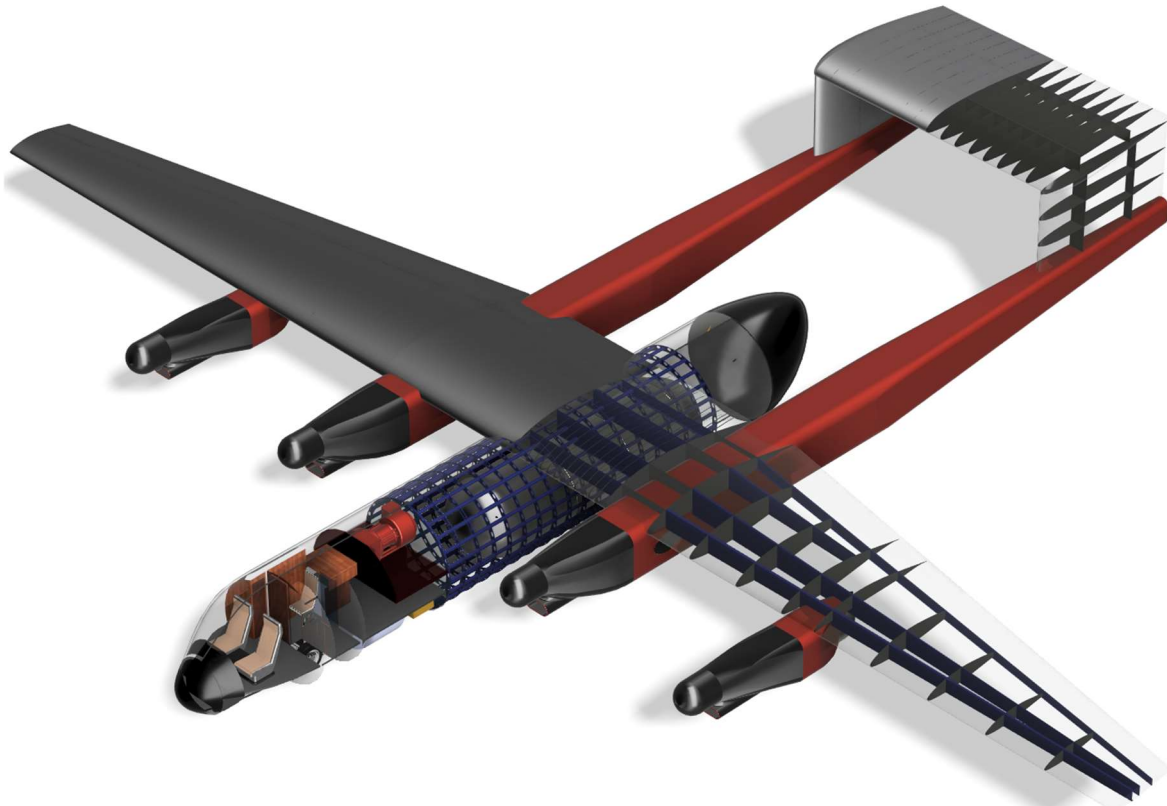
Table 1: Nerodia key design values.....	5
Table 2: Performance statement.....	7
Table 3: Drag breakdown.....	11
Table 4: Key propulsions system design values.....	12
Table 5: Relevant structural velocities.....	14
Table 6: Mass breakdown with CG's measured from nose Datum (shown in 3 view drawing).....	16
Table 7: Prices as of May 2022, adjusted for inflation.	17
Table 8: Operational cost comparison.....	17
Table 9: Operational Requirements.....	22
Table 10: Competitor benchmarking.....	23
Table 11: Down selection matrix evaluating the 7 streamlined concepts. 1: worst, 9: best.....	25
Table 12: PSC configurations, with selected attributes highlighted in bold italics.....	26
Table 13: Main wing parameters.....	31
Table 14. Aerofoil Comparison.....	32
Table 15. High-Lift Device Sizing.....	34
Table 16: Horizontal tail parameters.....	42
Table 17: Vertical tail parameters.	44
Table 18: Control surface specifications.....	44
Table 19: Aileron sizing parameters.	46
Table 20: Rudder sizing parameters.....	46
Table 21: Elevator sizing parameters.....	47
Table 22: Nerodia static stability derivatives.....	49
Table 23: Nerodia dynamic stability requirements and derivatives.....	50
Table 24: Typical high performance material examples.	64
Table 25: Key selected materials.	64
Table 26: Down-selection matrix evaluating the 4 chosen engine types. 1: worst, 9: best.....	73
Table 27: The 4 turboprop engines to be selected from [37]. DNA: Data Not Available.....	74
Table 28: The 4 turboprop engines assessed in both 2-engine and 4-engine layouts for the 11,000 kW requirement. Chosen configuration shown in purple text. DNMR: Does Not Meet Requirement	74
Table 29: Velocity, and total required power & thrust for varying flight conditions.....	76
Table 30: OpenProp input values.	77
Table 31: Propeller design specification at varying flight conditions.....	78
Table 32: Subsystem elements.	81
Table 33: Aircraft power requirements.	86

Table 34: Aircraft power sources.....	87
Table 35: Aircraft fuel tank quantities	88
Table 36: Aircraft landing gear specs.	89
Table 37: Aircraft landing gear specs II.....	90
Table 38: Estimated aircraft production rate.....	92
Table 39: Cost breakdown of existing FFA, and Nerodia.....	95
Table 40: Cost breakdown of loan and lease schemes.	96
Table 41: Risk matrix.....	102

21TTD009: Final Report

Nerodia: White Paper

Loughborough University & Virginia Tech



Loughborough
University

1. Introduction

The continuing changes to the climate of the planet, and the threat of wildfires, (especially in the western coast of the United States) has significantly increased over the past decade. In the year 2021, California had over 8,000 wildfires, 2.6 million acres burned, over 3000 structures damaged or destroyed due to wildfires, and a cost of \$5 billion dollars in insured damage. 2021 marked the 7th consecutive year that insured wildfires losses surpassed \$2 billion dollars. [1].

Furthermore, current firefighting aircraft are mainly modified from retired commercial or military aircraft. These aircraft usually have redundant internal space due to the different mission requirements between firefighting and passengers/cargo aircraft. Additionally, the typical mission profile increases the structural loads on the airframe, especially during extreme maneuvers. In most civil aviation scenarios, an extreme maneuver is anything that exceeds 30 degrees of bank, ± 10 degrees of pitch, or requires full deflection of any control surface [2]. A purpose-built aircraft could target firefighting mission requirements specifically which will significantly improve the capability and thus reduce the operational cost of the aircraft.

To meet all requirements accumulated from different operating locations, Nerodia adopts a design that includes 4 turboprop engines, a high wing, and twin-boom configuration. Turboprop engines have excellent efficiency within the speed range defined in the RFP, and relatively low maintenance cost compared to other types of engines. The high wing design gives a high ground clearance for propellers and a space for the payload tank by moving the center wing box to the upper part of the fuselage. Through the rear maintenance door, the whole payload system can be easily removed to maximize modularity and allows for rapid inspection, repairs, and replacement. Moreover, the twin-boom tail configuration minimises the fuselage volume and provides convenient placement for the landing gears as the width of fuselage is not sufficient to support traditional tricycle landing gear.

While all analysis was done using metric and SI units, some parameters in this report are displayed using imperial measurements (such as altitude and payload capacity) for intuition.

2. Mission Profile

According to research into the most effective methods of containing wildfires, the focus of design should lay in the methods of indirect aerial fire attack [3]. This involves the dropping of fire retardant in control lines within the vicinity of the fire to restrict its growth. From the knowledge of this drop architecture, a mission plan can be created using the requirements outlined in previous research - and is shown in Figure 1. The figure outlines three different mission plans; a nominal mission at the design radius (200nmi), a ferry mission, and an abandoned drop mission at the design radius.

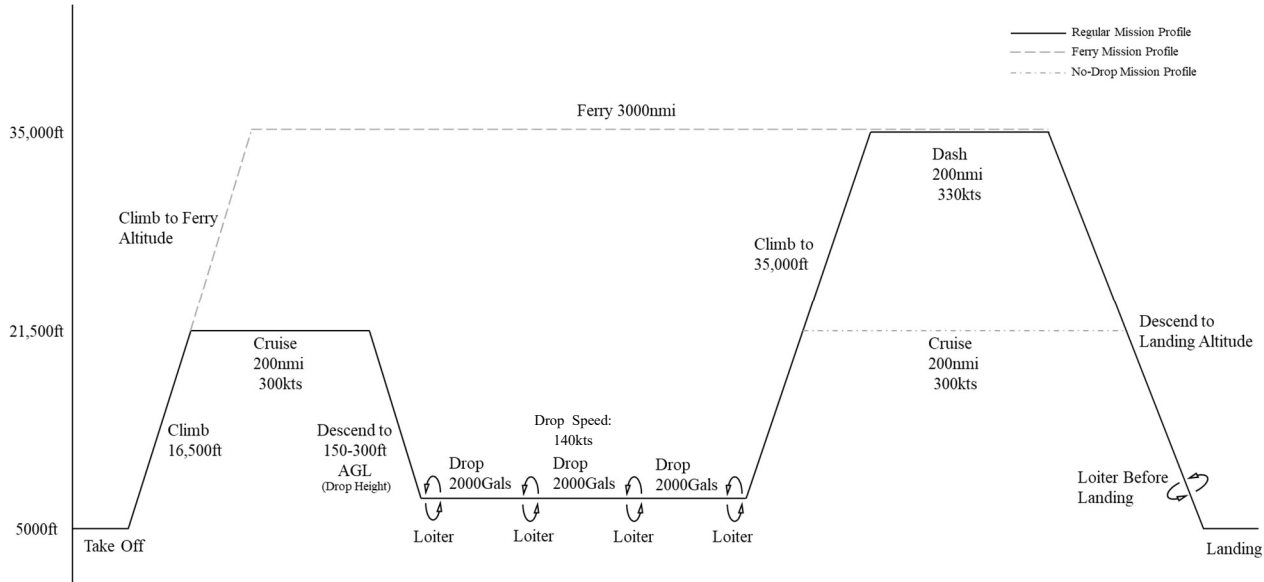


Figure 1: Mission profile showing 3 possible mission: standard aerial firefighting, ferry, and no-drop.

2.1 Regular Mission

The requirements state that the aircraft must be capable of taking off at 5000 ft (1524 m), therefore the regular mission profile reflects this. It then climbs with a 6000 US-gallon (22712.5 l) retardant payload to an altitude of 21,500 ft (6500 m) for cruise and cruises 200 nmi (370 km) to the design radius at a speed of 300 kts (154 m/s). Figure 2 shows that this design radius was chosen as a result of research which highlighted that the entirety of California (the state that the company used as a case study due to its high number of wildfires) could be reached by an aircraft with this design radius. The aircraft then descends to ~300 ft (91 m) Above Ground Level (AGL), at this drop height the aircraft performs three drops of 2000 gallons (7570.8 l) at a speed of 140 kts (72 m/s). Each drop is separated by repositioning and loitering towards a new drop position as the position of each drop is sometimes not known until the initial drops have commenced. Once the aircraft has completed its drops and no longer contains a retardant payload it climbs to a dash altitude of 35,000ft (12192m) where it cruises back to the operating airfield at a speed of 330 kts (170 m/s), before loitering (in a holding pattern or similar) and performing a landing.

2.2 Aborted Drop Mission

The aborted drop mission follows closely the manoeuvres of the above regular mission, the aircraft climbs to 21,500 ft to cruise 200 nmi at 300 kts to the drop zone before descending to ~300 ft AGL upon arrival at the drop zone. However, a malfunction of some description (or information from higher authorities) causes the aircraft to not be able to jettison the retardant payload and therefore the aircraft must climb back to the cruise altitude of 21,500ft and return to the operating airfield with the entire 6000 US-gallon payload. Despite this, the aircraft cannot land safely with a full retardant payload (the aircraft has the capability to land at this weight, but it has an elevated risk of structural fatigue and requires a longer BFL) and therefore must jettison some of the payload using the redundancy jettison lines at an appropriate location before attempting a landing.

2.3 Ferry Mission

The requirements of the aircraft state that the aircraft must be able to perform a ferry mission of 2000 nmi, which has been more than met by Nerodia which can operate a ferry mission of 3000 nmi (5600 km). This is a sizable range meaning the aircraft would not struggle to complete any transport between airports that was required of it. The ferry mission begins with a nominal take off at 5000 ft but with full fuel and empty payload, the aircraft then climbs to an altitude of 35,000 ft. At this altitude the aircraft performs a ferry of 3000 nmi at a cruise speed of 300 kts to the ferry radius. Then descends to land stopping to loiter before landing.

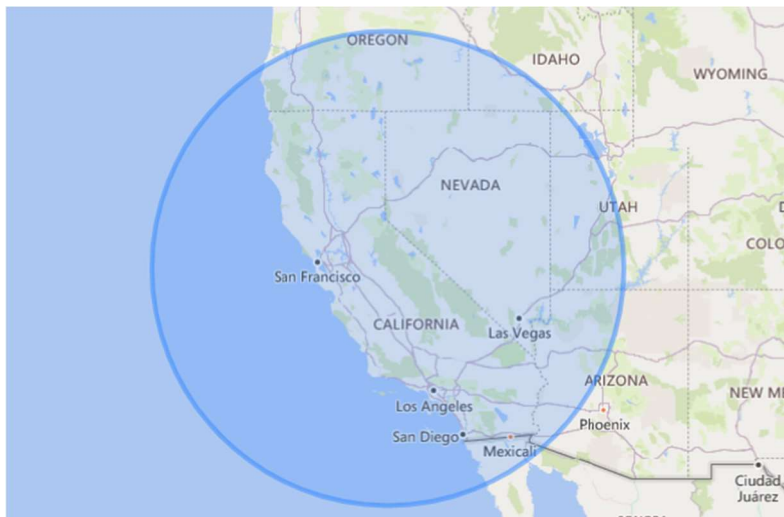


Figure 2: Illustrated design radius.

3. Design Summary

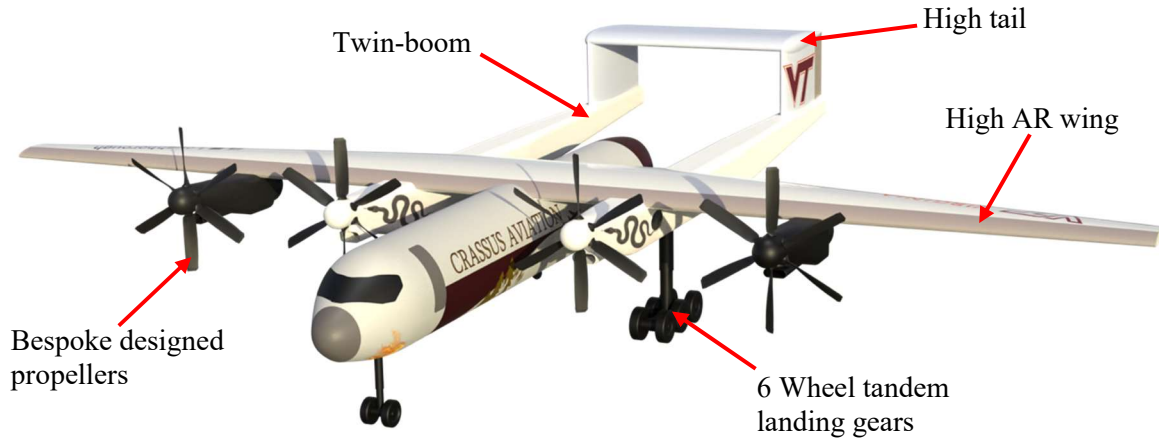


Figure 4: Nerodia's configuration (front view).

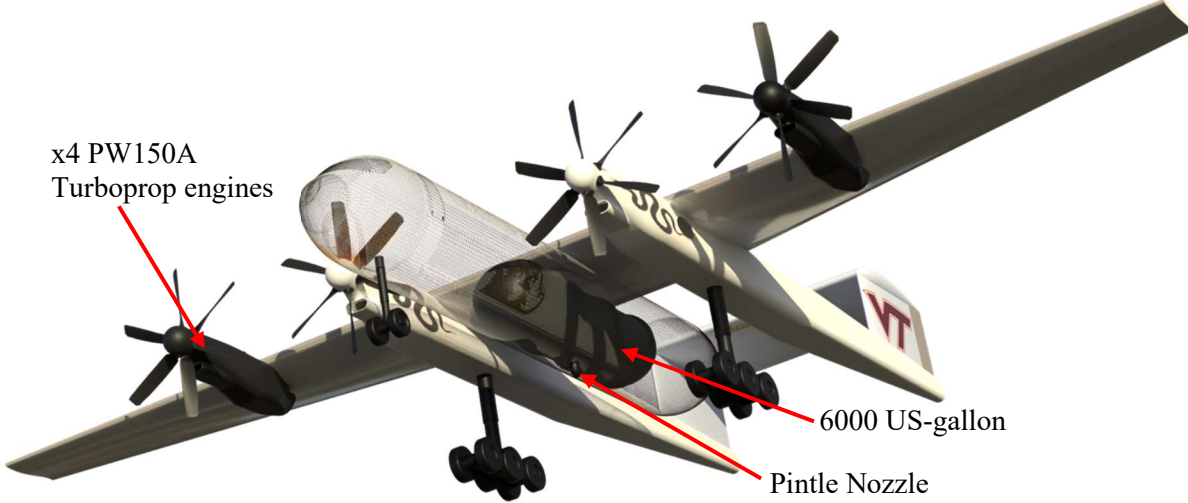


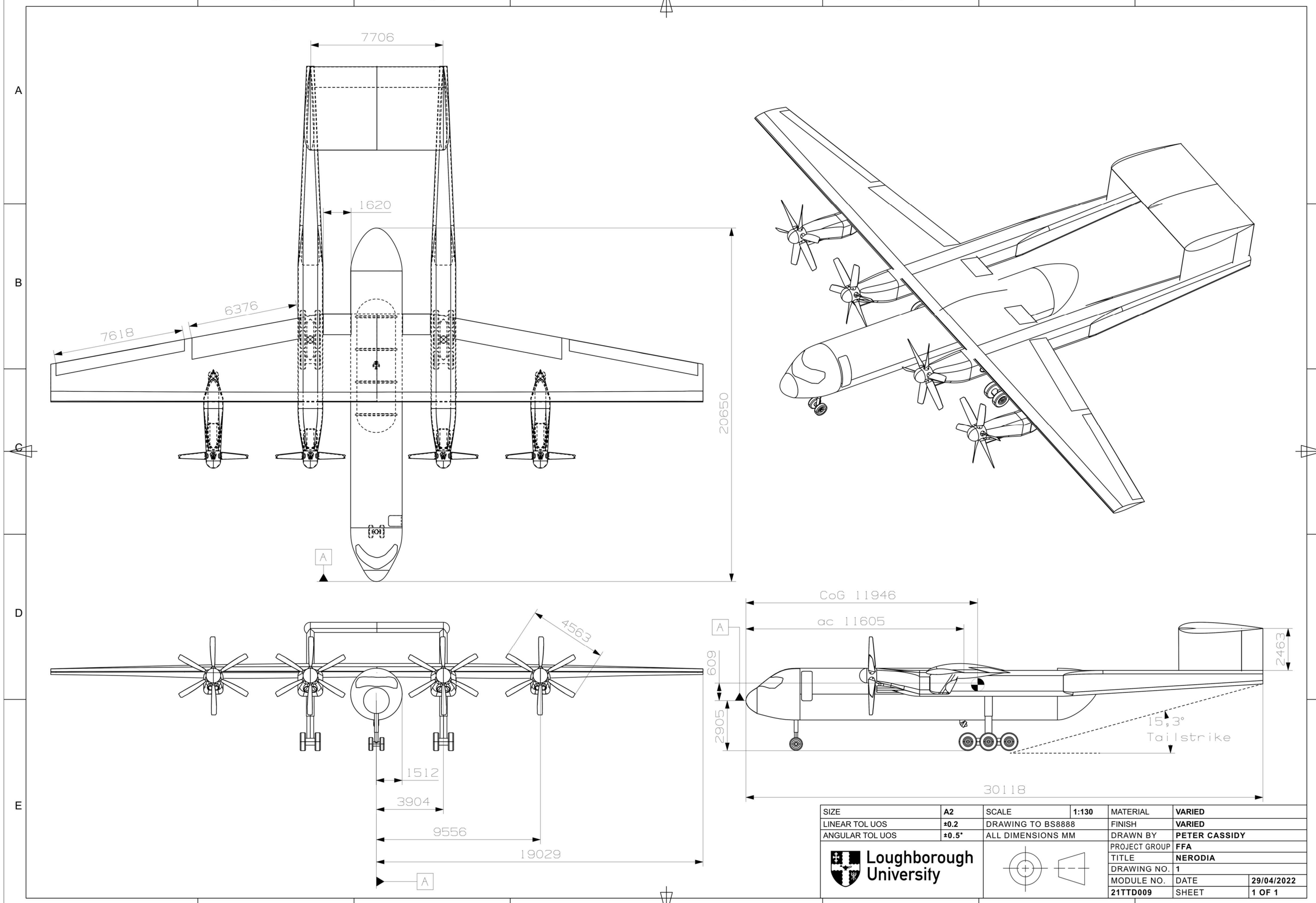
Figure 3: Nerodia's configuration (underside view). N.B. Fuselage is depicted as wireframe to illustrate payload location and size, all other internals omitted.

Nerodia is ultimately designed to perform its mission whilst providing maximum value to the customer. The following is a design summary of the aircraft, which is substantiated briefly by the White Paper and then further validated in the Supporting Information.

The traditional elements of the aircraft (lift generation, structures, control surfaces, systems, propulsion) have been designed in all aspects around the fundamental process of accurately dropping the payload in a timely and controlled manner. Nerodia is a twin-boom, high-wing large air tanker containing a 6,000 US-gallon pressurised tank designed for Phos-Chek LC95 retardant [4]. The retardant itself is contained within a 7.5 m long, 2.25 m wide, 2 m tall oval tank with half-ellipsoid end caps. The tank is outfitted with 14 internal baffles each containing 20 one-way valves to limit slosh and CoG travel during climb at worst-case volumes (half-full payload). A 38 m, 9.8 AR span main wing is paired with a 7.8 m span horizontal tail and two horizontal tails for lift generation and aerodynamic control. Four Pratt & Whitney PW150A turboprop engines propel the aircraft with fully bespoke propellers designed for optimal mission efficiency.

Table 1: Nerodia key design values.

Parameter	Value	Parameter	Value
MTOW (kg)	66,900	Wingspan (m)	38
OEW (kg)	29,000	Wing AR (-)	9.78
Payload Capacity (l)	22,700	Horizontal Tail Size (m²)	38.02
Payload Mass (kg)	25,000	Vertical Tail Size (m²)	32.7
Max Dispersal Rate (l/s)	6869	Subsystems Power Cons. (k W)	211.4
Max Payload Refill Rate (l/s)	101	Max Continuous Power (kW)	15124
Max Cruise Turn Rate (deg/s)	14.8	Unit Cost in 2030 (\$m)	119.9



4. Performance Statement

Table 2: Performance statement.

Performance Parameter	Value
Cruise Speed (m/s)	154
Cruise Altitude (m)	6,500
Dash Speed (m/s)	170
Dash Altitude (m)	10,500
Ideal Drop Speed (m/s)	72
Stall Speed (Fully Laden @ 5,000ft Take-Off) (m/s)	54
Stall Speed (Fully Laden @ Sea Level) (m/s)	50
Drop Height (AGL) (m)	46 – 92
Design Mission Radius (km)	750
Max Endurance (Full Payload) (hr)	13.1
Ferry Range (km)	5,600
Full Payload Capacity (l)	22,700
Service Ceiling (m)	13,260
Peak Flow Rate (l/s)	8,250
Propeller Efficiency (Cruise)	0.864
g-limits	-0.8 to +3.25
g-limits with override	-1.2 to +4.0625
MTOW (kg)	67,000
OEW (kg)	29,400
Wing Loading (Fully laden) (N/m²)	4,440
Balanced Field Length @ 5,000ft altitude (m)	1,370
Internal Fuel Capacity (l)	24,800
Total Trim Tank Capacity (l)	200
Rate of Climb (m/s)	11.2
Total Available Power (kW)	15,124
Thrust (at Cruise) (kN)	49.8

5. Payload Design

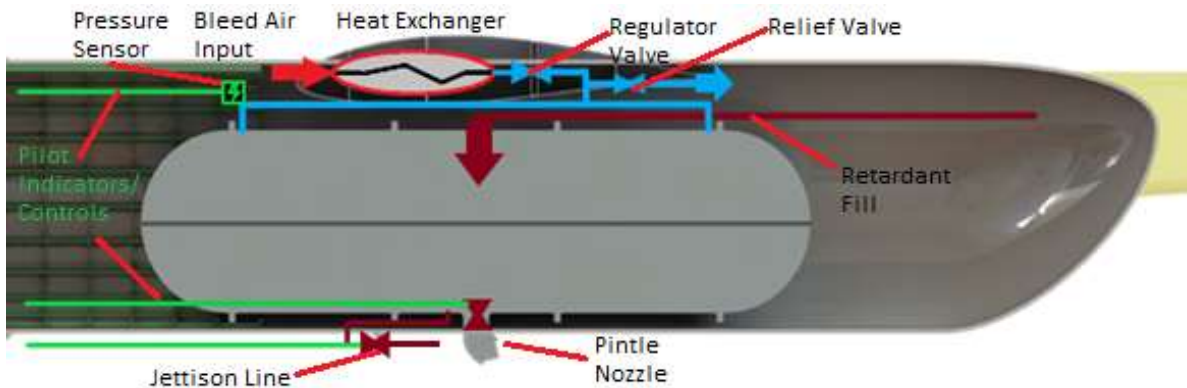


Figure 5: Internal payload configuration of Nerodia.

With the payload system being the most important system of any FFA, the rest of the aircraft was designed around it. The combination of a highly bespoke aircraft with a custom-built payload system has the potential to fight fires more efficiently and effectively than any current airtanker. The tank is slightly elliptical in shape, with a semi minor axis of 1 m and a semi major axis of 1.25 m. The material for the payload tank is Aluminium 5052 H32 due to its superior corrosion resistance. These dimensions results in an absolute volume of 6678 US-g, with total droppable payload volume of 6000 US-g (22700 l) when accounting for internal geometry and efficiency losses. To achieve an accurate retardant spread, a constant high flow rate is required and hence the payload tank is continually pressurised to 16.5 bar using engine bleed air of mass flow rate 1.44 kg/s from an inboard engine.

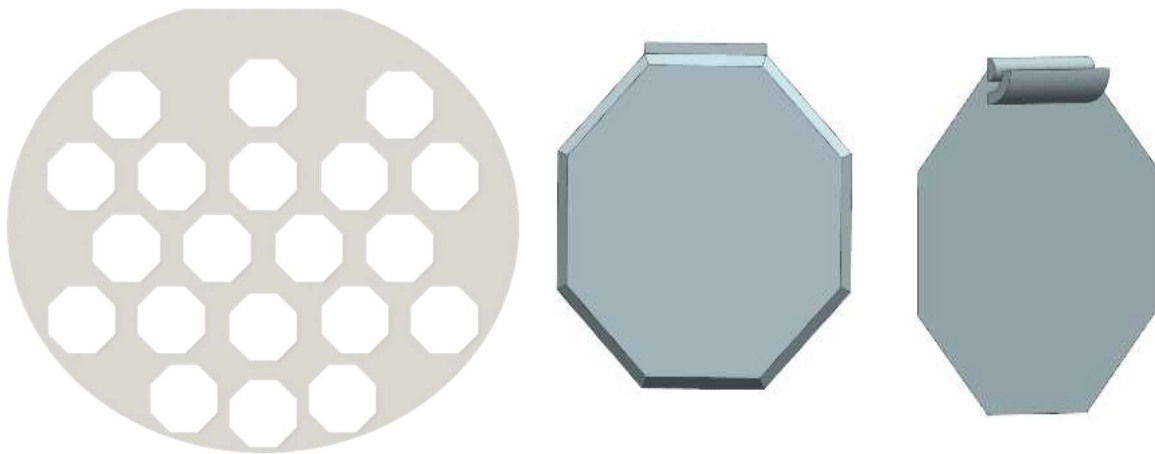


Figure 6: Baffle and One-way valve design.

Since the Nerodia will be subjected to high g-force manoeuvres which will cause ‘sloshing’ and CG shifts under payload deployment, a new baffle design was developed in conjunction with one-way valves. Optimisation code was developed and used to determine that 14 baffles would be optimal to suppress such effects. With an apothem of 0.140 m, the chosen baffle design is an octagon shape with a 45° chamfer on each length as shown by Figure 6 above.

DuPont Delrin [5] is the material of choice for the baffles, due to its resistance to corrosion and lightweight nature. Included are slot gaps of 0.0018 m^2 to permit pressurised air to move from the out-board cavities to the centre. The tank is slightly oversized to account for the capacity losses because of this. The one-way valves, also shown in Figure 6, have a hinge and stopper that acts like a flap that is capped at 45° so that the retardant is only allowed to flow in one direction. The designs of these individual components were created with the goal of conserving internal tank space while maintaining stability.

The outlet pipe of the tank has an inner diameter of 40 mm and can deliver a maximum flow rate of 6869 l/s to the pintle nozzle. As shown by Figure 6, a total of 20 one-way valves on each baffle (each with an area of 0.086 m^2) is required to meet the volume flow rate of the outlet pipe. The one-way valves are offset to allow for enough structural strength to remain within the baffle whilst also optimising the flow of retardant to the centre for discharge. The retardant is released from the tank using a pintle nozzle as shown by Figure 7.

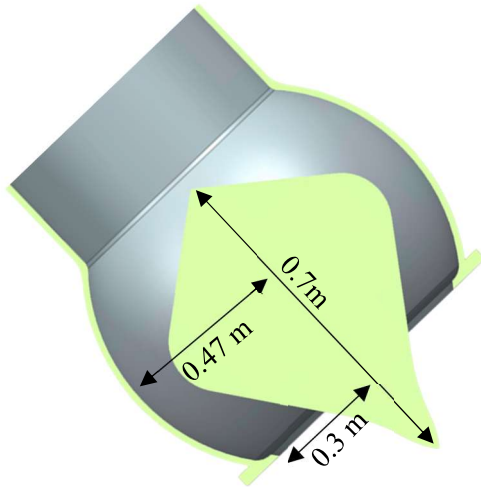


Figure 7: Pintle nozzle design. N.B. diagram not to scale.

The refill pipe inlet is located on the rear tail door and using the Waterous CSUC20C single stage fire pump [6] - the payload tank can be refilled in under 4 minutes. Crassus Aviation understands the importance of easy maintenance to an operator and hence a great effort has been put into designing the payload system of Nerodia as risk-free and as straight forward as possible. The payload system can be removed via the rear tail door for maintenance and repair. The tank includes a split casing around the lateral perimeter to provide access to the baffles for assembly and maintenance. 5 small maintenance hatches are present to detach and reattach the payload tank from the fuselage itself, whilst a larger maintenance hatch is present in the belly of the aircraft for detaching and reattaching the pintle nozzle to the outlet pipe.

6. Aerodynamic Design

As a bespoke FFA, the Nerodia must be able to fly with sufficient manoeuvrability at low level, whilst carrying a large payload. This without also compromising cruise speed and efficiency, so that it can respond to fires in a timely manner.



Figure 8: Main wing planform.

The main wing is a straight leading edge, semi-tapered design with a balance being made between the required high-lifting capabilities and the avoidance of tip stall during low-speed manoeuvres. A close-to-ideal taper ratio of 0.44 and an aspect ratio of 9.78 result in a moderately efficient wing in cruise while the straight leading edge and tip washout angle reduce the chance on tip stalling when flying close to the ground.

The NACA 63(2)-615 aerofoil provides a high section lift coefficient for the high-lifting capability and a high critical Mach number allows for the straight wing design without the risk of wave drag even while dashing at high altitude.

High-lift devices cover large areas of the available space on the wing not covered by the nacelles, booms, or ailerons to provide the required C_L of 2.88 to meet the balanced field length requirement.

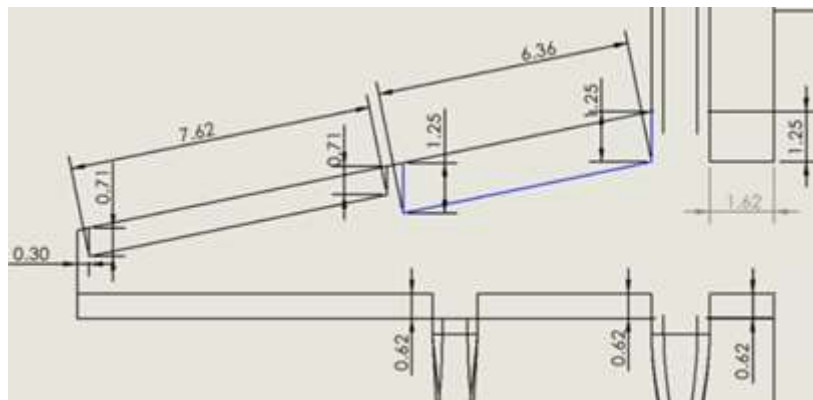


Figure 9: High-Lift Devices.

With the twin-boom, high-tail configuration used, some solutions have been employed to prevent the aircraft from deep stalling. Slotted flaps, slats, and inboard blown flaps all reenergise the flow over the wing surface. Nacelle strakes are also used to reduce the effect of the upwash caused by the nacelles. These measures delay flow separation, ensuring the horizontal tail is not covered in the turbulent wake when operating at higher AoA maintaining pitch control.

7. Drag Breakdown

The drag breakdown of the aircraft can be seen in Table 3. The zero-lift drag coefficients for each component was found using CFD, the process of which is briefly described in the supporting information of aerodynamic design. The induced drag at each phase of flight is also shown.

Table 3: Drag breakdown.

Component	Cd_0	Phase of Flight	Cd_i
Wing	0.0126	Cruise / Ferry	0.0124
Fuselage	0.007	Dash	0.008
Tail	0.0041	Drop (Full Payload)	0.197
Outboard Nacelles	0.00458	Drop (Half Payload)	0.126
Inboard Nacelles and Booms	0.0047		
Total	0.0333		

8. Propulsion Design



Figure 10: Engines and propellers on Nerodia's port side. Wireframe view showing engine inside nacelle, air intake, and exhaust port (wireframe not representative of actual nacelle).

The Nerodia aircraft is powered by a set of x4 Pratt & Whitney PW150A turboprop engines, located inside the fore sections of the booms, and inside the two outboard engine nacelles – arranged in a tractor configuration. The turboprop engines are outfitted with 6-bladed constant-speed (variable pitch) propellers that are a bespoke-design for optimal design mission efficiency. Each engine can deliver 3781 kW of continuous shaft power with an additional 3750 N of jet thrust [7] derived from the exhaust, all controlled via a FADEC system. 10% of the HPC airflow is

tapped off as bleed air (1.4 kg/s) from each inboard engine to pressurise the payload and provide air conditioning. Key propulsion design values can be seen in Table 4.

Table 4: Key propulsions system design values.

Parameter	Value
PW150A Rated Power (x4) (kW)	15,124
Take-off Required Power (kW)	3,840
Cruise Required Power (kW)	5,890
Take-off Required Thrust (kN)	44.1
No. Propeller Blades	6
Propeller Diameter (m)	4.55
Rotational Speed (RPM)	826
On-design Propeller Efficiency (%)	93.02
On-design Advance Ratio	1.79

9. Systems Breakdown

The scope of subsystems design work covers aspects such as power system design, avionics, fuel distribution systems, actuation, and miscellaneous topics such as de-icing and landing gear arrangement.

The power system is concerned with generation and distribution of electric & hydraulic power for use by various components on the aircraft. Design in this area has been aligned with the MEA concept. Alternators on the four engines supply ample power for all onboard loads. Separate power sources in the form of batteries, and onboard APU, and a connection point for ground-power add redundancy to the power system. These sources are also expected to be the initial power sources prior to and during engine start-up on the ground. Hydraulic power is provided by the APU for braking and steering by the landing gear. Once airborne, the aircraft has no hydraulic power needs. Avionics has been tailored towards operator convenience, particularly within the high-stress environment of aerial firefighting. Novel avionics suites planned for the aircraft allow safer, more frequent operation when compared to comparable aircraft of the same role. For example, night flying devices such as large headlights, radar altimeters, FLIR cameras, and EFVS permit the aircraft to continue effective low-altitude operation in poor visibility and low-light conditions. The avionics system also features a bespoke ‘ballistic aid’ suite. From the operator’s perspective this is represented by a ‘smart ballistic sight’ for augmentation of payload drops. This system makes use of inertia sensors, altitude, wind conditions, and visual cues to give operators a real-time preview of where their payload drops will impact on the landscape. Such a system will considerably improve airdrop precision – and hence promote the safety of ground-based personnel at each incident.

Fuel distribution systems have been built to satisfy needs for in-air trimming and extended range operations such as ferrying. Numerous trim tanks across much of the length of the airframe allow

rapid reconfiguring of the aircraft in response to rapid changes in weight distribution caused by the payload tank. Excess capacity also permits greatly improved aircraft range where necessary – of particular use during ferrying or alternate use cases. Aircraft maximum ferry range is calculated as 4980km on standard tanks, this increases to just over 6,500km when trim and surge tanks are also filled.

Actuation of control surfaces, lift devices, and landing gear has been aligned with the MEA concept. As such, electromechanical and electro-hydraulic devices are used throughout the aircraft. This eliminates the need for hydraulic lines throughout the airframe – enabling more efficient use of the remaining space for alternative systems and strong structures. To compensate for the lack of direct connection, force feedback for the operators is simulated virtually.

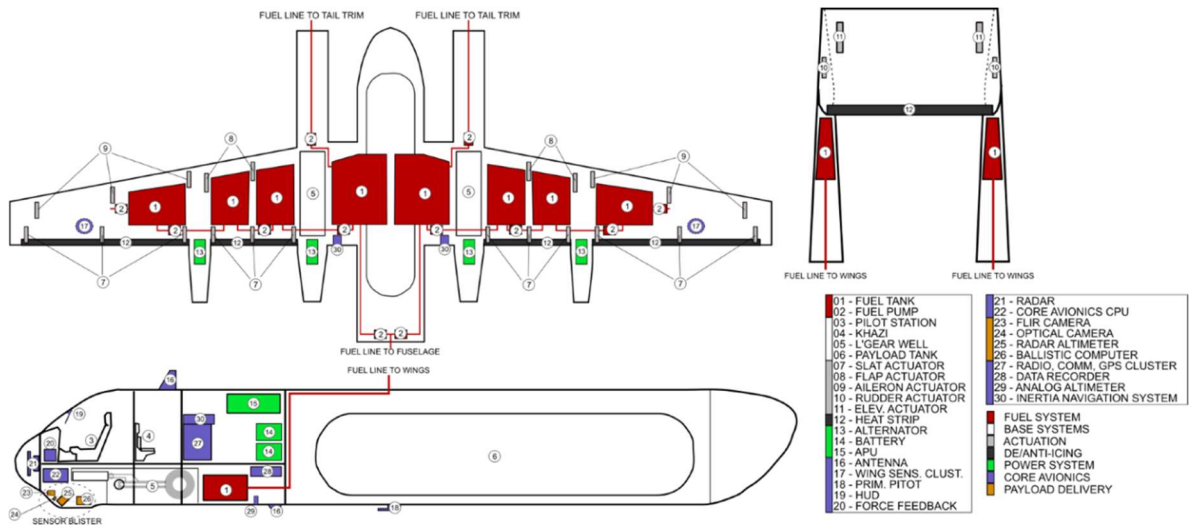


Figure 11: Subsystems layout of Nerodia.

The above figure displays the layout of various subsystems about the aircraft. The bulk of subsystem components are concentrated in the forward fuselage and about the wings. Fuel distribution systems are displayed in red, with points for fuel jettison located towards the wingtips. Actuators are listed in grey. Power systems in green, core avionics in blue, and ballistic aids in orange.

Key areas of note are the ‘sensor blister’ below the aircraft’s nose. This features many of the key components required for night-vision capabilities and the ballistic aids. Between the crew station and the payload bay is the ‘subsystem bay’. This large space contains key components such as batteries, the APU, control electronics, communications equipment, and other such devices. The space is designed to be accessible from outside and highly configurable depending on future mission needs.

10. Structures

The Aircraft is designed for a no fatigue load limit of 3.25g with a FCS to prevent straining load from being applied to the aircraft. The FCS allows the limit to be temporarily increased to 4g to avoid terrain with pilot operation of a paddle on the control column.

The Flap speeds are designated with sufficient headroom to allow the FCS time to automatically close the flaps as the plane accelerates.

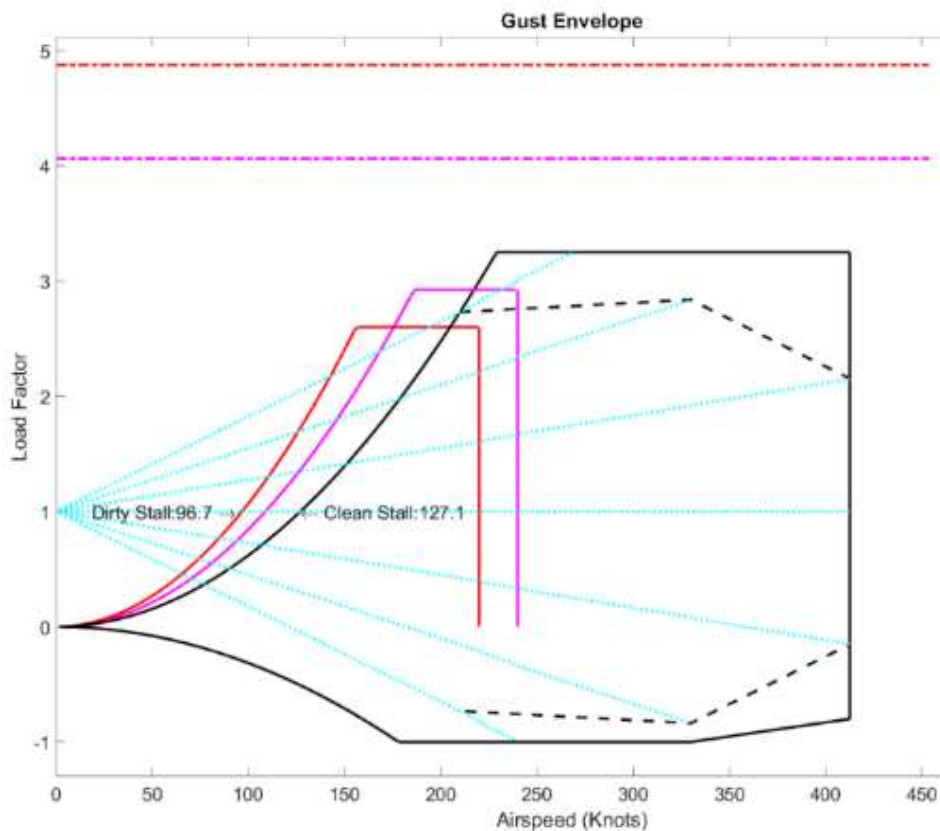


Figure 12: Combined gust and V-N diagram.

Table 5: Relevant structural velocities.

G-Limit Normal	G-Limit Override	G-Limit Structural	V _a Manoeuvre (kts)	V _b Gust (kts)	V _c Cruise (kts)	V _d Dive (kts)	V _f Flap (kts)
3.25	4.06	4.875	230	210	300	412	210

Nerodia's primary configuration drawback is the structurally inefficient twin boom design. This configuration causes massive torsional loads to be driven into the wing during higher alpha, high elevator deflection manoeuvres. For this reason, careful consideration has been taken to design a highly stiff, optimised wing section to ensure the aircraft can withstand the wear and tear of typical FFA flight patterns, with a control system to further assist in increasing longevity and minimising maintenance time. The aircraft is designed such that typical tail loads do not surpass half the maximum pre-fatigue load to reduce fatigue risk.

Materials have been selected to ensure low mass, high stiffness before failure, and a predictable, smooth-yielding dynamic that, in the event of catastrophe, will allow the aircraft to safely return. The FCS is inspired by modern fighter aircraft design, keeping the aircraft within the structural capabilities with an option for the pilots to pull the “Terrain Avoidance Paddle” located on the stick, temporarily increasing FCS limits to allow 100% load. This has been designed that in a worst case a pilot could reach 100% of the aerodynamic load capability of the aircraft 27 times before catastrophic failure occurs. Using this feature even once would require a full inspection of key structural components. Aluminium is one of the best researched materials in fatigue with signs of fatigue well understood with easily detectable indicators. This combined with sensibly designed access hatches allows the inspection of the airframe to give good confidence in the real condition of the parts without need for expensive, high-tech composite analysis (NDT).

Figure 13 show some examples of FEM models undertaken to unsure high confidence in a/c structure and payload mounting. More detail explaining these is covered in the supporting content.

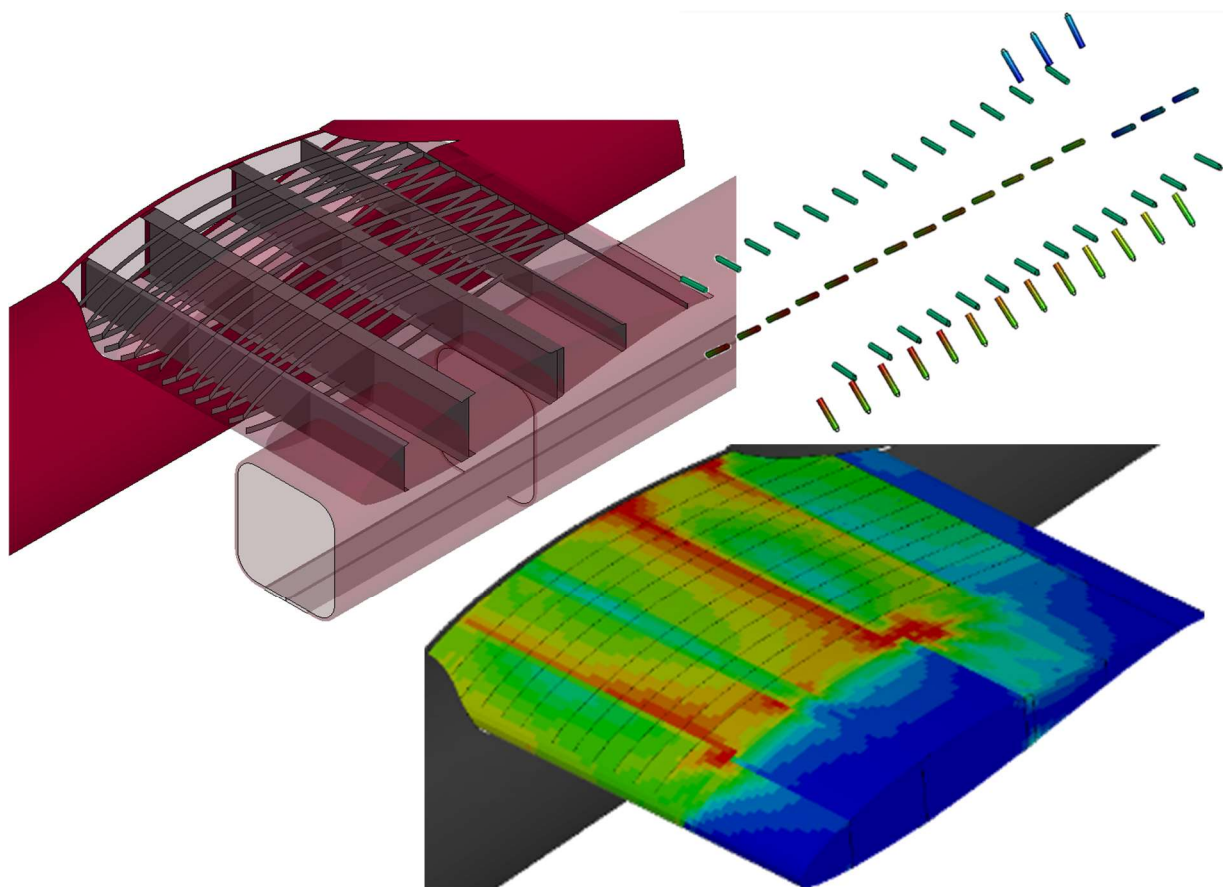


Figure 13: Examples of FEM analysis carried out in supporting information.

11. Mass Breakdown

Table 6: Mass breakdown with CG's measured from nose Datum (shown in 3 view drawing).

Component	Mass (kg)	CG Chordwise (m)	CG Spanwise (m)	CG Vertically (m)
Engine #1	718.00	9.96	-9.71	1.08
Engine #2	718.00	9.96	-3.88	1.08
Engine #3	718.00	9.96	3.88	1.08
Engine #4	718.00	9.96	9.71	1.08
Main Wing	6715	12.62	0.00	1.40
Fuselage	4303	10.94	0.00	0.00
Horizontal Stabilizer	747	25.52	0.00	4.62
Vertical Stabilizer	1726	24.04	0.00	3.15
Electronics Payload	1067	3.50	0.00	-0.12
Fuel	13362	12.00	0.00	1.35
Fuel Systems	416	12.00	0.00	1.15
Nose Landing Gear	222	2.79	0.00	-1.30
Main Landing Gear	1795	12.79	0.00	0.50
Booms	3301	19.57	0.00	0.50
Retardant Tank #1	1565	11.60	0.00	0.00
Retardant in Tank #1	24494	11.60	0.00	0.00
Avionics Systems	14101	3.00	0.00	-0.20
APU	295	20.48	1.40	-1.13
Hydraulics System	1395	5.00	0.00	-0.12
Cockpit and Instrument Systems	124	2.00	0.00	-0.20
Pilots	181	3.00	0.00	0.60
Air Conditioning	869	4.00	-0.30	-0.75
Total / Overall CG (kg / m)	66859	11.95	0.002	0.61

12 Project Viability

Compared with contemporary FFA, the Nerodia offers enhanced capabilities over the competition.

A payload capacity of 6000 US-g fits into the classification of a large tanker. Aerial performance and stability is also impressive with the aircraft boasting a good power-to-weight ratio, very good ferry range, and numerous stability & trimming mechanisms to compensate for weight distribution changes after dropping of payload. If produced, the Nerodia would be only 1 of 2 multirole aerial firefighters built and supported by an OEM, alongside the DHC-515.

Table 7: Prices as of May 2022, adjusted for inflation.

Aircraft Type	Payload Capacity (us gal)	Ferry Range (nm)	Unit cost in 2022 (\$ million)
Nerodia	6000	3000	94.6
DHC-515	1850	1200-1600	~30
CL-415	1600-1850	1500	20.65
C-130J w/ MAFFS II	3000	2400	82.8

The aircraft also offers avionics capabilities not widely found on competitor FFA. The night flying package enables safe and effective operation of the aircraft in low-visibility and dark conditions at low altitudes – permitting the aircraft to respond to emergencies regardless of the time of day. This alone represents a step-change compared to existing FFA - with all aircraft currently unsuitable for low-level night flying. Improvements to payload delivery including a bespoke tank baffle design and a ballistic aid system offer enormous improvements to the consistency, precision, and safety of payload drops compared to current aerial firefighting methods. Further, the modular approach to design of the payload bay allows adoption of a wide range of alternative roles.

Table 8: Operational cost comparison.

	Nerodia	DC-10	CL-415	BAE 146	C-130
Total Cost/Drop (\$ in 2030)	43,400	78,800	17,100	9,500	31,100
Cost/US Gallons (\$ in 2030)	7.23	8.38	10.69	9.43	10.37
% diff. in DOC from Nerodia	-	16	48	30	43

However, the business case for the aircraft somewhat falls flat. Given the very low volume of aircraft anticipated for production and the large unit cost of each aircraft it is apparent that it would be uneconomical for a client to operate a fleet of these aircraft without considerable additional subsidy. Hence, private contractors and NGOs are unlikely to be swayed to purchase any of these aircraft despite the great leap in performance they would offer over their current fleets.

Government organisations are another matter, however. Given their large budgets ~~and general fiscal irresponsibility, especially in California~~ it remains possible that such organisations in locations prone to wildfires may be swayed to rise to the purchase of a fleet of aircraft. In a way,

such a client may seek to convert financial capital into political capital instead. However, this is hardly a mentality to build a sound business case on.

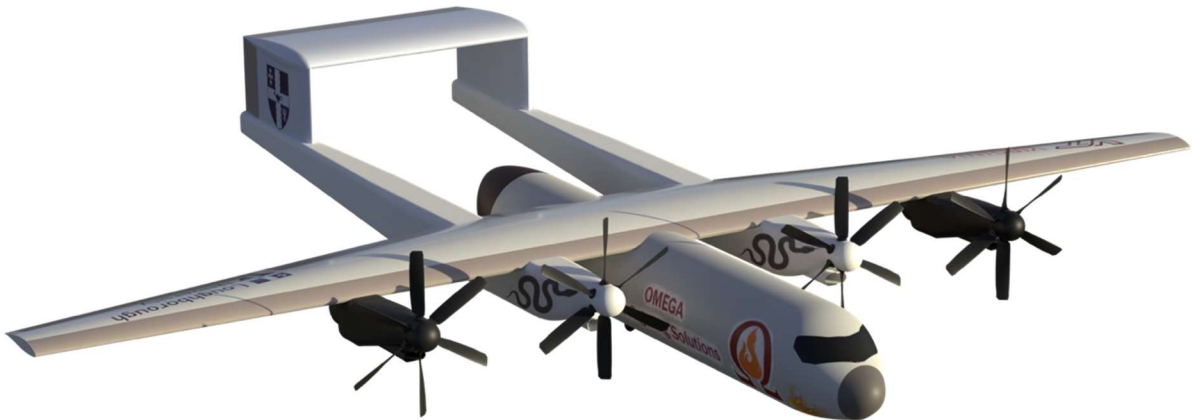
12. Conclusion

Crassus Aviation has completed the detailed design of an effective aerial firefighting aircraft – Nerodia. Nerodia boasts state-of-the-art design features including a high-wing with AR of 9.78, four PW-150A turboprops, a twin-boom tail design, 6000 US-g ellipsoid pressurized payload tank with a pintle exit nozzle. The chosen payload tank configuration combined with CA's all new one-way valve baffle system achieves the highest payload possible with minimal CG shift. It allows Nerodia to perform multiple highly accurate payload drops whilst veering away from a VLAT title. Each of Nerodia's engines are fitted with a bespoke propellor designed for maximum mission efficiency. The combined total power of over 15,000 kW leaves ample power for the heat exchanger and systems IDG. Furthermore, the aerodynamic analysis optimises cruise efficiency, low speed handling and take-off characteristics. The inclusion of effective high lift devices provides an additional C_L of 1.21 resulting in the total C_L of 2.88. Nerodia's cost per US-g dropped is \$1.15 (2030 U.S dollar) cheaper than the next best competitor FFA. The technical brochure reveals Nerodia as the “new and improved” approach to aerial firefighting. Nerodia completes the mission profile in the most efficient manner possible compared to any other existing LAT.

21TTD009: Final Report

Nerodia: Supporting Information

Loughborough University & Virginia Tech



1 Design Brief and User Requirement

1.1 Operational Environment And FFA Regulations

Through research of various locations with high probability of wildfire occurrence, California has the most consistent wildfires resulting in immense damage. Given this fact, Cal-Fire still consists of one of the largest fleets of firefighting aircraft and equipment in the world [1]. Crassus' objective is to surpass the operational prowess of all other FFA such as those in Cal-Fire's current repertoire. The challenges encountered by CAL-Fire give insights into Crassus' initial focus. Mountainous, remote terrain in unfavourable climates with pilots pushing the aircraft to their limits make up a unique design problem.

There is a grey area regarding bespoke firefighting aircraft regulations. Upon contacting current market leaders, it's shown that current regulations are in place only to account for the old airframes in use. Majority, if not all current FFA in service are repurposed commercial or transport airframes. Furthermore, the Australian National Aerial Firefighting Centre (NAFC) delivered an in-depth document outlining the Australian firefighting regulations. The document paved the development of regulations created by Crassus Aviation. Hence, Crassus Aviation began accumulating regulations that abide by ones already in place within the firefighting authorities of various states and countries, as well as those bespoke to our FFA.

1.2 Key Technologies

Crassus Aviation aims to bring a new approach to firefighting. A part of this is developing upon existing technologies that clearly have room to improve. The main point of focus in our FFA design is the payload system. The majority of FFA currently use the RADS and MAFFS modular aftermarket system, consisting of multiple pressurised tanks placed in the fuselage. This format is a very inefficient use of the fuselage space. Crassus Aviation intends to research the viability of a singular large, pressurised tank system which most effectively uses the entirety of the fuselage space available.

More lethargic FFA require a higher drop height compared to nimble FFA, with higher non-pressurised drop height resulting in a more dispersed drop. Pressurisation of the payload tank is a method used to combat low accuracy of drops, and thus is a field of improvement to allow Crassus Aviation to incorporate a large payload with accurate retardant drops.

Most effective firefighting strategies correlate to good exchange of information between aerial and ground teams. Hence, communication is paramount and Crassus Aviation's FFA must include state-of-the-art communication systems on board.

Night flying is a sector not yet touched upon by current FFA in the market. The ability to combat fires at night will place Crassus Aviation's FFA vastly ahead of its competition.

1.3 QFD

GDP FFA QFD

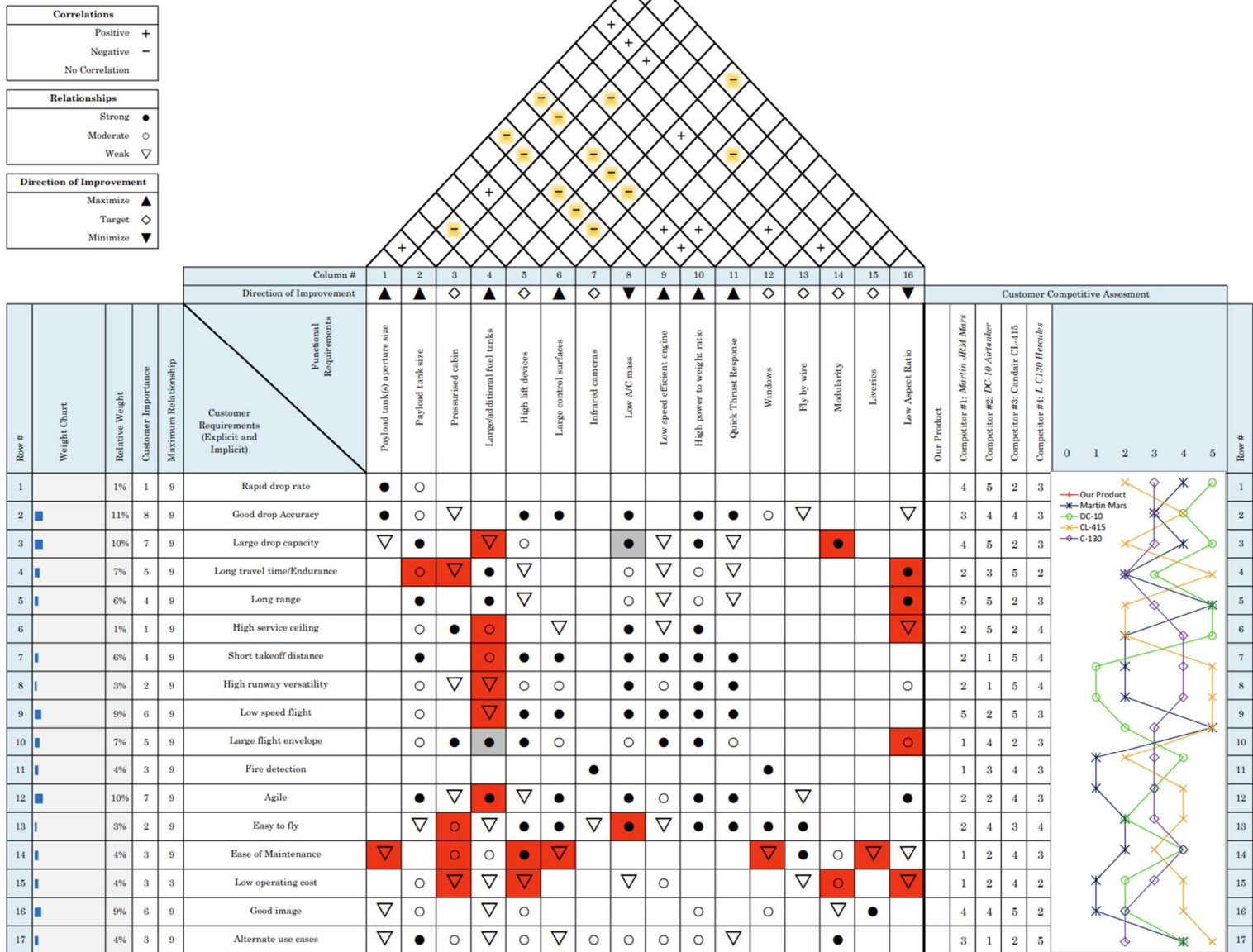


Figure 14: Quality Function Deployment for firefighting aircraft.

A QFD analysis provided Crassus Aviation with a score for each key design element. This score allows for a comprehensive observation of its effect on each customer requirement. Certain design features have a greater effect on more than one customer requirement than others, which can be clearly seen through QFD. As a result, each design feature can be concluded as performing favourable or not. Following the QFD analysis, the Martin Mars is the worst performing FFA whilst the CL-415 performs most favourable, achieving the highest score. Hence, the performance of the CL-415 can opt as a starting point for Crassus Aviation's FFA.

1.4 Requirement Statement

The operational requirements displayed in Table 9 are accumulated and deduced from various firefighting authority regulations. The NAFC regulations are fulfilled whilst the outperformance of

current FFA transcends through the requirements table. The current value of Crassus Aviation's FFA below is compared to the initial estimations put in place prior to design freeze.

Table 9: Operational Requirements.

Requirements	Initial Values	Final Values
Total Payload Volume (Litres)	22,700 - 30,000	22700
Minimum Drop Flow Rate (Litres/Second)	2,000	2,000
Number of Payload Tanks	3-4	1
Drop Flight Speed (m/s)	67	72
Dash Speed (m/s)	170	170
Drop Height (m)	70 – 76	46-92
Take-Off Distance (km)	1.2	1.524
Take-Off Speed (m/s)	58	65
Design Radius (km)	750	750
Ferry Range (km)	6,000	6500
Crew	2	2
Aspect Ratio	<10	9.78

2 Competitor Benchmarking

Through competitor analysis, Crassus Aviation alongside Omega Solutions have produced a bespoke firefighting aircraft that succeeds its predecessors in the field. A gap in the market was established as there are a multitude of single engine air tankers (SEAT) and a few very large air tankers (VLAT) and little to no large air tankers within the 6000 US-gallon payload margin.⁴ 4 competitor aircraft were chosen for the basis of Nerodia's design. The Martin Mars is not considered a historically successful aircraft; however, it was widely used for a long period due to a gap in the market which we intend to exploit. Unfortunately, the cost of running such a large air tanker has surpassed its necessity and therefore flew its last mission in 2016. The CL-415 is rated for the lowest drop height which is partly responsible for its highly accurate dispersals. The C-130J Hercules is an all-rounder, hence is also our direct competitor in terms of existing FFA. Nerodia benefits from new technologies alongside a bespoke space efficient design, allowing Nerodia to bring an all-new operational capability to fighting forest fires. Nerodia's place in the market can be in Figure 15, and it's parameters when compared to other FFA can be seen in Table 10.

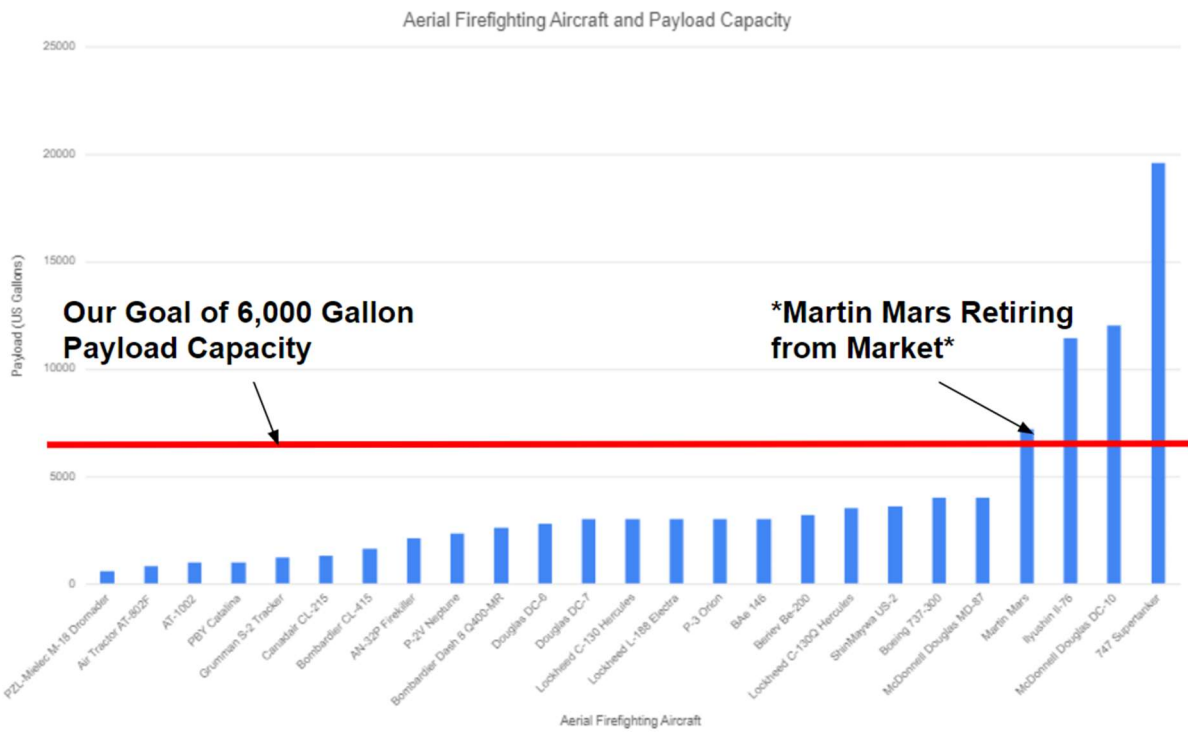


Figure 15: Payload capacities of varying FFA, with Nerodia's design goal highlighted.

Table 10: Competitor benchmarking.

Parameter (0 Q _{NH})	Martin JRM Mars	DC-10 Air Tanker	Canadair CL-415	C-130 Hercules	Nerodia
Span (m)	60.96	47.35	28.38	40.4	38
Length (m)	35.7	55.6	20.4	29.8	30.12
Wing Area (m²)	342.4	330	100	162.1	148
Aspect Ratio	10.85	7 - 7.5	8	10.1	9.78
MTOW (kg)	74840	195000	19890	70300	67000
OEW (kg)	34280	108940	13600	34380	29400
Max Operating Speed (m/s)	98.8	261	100	165.4	170
Stall Speed (m/s)	62	62.6	34.9	51.4	50
Take off Balanced Field Length (m)					
	-	2700	783 / 814	1090	1370
Drop Capacity (litres)	27276	45000	6137	13250	22713
Range (km)	7964	6500	2443	3800	5600
No. of Engines	4	3	2	4	4.69
No. of Crew Members	2	3	2	2	3
Service Ceiling (Payload) (m)					
	4500	12800	4481	7000	13250
Fuel Capacity (litres)	24550	82380	5790	30460	24800
Drop Rate (l/s)	3030	5750	2320	5340	6870
Drop Height (m)	46 - 61	61 - 91	30 - 45	61 - 91	70

3 Concept Generation

3.1 Initial Concepts

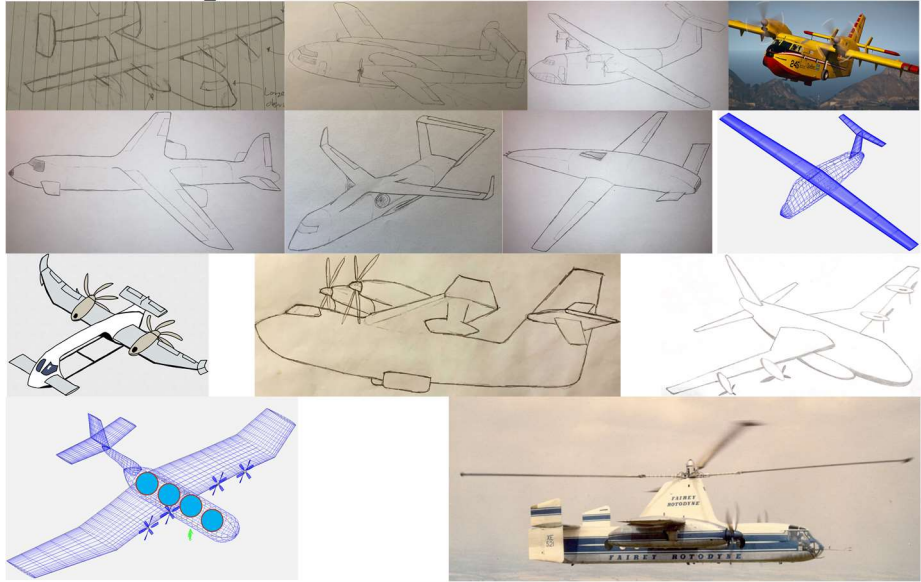


Figure 16: Crassus' initial concepts.

The derived requirements and customer needs from Section 1 guided LU's (Crassus') initial concept generation phase, whereas VT would be constrained by a request for proposal from the AIAA (more in section 3.3). Any conceived concept must fulfil the requirements but also bring about unique solutions to the firefighting problem. To aid the concept generation phase, a reverse-thinking exercise was carried out which aimed to highlight what could possibly be the worst firefighting aircraft, with the hopes of reversing the characteristics for the initial concepts. The result was an aircraft that would have poor lifting capacity (e.g. low lift wings, large sweep angle), be unreliable and/or difficult to service (e.g. poor engine choice, terrible parts availability, age causing lack of certified technicians, complex components), be “awful to fly” (e.g. poor stability, lethargic control response, poor field of view), and be unfit for the mission (e.g. low payload capacity, short operational radius, low drop accuracy, slow turnaround times). A select number of initial concepts are shown in Figure 16 with a variety of unique solutions to the firefighting problem.

Idiosyncratic concept aircraft are useful in that they highlight features and functionality that would otherwise be missed from more conventional aircraft. The presented concepts were thus streamlined/combined to form 7 concepts, each with defining aspects, ready for down-selection.

3.2 Down Selection

The customer requirements derived during the QFD process provided good objective analysis of competitor aircraft. However, they tend to dilute the more important attributes, especially when applied to concepts where the characteristic values are not truly objective. Thus, a reduced number

of attributes were used for the purposes of down selecting our own. Table 11 shows the down selection matrix; attributes (and associated weights), 7 streamlined concepts, and ratings (using genuine data if modelled off current aircraft, or accurately guessed if more unique).

Table 11: Down selection matrix evaluating the 7 streamlined concepts. 1: worst, 9: best.

Attribute and Weight /9	Good drop accuracy	Large drop capacity	Long travel time	Large flight envelope	Easy to fly	Ease of maint.	Alternate use cases	Final score	Norm.
	8	7	5	5	2	3	3		
Concept	Figure of Merit /9								
Rotodyne	9	6	5	8	3	2	6	209	100%
Thunderboxcar	6	8	6	4	6	7	6	205	94.8%
Piaggio	2	2	8	4	3	5	7	132	0%
Marcus	4	7	6	6	6	7	7	195	81.8%
Combination	3	7	7	6	5	5	5	178	59.7%
Catalina	4	6	8	4	7	5	4	175	55.8%
Alula	6	7	7	4	5	6	4	192	77.9%

Out of the down selection process, 4 concepts emerged with promise. The top 2, Rotodyne and Thunderboxcar, were taken forward for further analysis of design suitability and viability.

The thunderbox car presented several clear benefits, as well as its own problems. Primary benefits were its exceptional downward visibility due to the combination high wing, and blunter nose allowing the pilots to be very close to the front of the airframe with clear visibility of the terrain. Additionally, the high wing and elevated tail are advantageous at allowing unrestricted drops for the retardant, with minimal chance of splashing corrosive retardant onto the aircraft. The straight wing design allowed for large control surfaces, ensuring effectiveness even at low speeds. The mated airframe also retains the required agility to carry out accurate, safe drops.

However, the high tail design presents large issues with a stalling / high alpha airframe, as it can get stuck into a “deep” stall where the wake from the main wing stalls the tail, resulting in a nigh unrecoverable stall condition. Secondly, the twin boom design means the force from the tail is being transferred into the fuselage at an offset, requiring a strong wing section to resist the load and more complex plumbing.

The rotodyne concept was plagued with several issues, primarily based around the size and complexity involved in making a rotorcraft with a payload capacity meeting the 6000 US-g minimum requirement. For reference, the largest helicopter by MTOW, the Mi-26, would hold 5000 gallons if you were to completely ignore tank and dropping system mass, and at this mass, would be limited to extremely low speeds / loiter times. The research and development to produce a rotorcraft of this size was estimated by a consulted industry professional to be around 6-7 billion dollars, making this project grossly non-viable. Cost per flying hour is another major concern. With 7 tonne helicopters costing around \$3,000 per flying hour, a 70 tonne rotorcraft would be expected

to be on the order of \$20,000-\$30,000 per flying hour. Beyond pure cost issues, there would be a series of issues stemming from tip speed limitations and structural limits to maximum disk area. Finally, and most importantly, the rotodyne or similar would functionally dash slower than any conventional tanker, and dash speed is critical to firefighting. As fires grow exponentially, so too does the work of the team and the FFA. Any delay, or slow response can mean an otherwise manageable fire becomes a major source of economic drain to suppress.

Taking the thunderbox car as LU's primary design, VT and LU met to discuss similarities with the PSC. The merger would share many aspects from both designs, with primary configuration decisions being the twin boom and reduced payload capacity of the LU design while taking much of the internal configuration and performance requirements from VT. Most notable of these being the step increase in balanced field length, allowing for a lower power requirement and better optimisation of the wing for cruise condition.

Table 12: PSC configurations, with selected attributes highlighted in bold italics.

School	Layout	AR	Wing	Power Unit	Payload (USG)	BFL (ft)
LU	<i>Twin Boom</i>	9	Straight	<i>4 Turboprop</i>	<i>6000</i>	4000
VT	Conventional	<i>10.2</i>	<i>Tapered</i>	<i>4 Turboprop</i>	8000	<i>5000</i>

3.3 VT-LU Merger And Evolution

In early 2022, Crassus Aviation joined forces with Omega Firefighting Solutions, the latter being based out of Virginia Tech in the USA. Omega had initially been working towards a request for proposal (RFP) from the AIAA as part of a design competition. A team size greater than 10 excludes them from the competition and so our derived requirements were able to be merged ceremoniously with their RFP to form a unique set of customer needs.

A series of compromises had to be made with requirements and our proposed concept aircraft. Most importantly, the payload volume differed where Omega proposed an 8000 US-g capacity, and Crassus a 6000 US-g capacity. Crassus' figure aimed to fill the gap in the market of the now retiring Martin JRM Mars, and to achieve a low enough weight to satisfy many US small airfield requirements (68 tonnes [8]). The balanced field length requirement was set to 5000 ft for full

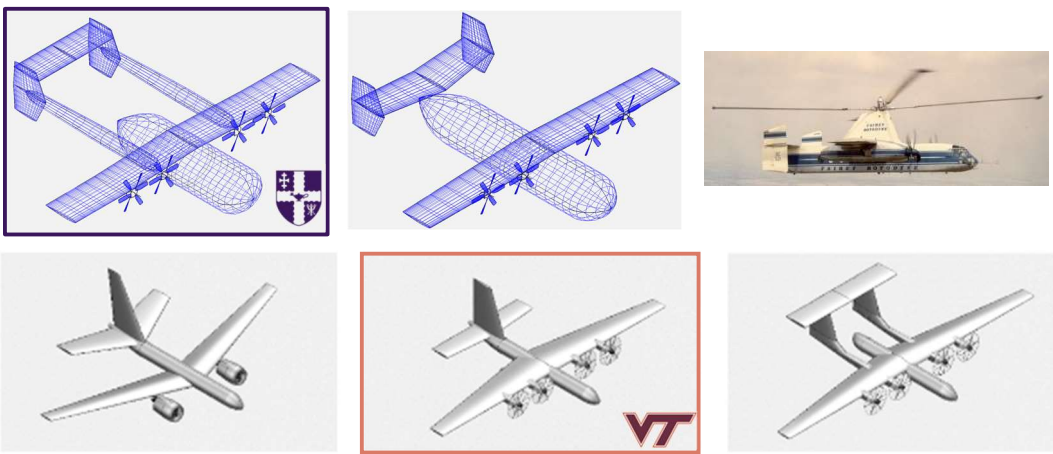


Figure 17: LU and VT shortlisted and ultimately selected concepts.

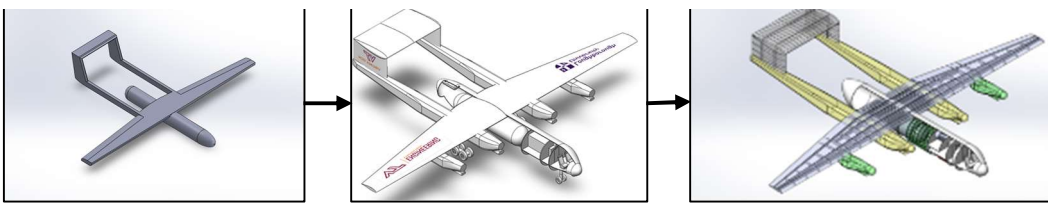


Figure 18: LU and VT merged and evolved concept: Nerodia

payload operation as this was the required size expected to be available at airfields with sufficient ground resource to support and a/c of this class.

As the merger evolved, aspects of both teams' other designs were compared against to create the Frankenstein of requirements that would then be used to encapsulate Nerodia. The main aspects drawn were the interest in the smaller diameter fuselage (selected due to the reduced drag capability that a carefully designed small fuselage could accomplish, allowing greater dash speeds for a given power requirement) and the high tail, ensuring the tail stays well clear of retardant even while pulling G in a drop. This is highly beneficial as retardant is corrosive, meaning a highly corrosion resistant tail would be needed, heavily limiting material selection options and likely increasing cost.

While the general configuration of Nerodia retained its structure from here, the design continued to evolve as part interactions and inter-subsystem requirements were further integrated, the geometry evolved to account for different subsystems needs. The wing geometry was adjusted, increasing the straight section of chord to fill out until the booms allowing the wing structure and flap systems to be significantly less complex. The engine placement varied to ensure good clearance as propeller size changed. Fuselage geometry shifted as payload requirements changed. Initially Nerodia was planning on using multiple separate spheres for payload dropping to ensure no shift due to partially emptied tanks. This later changed to a class-leading CG resistant single tank system, allowing the fuselage to shrink, forcing some systems into the wing box and adjusting wing thickness requirements.

4 Mission Performance

This section covers the performance parameters that are not otherwise derived in other sections of the supporting information.

Ferry range

$$R = \frac{V}{g} \frac{1}{c_t} \left(\frac{L}{D} \right)_{max} \ln \left(\frac{W_1}{W_2} \right), \quad R = \frac{154}{9.81} * \frac{0.864}{1.67 * 10^{-5}} * 13.26 * \ln \left(\frac{49400}{29400} \right) \approx 5,600 \text{ km}$$

Where [9]:

c_t = Specific Fuel Consumption w/ propeller efficiency

W_1, W_2 = Starting and final mass respectively

Endurance (max payload)

$$E = \frac{1}{c_t} \left(\frac{L}{D} \right)_{mp} \ln \left(\frac{W_1}{W_2} \right), \quad E = \frac{0.864}{1.67 * 10^{-5}} * 4.19 * \ln \left(\frac{67000}{53890} \right) \approx 13.1 \text{ hrs}$$

Where [9]:

L/D_{mp} = Lift-to-Drag ratio at minimum power

Rate of Climb

$$RoC = \frac{thp_{avail} * 33000}{W}, \quad RoC = \frac{4000 * 33000}{59530} \approx 2,200 \text{ ft/min} = 11.2 \text{ m/s}$$

Where [10]:

thp_{avail} = excess thrust horse power available

W = Aircraft mass in pounds (lb)

Service Ceiling

Service ceiling is defined as the altitude where the maximum rate of climb is 500ft/min for jet powered aircraft [10]. By rearranging the above formula for the rate of climb the excess thrust horsepower can be found. Using engine and propeller performance at given altitudes the service ceiling can be found to be 43,500 ft or 13,260m.

Ideal Drop Speed

The ideal drop speed is defined as $1.3V_{stall}$. At dropping altitude of 10,000 ft, V_{stall} is 55.4 m/s so the ideal drop speed is therefore 72 m/s.

Turn rate Diagram

Figure 19 shows different turn rates WRT speed at cruise altitude and max power. Max turn rate (intersection of stall limit and structural limit) and sustained turn rate envelope (achievable turn rates without incurring loss of altitude).

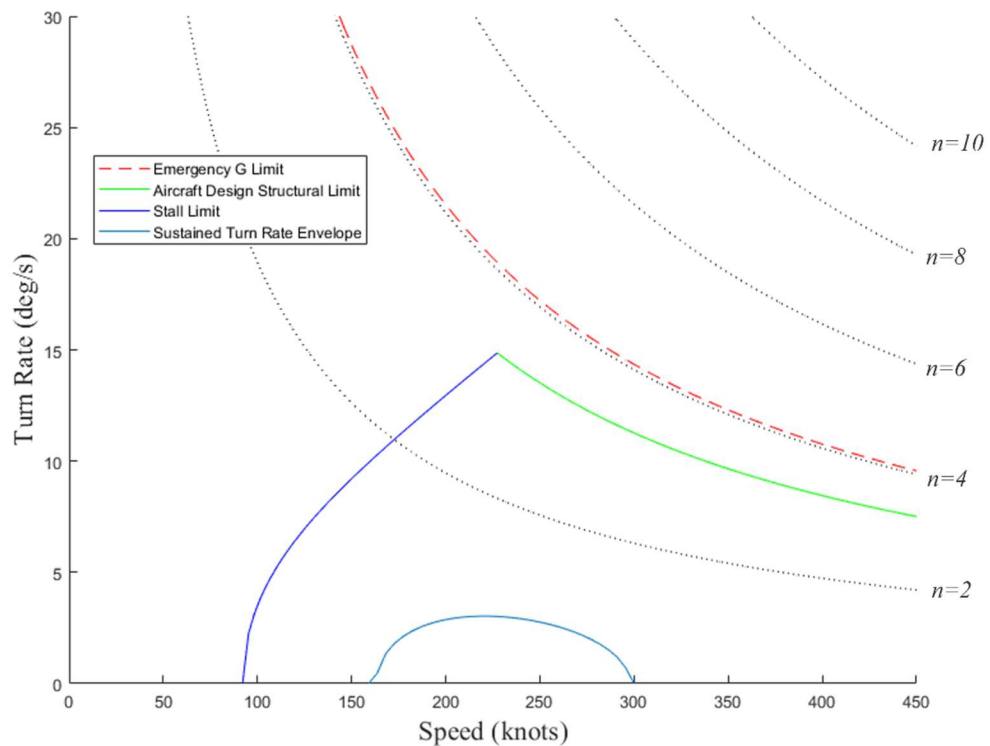


Figure 19: Turn rate diagram.

5 Aerodynamics

Aerodynamic analysis was critical in maximizing the aircraft's cruise efficiency, low speed handing, and take-off characteristics. Mitigating stall was an important consideration given the environment the aircraft will be operating in. The following section outlines the design process in the main wing, high-lift devices, and stall considerations.

5.1 Requirements And Initial Sizing

The design of the main wing was driven by a set of requirements mainly concerning other disciplines, these included the planform area and loading, take-off and landing distances, engine thrust, operating range, and stall behaviour. These values were quantified in a series of equations derived from chapter 5 of “*Aircraft Design: A Conceptual Approach*”, by Daniel P. Raymer [11]; [12] and a NASA reference publication by Laurence K. Loftin, Jr. [13]. MATLAB was used to generate a plot of power and wing loading required to meet all mission performance constraints mentioned earlier, as shown in Figure 20.

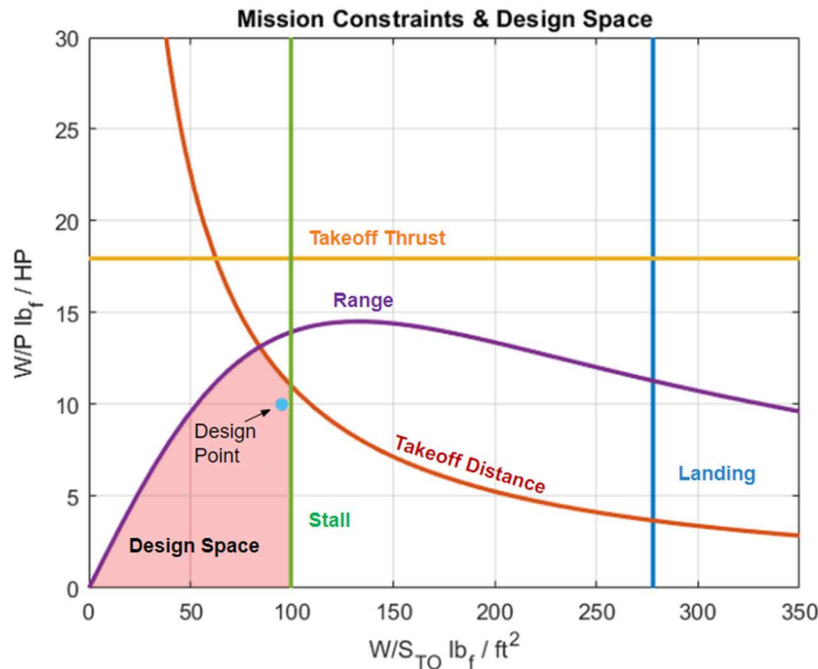


Figure 20: Constraints Diagram.

This yielded a “design space” from which was selected an initial operating point, (shown in red). From a top-down design approach the conceptual aircraft’s wing loading was targeted at $95 \text{ lb}_f/\text{ft}^2$ (4550N/m^2), this was used to find wing planform area required. After the final bottoms-up design, wing loading shifted to $92.76 \text{ lb}_f/\text{ft}^2$ (4441N/m^2), based on actual estimates of MTOW and wing planform area. The following section covers wing dimensions in greater detail.

5.2 Main Wing

The wing planform was created using XFLR5 which has a built in “Wing and Plane Designer” allowing for easy modification to the wing design.

Table 13: Main wing parameters.

Parameter	Value	Parameter	Value
Wing Area (m^2)	148	Tip Chord (m)	2.2
Wingspan (m)	38	Mean Aerodynamic Chord (m)	4.1
Aspect Ratio	9.78	Quarter Chord Sweep ($^\circ$)	0
Taper Ratio	0.44	Root Incidence ($^\circ$)	1.2
Root Chord (m)	5	Tip Incidence ($^\circ$)	0.7

With the wing area defined from the design point, various other parameters for the wing planform had to be balanced against other desired parameters such as the aspect or taper ratios. Initially an aspect ratio of 10 was the target to balance other wing requirements with a high span efficiency and manoeuvrability in roll rates roughly equivalent to similar sized transport aircraft. After the wing was fully designed, the aspect ratio was reduced to 9.78. Taper ratios around 0.4 are the most desirable due to lift distributions that generate the least amount of induced drag as can be seen in Figure 21. Tapered wings also have the benefit of reducing the mass of the wing towards the tip allowing for a lighter wing structure to balance the bending moment.

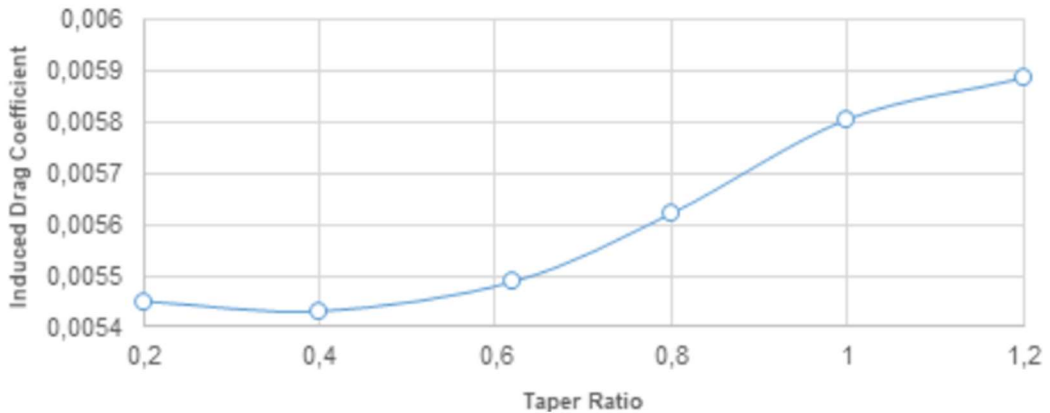


Figure 21: Induced Drag vs Wing Taper Ratio [14].

The inboard wing has a constant chord before the taper begins. This is to provide a rectangular wing section up to the booms primarily for structural considerations and will be discussed in more depth in Section 8.

The aerofoil selection began with a series of derived lift coefficient requirements from chapter 5 of “Wing Design” by Sadraey [15]. An aerofoil of the appropriate ideal lift coefficient (Cl_i) of 0.456 and maximum section lift coefficient (Cl_{max}) of 1.63 was chosen from Figure 5.23 of “Wing Design” [15] based on planform area and other requirements derived from the mission constraint study. A few aerofoils (see Table 14) were selected around this point for some additional analysis using the panel method solver, X-Foil, as part of the XFLR5 package, to compare them in the

expected cruise conditions (Reynolds number of 30million and at 0° AoA) rather than comparing just the maximum lift coefficient.

Table 14. Aerofoil Comparison.

	NACA 63(2)-615	NACA 64(3)-618	NACA 4415
C_{L0}	0.546	0.515	0.490
C_{D0}	0.00439	0.484	0.00503
$C_{L Max}$	1.59	1.25	1.56

The NACA 63(2)-615 aerofoil was chosen for its high lift coefficient, and low drag at high speeds that the aircraft will be cruising at, while still leaving adequate internal space for components and fuel storage. A side profile of this aerofoil is shown in the following figure. One major downside of this aerofoil however was its poor stall characteristics, and tendency to stall suddenly due to the sharp peak of the lift curve.

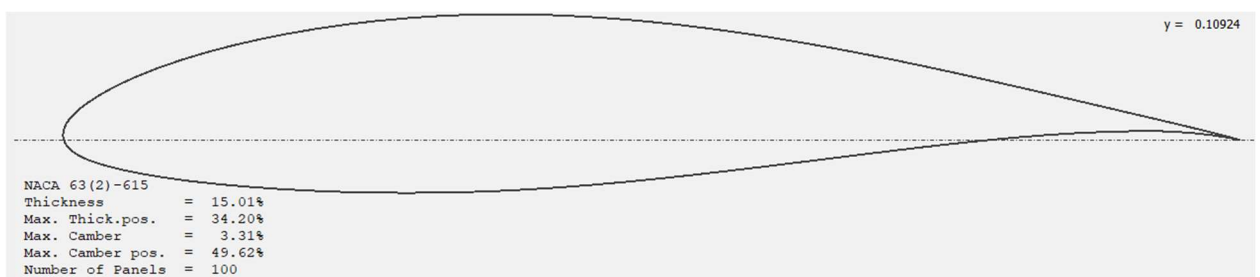


Figure 22: Main wing aerofoil profile NACA 63(2)-615.

The incidence of the wing was set with both aerodynamic efficiency and reducing the risk of tip stalling in mind – with the potential for the FFA to be operating relatively close to the ground, when dropping, combined with the tapered wing, the avoidance of tip stall was a major consideration.

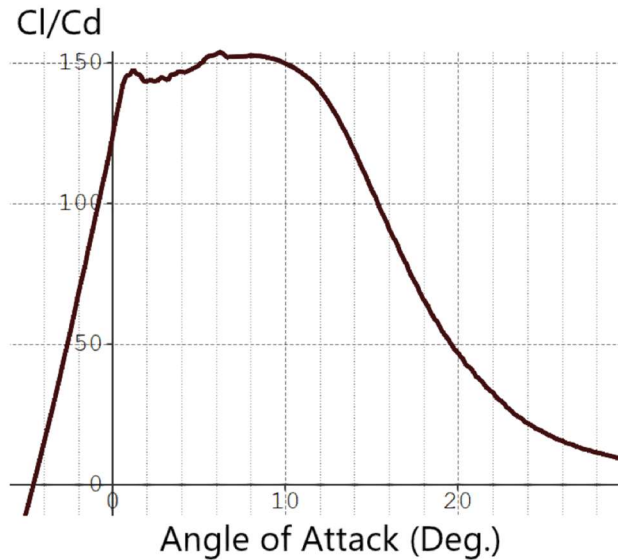


Figure 23. Cl/Cd plot of NACA 63(2)-615 from XFLR5.

Figure 23 shows how the peak of the Cl/Cd graph roughly plateaus between 1° and 10° AoA. The incidence at the wing root of 1.2° benefits from being in this region while minimising the incidence angle. This will reduce the overall drag of the wing while in cruise (given the wing can produce adequate lift) and keep the wing as far as possible away from stalling. Tip incidence of 0.7° provides washout.

The main wing has no leading edge or quarter chord sweep, a decision made by checking the critical and drag divergence Mach numbers against the expected Mach number of 0.574 at the “dash” flight condition. Using the following equation to relate pressure coefficient and Mach number the critical Mach number can be found. By equating the minimum (from aerofoil analysis) and critical pressure coefficients the critical Mach number of an aerofoil section can be found.

$$C_p = \frac{2}{\gamma M^2} \left(\left(\frac{1 + (\gamma - 1/2) M^2}{1 + (\gamma - 1/2)} \right)^{\frac{\gamma}{\gamma-1}} - 1 \right)$$

The critical Mach number therefore can be found to be 0.644. The influence of wave drag is negligible when flying below the critical Mach numbers so no further modifications (i.e. sweep) have to be made to the wing to combat wave drag.

A straight wing has advantages over a swept wing particularly for low-speed flight – useful for the payload dropping and loitering over the mission area specific for this aircraft. Swept wings generate spanwise flow, most noticeably at lower speeds, due to the sweep of the forward leading edge. Spanwise flow essentially means the air towards the wingtips have travelled further so have larger boundary layers, effectively reducing the efficiency of the aspect ratio and most importantly promoting flow separation at the wingtips, and as a result will be more susceptible to wing stall. As

wave drag will not be an issue for the flight conditions expected of the FFA, straight wings can be used, improving the aerodynamic efficiency of the wing and reducing the chance of tip stalling.

5.3 High-Lift Devices

High lift devices were critical to meeting key-performance parameters. The primary drivers of the HLDs were balanced field length and stall requirements. Stall speed should be comfortably below drop speed for crew safety, and HLDs were necessary to meet this requirement.

Based on the aircraft configuration, a Cl requirement to meet the 5,000 ft balanced field length as defined by the RFP was found. Having already an understanding of the Cl produced by the main wing, the additional change in lift provided by the HLD was found.

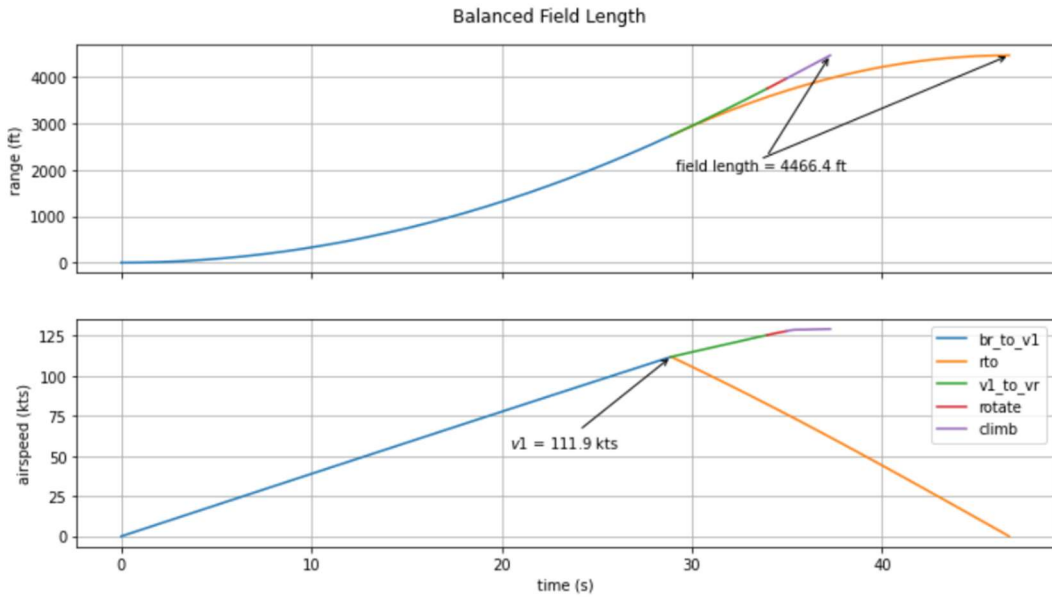


Figure 24. Balanced Field Length.

Figure 24 shows the V_1 speed around 112 kts with an estimated ideal drop speed of 140 kts meaning the required Cl for field length became the main driver to calculating the sizes of the HLD. The maximum take-off angle was set to 14° , limited by the tail strike angle of 15.3° , generates a “clean” (wing configuration with no HLD deployed) Cl of 1.67 from full plane analysis of XFLR5. To meet the requirement for the 5,000 ft balanced field length, an additional Cl of 1.21 (0.48 for ideal dropping speed with full payload) had to be generated from the HLD.

Table 15. High-Lift Device Sizing.

Parameter	Trailing Edge	Leading Edge
Type (see Figure 26)	Single-Slotted	Slotted Leading Edge (Slat)
Wing Semi-Span Coverage (%)	42.6	84.5
Chord Coverage (% of MAC)	28	15
Max Deflection ($^\circ$)	45	15
Additional Cl (at Max Deflection)	0.7	0.51

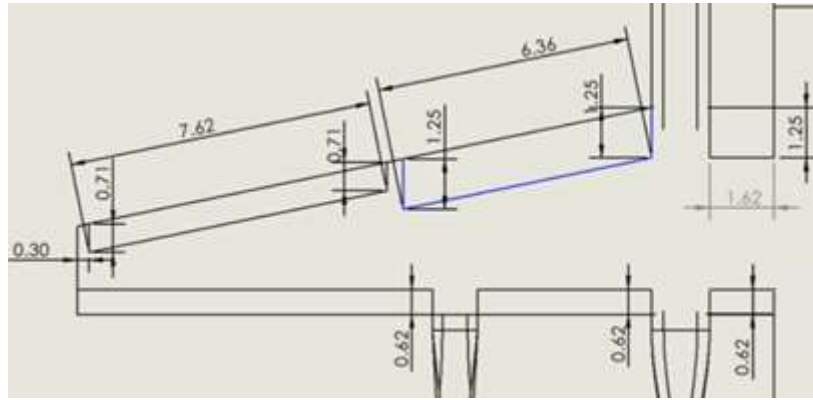


Figure 25. High Lift Device Placement and Sizing.

A summary of the HLD can be found in *Table 3* with a visual representation shown in *Fig 7*.



Figure 26. Single-Slotted Flap and Slat.

The available space for HLD on the wing was limited by the aileron and boom for the flaps and the nacelles for the slats. Using a series of figures from DATCOM 1978 [16], relative factors that consider things such as relative flap/slat chord or relative deflection angles, an increase in the maximum lift coefficient of an aerofoil section can be found by the deployment of flaps and slats using the following equations.

$$\Delta C_{l \max, flaps} = k_1 k_2 k_3 (\Delta C_L \max)_{base}$$

$$\Delta C_{l \max, slats} = C_{l \delta, slats} \eta_{\max} \eta_{\delta} \delta_f \frac{c'}{c}$$

Where [16]:

k_1 = factor for relative flap chord

$C_{l \delta, slats}$ = theoretical slat efficiency

k_2 = factor for relative flap deflection angle

η_{\max} = factor for relative leading-edge thickness

k_3 = factor for relative flap kinematics

η_{δ} = factor for optimum angle of deflection

c'/c = relative slat chord length

δ_f = slat angle of deflection

The total ΔC_L of the wing with the HLD deployed can be found by multiplying the lift increase of the aerofoil section by the area ratio the HLD cover on the wing. Since the required total ΔC_L is known, the factors used in the above equations can be adjusted so that the sizes of the HLD fit into the available space on the wing which is what defines the final values listed in Table 15.

5.4 Stall

Stall analysis was a critical area of study for this aircraft, as NACA 6-series typically have poor stalling characteristics. While panel methods previously used give accurate results for moderate angles of attack up to stall, they cannot accurately predict stall or post stall behaviour.

Because of this, it was necessary to use CFD coupled with wind tunnel testing to reveal flow behaviour.

The XFLR5 analysis of the full 3D wing revealed that the stall angle to be in excess of 18° (Figure 27) before the VLM solver couldn't resolve at this large AoA.

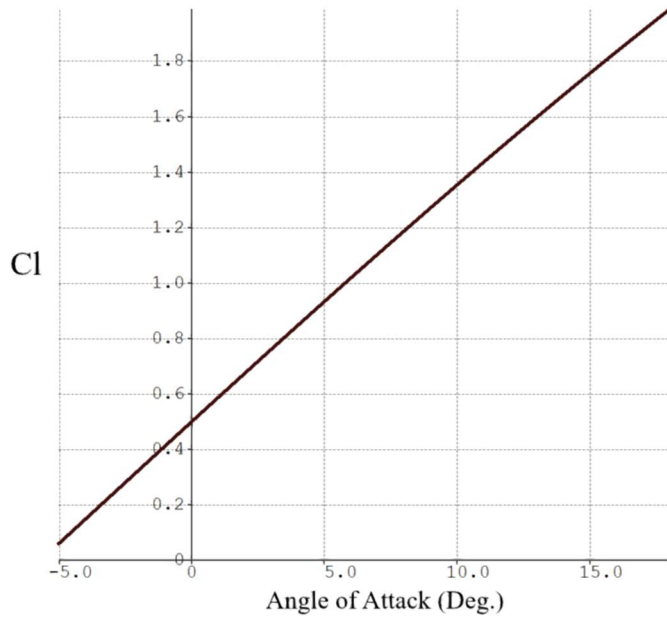


Figure 27. XFLR5 Cl vs Alpha Main Wing.

Due to the limitations of VLM, it was necessary to further investigate the stall angle of the wing using experimental methods by a wind tunnel experiment. While flow characteristics were drastically different between the scale model and the full-sized aircraft, the experiment still revealed useful insight to the flow behaviour. Stall was found to occur at around 19° AoA on the scale model at 25 m/s flow velocity and at a Reynolds number of around 100,000. Because the flow similarity was so different, around an order of magnitude different, CFD at full aircraft scale was needed to further understand flow at real aircraft scales. The flow separation can be seen in Figure 28. This region of separation correlated well with further CFD analysis.



Figure 28. Wind Tunnel Testing Flow Separation.

It was initially expected the wing would require stall fences around the ailerons due to the taper ratio and risk of tip stall. However, wind tunnel testing instead revealed the main issue lies around the inboard nacelle (see Figure 29), due to the upwash it causes. As a result of the findings from the wind tunnel, it was decided to use CFD to further investigate this area of interest.

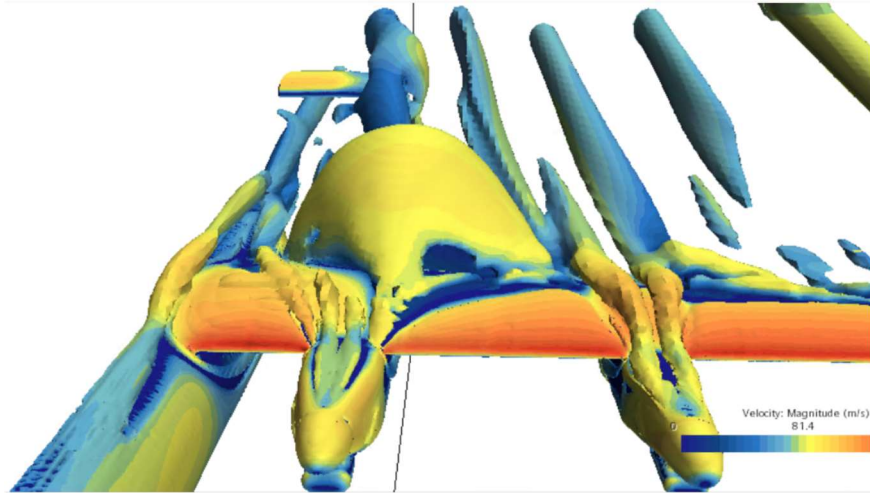


Figure 29. Flow Separation due to the nacelles (Isosurface of Q-Criterion).

A CFD simulation was set up using STAR-CCM+ using a half-span model with a symmetry plane bisecting the fuselage. The physics model was set to a Reynolds number of 10 million to represent the expected low-speed flight conditions of the FFA. Figure 29 shows the initial analysis of the FFA at 15° AoA. This value was selected as it is close to 14° AoA already used in take-off, and it would be important to investigate the flow behaviour in depth at this important phase of flight. Figure 29 shows the results of the simulation with an isosurface of Q-Criterion ($Q>50$) to represent the regions of strong vortices and therefore potential separation. Like in the wind tunnel

experiment, it shows a large area of separated flow at the rear of the wing due to the inboard nacelle. This nacelle both causes upwash on the flow, increasing the local AoA, and generates vortices of its own at the interface between the nacelle and the wing leading edge. These factors combine to induce early separation of the flow over the wing. It also causes a strong, slow-moving vortex behind it which covers part of the horizontal stabiliser. This could lead to the loss of pitch control while already at a high AoA and deep stalling which was the most concerning aspect. Strakes were eventually chosen to tackle this problem. A PhD paper by Sibilli [17], investigated the effects of nacelle strakes on wings and found an increase in stall angle (indicating a delay to flow separation). Simple strakes were added to the model to investigate any potential benefits they may have for the flow field. Figure 30 shows the placement of the strakes on the model.

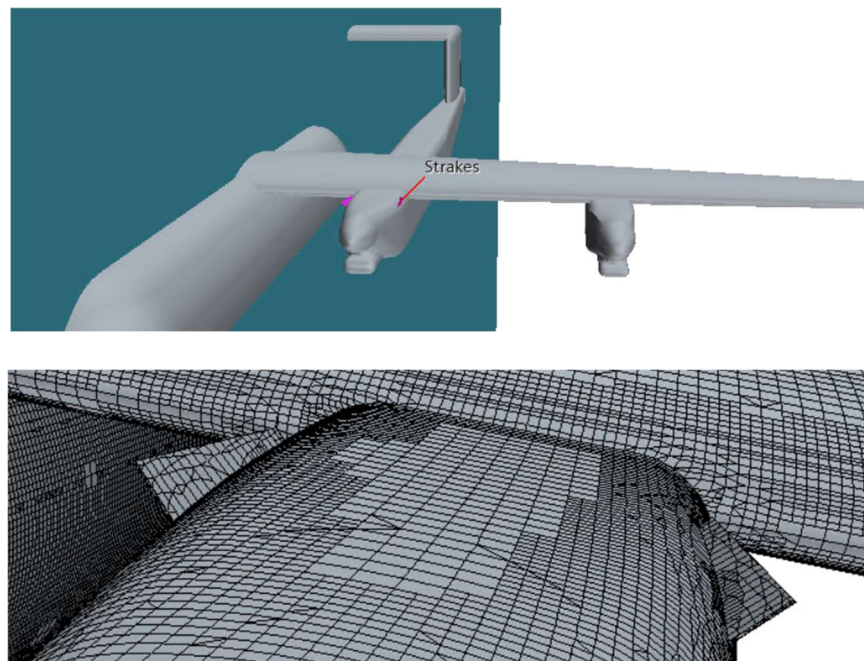


Figure 30. Engine Strakes of CFD model.

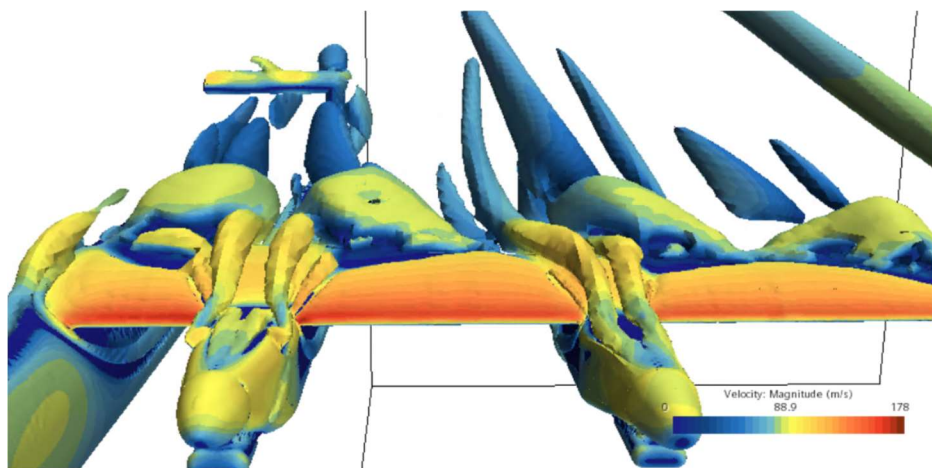


Figure 31. Strakes effect on flow separation.

Figure 31 shows the repeated simulation done in Figure 29 but with the strakes included in the model. While separation is still present over the rear of the wing the magnitude of it has been reduced. The vortex that had previously covered the horizontal stabiliser has been lowered so that pitch control can be retained at higher AoA than without the strakes. Also, the inclusion of strakes was also found to reduce drag by 2% at 15° AoA.

Some other features of the wing will also aid in improving the stall performance of the FFA. The previously mentioned slotted HLD aid in delaying the flow separation over the wing. The slots allow accelerated flow back over the upper surface of the flap reattaching the flow which would help in delaying stall and reduces the negative effects of separated flow which is illustrated in Figure 32.

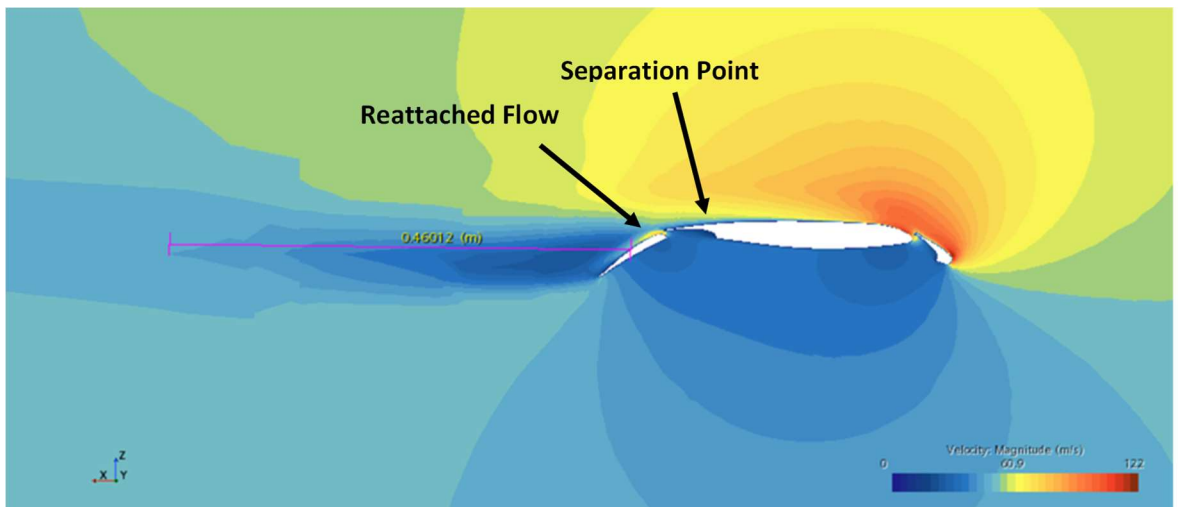


Figure 32. CFD simulation done as part of the HiLift-2 Prediction Workshop [18].

Blown flap surfaces are found on the inboard section of the wing (due to the placement of the tail directly behind). They will use excess flow from heat exchanger that would have otherwise been lost during payload pressurization. The placement of the propeller and its wake will also aid in inducing velocity through the HLD. These will re-energise the boundary layer over the flaps and delay separation as shown in Figure 33.

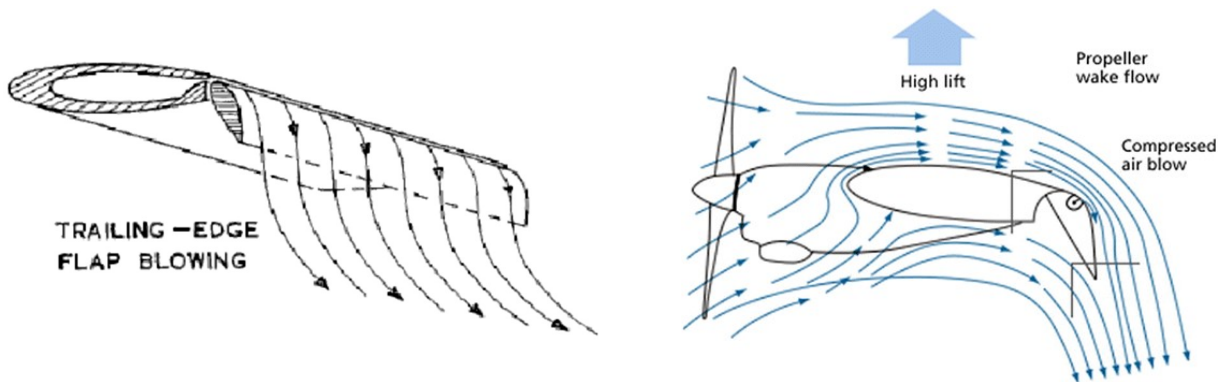


Figure 33. Left: Blown Flaps [19], Right: Propeller Wake Influence [20].

5.5 Drag Breakdown

To obtain the drag breakdown of individual components CFD was used, as hand calculations based on empirical data and suggestions from Raymer [12] and Torenbeek [21] provided poor estimations for a twin-boom, high-wing design. This method suggests that the FFA would have an equivalent C_{D0} than conventional transport planes, unlikely due to the configuration of the aircraft. The CFD model was separated by surfaces as shown in Figure 34 and the CFD simulation run at cruise conditions. Finally, drag force reports were then used on each surface to provide a drag breakdown shown in Table 3.

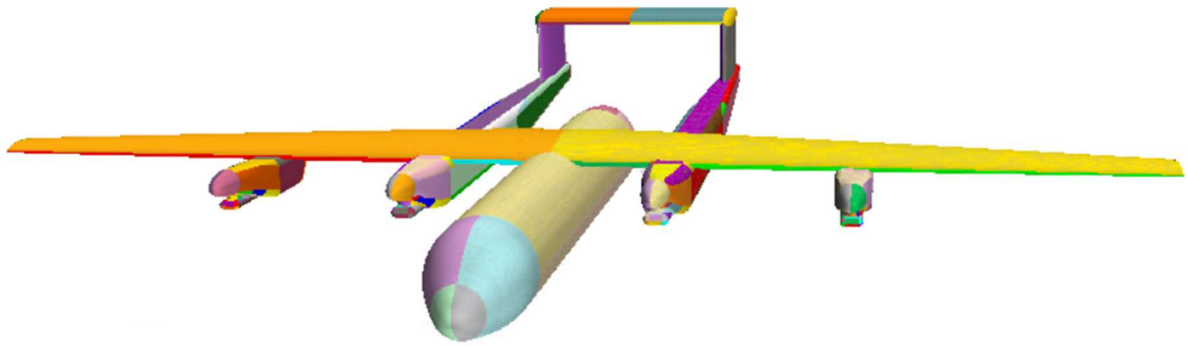


Figure 34. CFD model to be separated by patch.

6 Performance, Stability and Control

The design of the control and stability of any aircraft is of critical importance, especially to an aircraft intended to fly within proximity to the ground. Nerodia must remain nimble whilst maintaining the mandated stability of the FAA [22] and a suitable Cooper-Harper handling qualities pilot rating. The static and dynamic stability (which directly influence ease of control and pilot workload) have been continually assessed through methods outlined in the following sections to derive control surface and empennage sizing.

6.1 Empennage Configuration And Sizing

6.1.1 Tail Disposition

Driven by the unique nature of the twin boom design, the aircraft incorporates an empennage configuration with two vertical stabilisers joined at the highest point by a horizontal stabiliser. This configuration ensures easy access to the rear of the fuselage allowing the operator to benefit from not only ease of maintenance on the bespoke payload and its connections within, but also the entire removal of the payload tank through means of a hinged rear section of fuselage only made possible through the implementation of a twin boom design. Additionally, due to the twin boom design the large horizontal tail can be mounted high above the disturbed airflow of the wing and is of sufficient size to incorporate a large elevator to aid in pitch control authority. Also, another benefit of the twin boom design and high tail is the distancing of aircraft body from the flow of retardant, the retardant is slightly corrosive and therefore must remain away from the body of the aircraft. The aircraft also benefits from an end-plate effect caused by the attachments of the vertical stabilisers.

The horizontal stabilizer used an inverted NACA 23012 to impart a downforce that cancelled the moment generated by the main wing. An inverted aerofoil was chosen to allow the horizontal stabiliser to sit flush on the top of the vertical stabilisers while still generating downforce. The vertical stabilizer used a symmetrical NACA 0009 aerofoil due to the desire to have no lift forces generated at 0° side slip angle and the small drag force a thin aerofoil will create. Both aerofoils have been used extensively within other aircraft and therefore have well known aero characteristics.

6.1.2 Horizontal Stabiliser

The sizing of the horizontal stabiliser was initialised through the assumption of a horizontal tail volume coefficient. Raymer [12], Roskam [23], and Torenbeek [21] were used to arrive at an initial value of $\sim 0.9-1$ under the understanding that the aircraft behaved equivalently to either a civil regional turboprop or a large military transport aircraft. However, to expedite the selection of a horizontal stabiliser volume coefficient, a scissor plot was created to define the limits within which

the coefficient could exist. Torenbeek [21], and Hays [24] both provide details as to the procedure to arrive at a suitable value of horizontal stabiliser volume coefficient which was followed to produce Figure 35. This shows a scissor plot which arrives at a design coefficient value of 0.94 from: a CG derived aft static margin stability limit, constrained to 10%MAC (as suggested by Roskam [23]) below the neutral point limit locus, and the forward CG limits of both a take-off rotation (performed at take-off speed with appropriate aerodynamic devices), and a landing flare

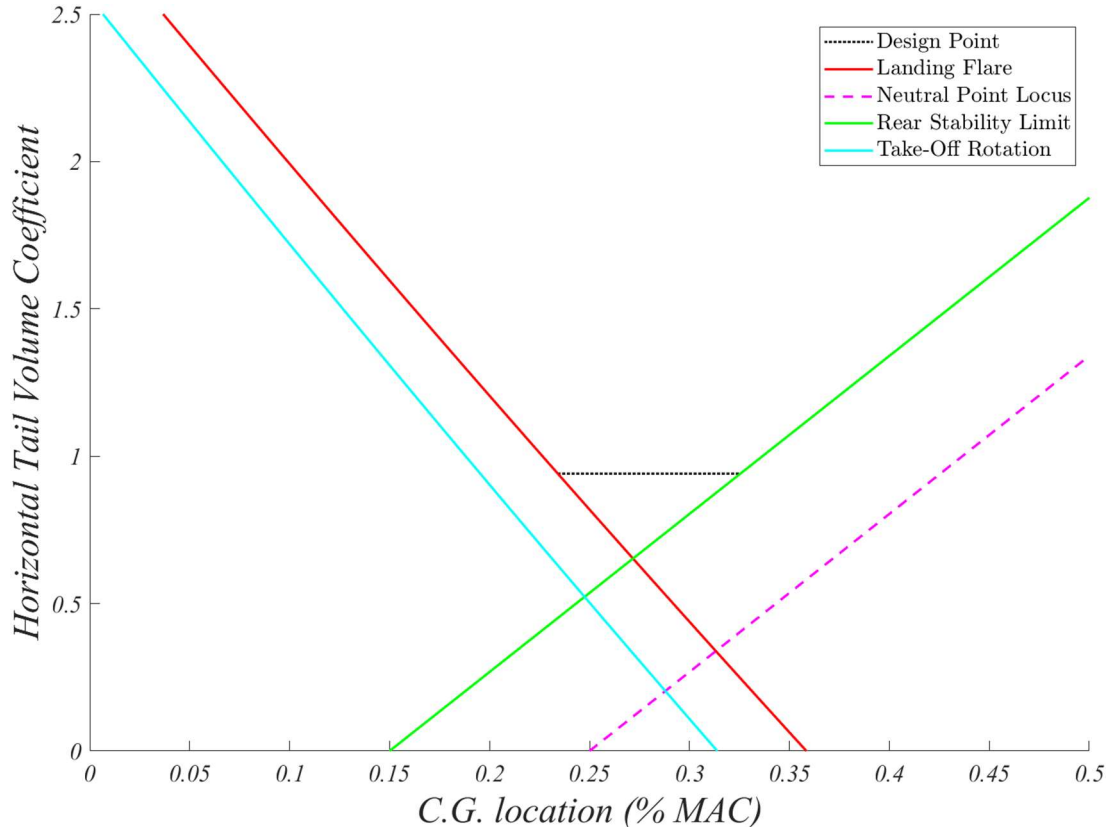


Figure 35: Horizontal tail volume coefficient scissor plot.

(utilising appropriate landing speed and full aerodynamic devices).

Due to the nature of the mission the aircraft is subject to involving large drops of payload at altitudes of around 300ft AGL the manoeuvrability of the aircraft was of primary concern, however it has been identified that the inherent sloshing capability of the payload leads to a larger CG travel as loads move in the fore and aft direction. A compromise was therefore made between allowing the aircraft to be suitably stable for ease of pilot control whilst remaining manoeuvrable; these two requirements lead to the selection of a volume coefficient of 0.94 – as shown in Figure 35. Which subsequently leads to the horizontal stabiliser sizing shown in Table 16.

Table 16: Horizontal tail parameters.

Area (m ²)	Span (m)	Aspect Ratio	Root Chord (m)	Tip Chord (m)	Taper Ratio	MAC (m)	L.E. Sweep (°)
38.02	7.75	1.58	4.90	4.90	1.00	4.90	0.00

6.1.3 Vertical Stabiliser

Following the same process as the horizontal stabiliser sizing, the sizing of the vertical stabiliser was initialised through an assumption of the vertical tail volume coefficient. Again, the findings of Raymer [12], Roskam [23], and Torenbeek [21] were used under the understanding that the aircraft was of the same nature as a civil regional turboprop or a large military transport aircraft. This meant that a rough estimate of the vertical tail volume coefficient was 0.07-0.09, however it is noted that there should be a significant reduction (up to 5%) in vertical stabiliser volume coefficient for aircraft with twin boom tails resulting in a coefficient estimate of 0.0665-0.076. To arrive at the true required value of vertical stabiliser volume coefficient, for an aircraft with multiple engines, the requirement of FAA 14 CFR Part 25.149b [22] that states “when the critical engine is suddenly made inoperative, it is possible to maintain control of the airplane with that engine still inoperative and maintain straight flight” must be adhered to. This means that the aircraft must have a vertical stabiliser of appropriate size to allow for the pilot to correct the yawing moment due to asymmetric thrust using the rudder. The side force experienced by the rudder is given in terms of the area of the vertical stabiliser by the following equation:

$$F_V = \frac{\partial C_F}{\partial \delta_r} \cdot \delta_r \cdot q \cdot S_V$$

Which can then be written in terms of vertical stabiliser volume coefficient and then expanded as the following:

$$\begin{aligned} F_V &= \frac{\partial C_F}{\partial \delta_r} \cdot \delta_r \cdot q \cdot \left(\frac{C_{VT} \cdot b_W \cdot S_W}{l_{VT}} \right) \\ \frac{(T_1 + D_{engine out}) \cdot y_{E1}}{l_V} &= \frac{\partial C_F}{\partial \delta_r} \cdot \delta_r \cdot q \cdot \left(\frac{C_{VT} \cdot b_W \cdot S_W}{l_{VT}} \right) \\ C_{VT} &= \frac{(T_1 + D_{engine out}) \cdot y_{E1} \cdot l_{VT}}{\frac{\partial C_F}{\partial \delta_r} \cdot \delta_r \cdot q \cdot b_W \cdot S_W \cdot l_V} \end{aligned}$$

Where C_{VT} is the vertical stabiliser volume coefficient, F_V is the rudder side force (N), l_{VT} is the moment arm of the vertical tail (m), $\frac{\partial C_F}{\partial \delta_r}$ is the change in force per unit rudder deflection, δ_r is the rudder deflection in radians, q is the dynamic pressure (Pa), b_W is the span of the main wing (m), S_W is the area of the main wing (m^2), T_1 is the thrust of engine one at minimum control speed (N), $D_{engine out}$ is the windmill drag of the inoperable engine, y_{E1} is the lateral distance from engine centreline to inoperative engine (m), and l_V is the vertical distance between the cg to the MAC of the vertical stabiliser (m).

Using the above equations the vertical stabiliser volume coefficient was determined to be 0.073, a value that comfortably fits within the general trends of similar aircraft as described in Raymer [12]

and Torenbeek [21] as well as providing the adequate sizing for the support of the large horizontal tail. This value also more than satisfies the CFR Part 25 requirement for directional control under a one engine inoperable condition at a rudder deflection angle of ~20 degrees. Torenbeek [25] does suggest a maximum rudder deflection of ~25-30 degrees however the more conservative value of ~20 degrees was selected to allow for some margin of control for the pilots under OEI conditions. With this, the sizing of the vertical tail was now defined, the dimensions of which are displayed in Table 17.

Table 17: Vertical tail parameters.

Area (m ²)	Span (m)	Aspect Ratio	Root Chord (m)	Tip Chord (m)	Taper Ratio	MAC (m)	L.E. Sweep (°)
16.70	3.30	0.65	5.23	4.90	0.94	5.07	15.79

6.2 Ailerons, Rudders, And Elevator Sizing

The sizing of the aircraft control surfaces was an iterative process, first done by extrapolating historical data provided by Raymer [12], then refined through analysis of required performance capabilities. Table 18 shows our initial values for the chord of each control surface, and the ratio of these chords relative to the chord of each control surface's respective lifting surface. For reference, span in this case refers to the control surface length on one wing (aileron) or vertical stabilizer (rudder).

Table 18: Control surface specifications.

Control Surface	Chord (m)	Control surface to lifting surface chord ratio	Span (m)
Ailerons	0.71	0.32	10.67
Rudders	1.30	0.32	3.20
Elevator	1.23	0.25	7.62

The ratios were then compared to Figure 36 from Sadraey [26], which gave us an idea of the control surface effectiveness.

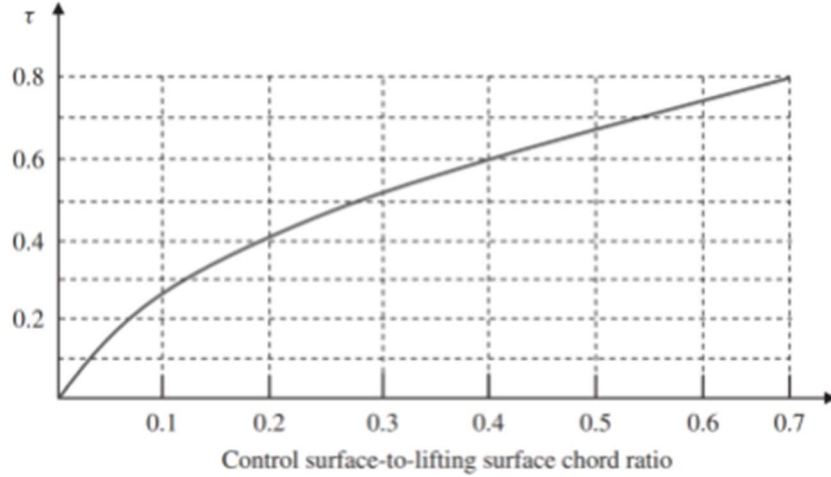


Figure 36: Control surface efficiency plot.

6.2.1 Aileron Sizing

Shown in Figure 36 is the control surface effectiveness; a measure of how effective the aileron is at producing the desired rolling moment, with the roll control of the aileron being the driving factor behind its design. As the FAA 14 CFR Part 25 [22] documentation is not as quantitative as is needed for appropriate design, MIL-F-8785 B will be used in its stead as it provides requirements to design the aircraft within that meet or even exceed the requirements of the FAA. Under the assumption the aircraft behaves as a medium sized cargo aircraft the requirement for the roll rate of the aircraft was to accomplish a required roll of 45 degrees in 1.4 seconds [12]. Using the known information of the initial size of the aileron, the roll rate could be determined

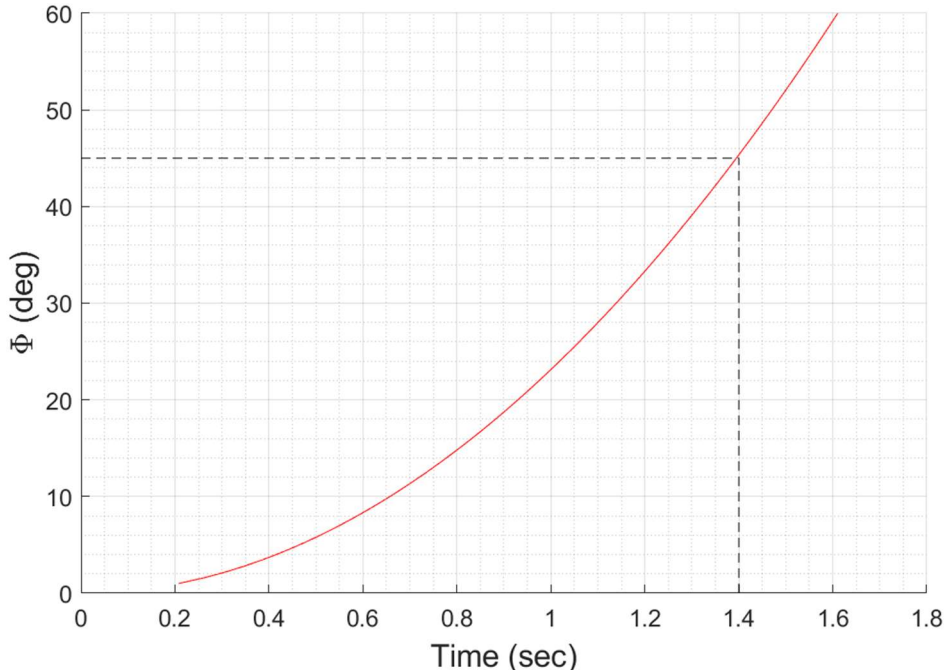


Figure 37: Bank angle against time at approach speed and max aileron deflection.

under the assumption that the max upward deflection of the aileron was 25 degrees (a value used by similar aircraft given in [26]). This gave a roll rate of 0.7642 rads/s², a figure that would cause a roll to 45 degrees in slightly over 1.5 seconds which does not fit within the requirements of the MIL-Spec, therefore it was determined that, to satisfy the 1.4 second roll requirement, the max deflection of the aileron be extended to 27 degrees upward. Figure 37 shows the aircrafts roll performance at approach speed and max aileron deflection under this configuration.

Table 19: Aileron sizing parameters.

Area (m ²)	Span (m)	Chord (m)	C _a /C	Max δ_a	Y _i (%b)	Y _o (%b)
7.58	0.71	10.67	0.32	+27° -20°	59	95

6.2.2 Rudder Sizing

The sizing of the rudder was completed to abide by the two requirements defined by [26] as “the most critical flight conditions for a rudder on a multi-engine transport aircraft (with wing-installed engines)”, these requirements are for control authority under:

- Asymmetric Thrust
- Crosswind Landing

As defined in the vertical tail section, the rudder is already of an appropriate size to fulfil the requirements of a One Engine Inoperative (OEI) climb, therefore it is the crosswind landing that needs verifying. This crosswind requirement was stated as: the pilots needing to remain in control of the aircraft when experiencing up to a 40 knot cross wind on landing. Therefore, using the pre-defined knowledge of the rudder sizing it was calculated that for a 40 knot cross wind at approach speed the rudder deflection was only required to be 17.07 degrees to remain in control of the aircraft and therefore was comfortably below the maximum allowable rudder deflection of 30 degrees. This meant that no amendments to the rudder were required, and the aircraft admirably controllable in cross wind.

Table 20: Rudder sizing parameters.

Area (m ²)	Span (m)	Chord (m)	C _R / C _{VT}	Max δ_R
4.16	3.20	1.30	0.32	±30°

6.2.3 Elevator Sizing

When sizing the elevator there were two requirements outlined in [26] that must be met for a large transport aircraft when the C.G. is located at its most forward location, these being:

- A Rotation Time During Take-Off between 3-5 seconds
- A Take-Off Pitch Angular Acceleration between 4-6 deg/s²

In order to satisfy both requirements a take-off pitch angular acceleration of 5deg/s² was chosen to calculate the appropriate ratio of horizontal tail chord to elevator chord. Assuming the elevator has a maximum deflection of 20 degrees (a value slightly lower than the norm due to the large size of the elevator) an elevator efficiency of 42.78% was calculated which (using Figure 36) corresponds to a control surface to lifting surface chord ratio of 0.22 and an elevator chord length of 1.08m. This sizing met both requirements and therefore the sizing of the elevator had to be amended from its initial estimate to a size slightly smaller to align properly with the requirements, subsequently limiting the forces felt upon the elevator.

Table 21: Elevator sizing parameters.

Area (m ²)	Span (m)	Chord (m)	C _E /C _{HT}	Max δ_E	ϵ (Rads)	τ_E (%)
8.23	7.62	1.08	0.22	$\pm 20^\circ$	0.104	0.4278

6.3 Static Stability And Centre-Of-Gravity Envelope

Static stability governs an aircraft's response to a minor change in the external forces acting upon itself and its speed, and can either be positive, neutral, or negative [27]. An aircraft is only said to be statically stable (inhibit positive static stability) if after a disturbance the aircraft returns to its initial speed and orientation without input of the pilot. The two requirements for positive static stability are defined in Hays [27] as: for a positive angle of attack

- “The derivative of pitching moment ($C_{m_{cg}}$) with respect to lift coefficient (C_L) must be negative.”
- “When $C_L = 0$, the airplane must exhibit a nose-up pitching moment ($C_{m_0} > 0$).”

These requirements both are satisfied if the aircraft exhibits a positive static margin, the static margin is the percentage (of MAC) distance of the centre of gravity from the neutral point and is defined by the following equation [12]:

$$\text{Static Margin (SM)} = (\bar{X}_{np} - \bar{X}_{cg}) = -\frac{C_{M_\alpha}}{C_{L_\alpha}}$$

Therefore, from this equation it can be attested that for all different configurations with respect to the loading of the aircraft (especially with respect to the payload and the fuel consumption) the centre of gravity position must remain forward of the neutral point to ensure positive stability. Additionally, the equation shows that the greater the static margin the more stable the aircraft, which in flight manifests itself as a less manoeuvrable aircraft. Therefore, the centre of gravity should be positioned as to provide constant static stability for the aircraft whilst also allowing the appropriate level of manoeuvrability to complete the firefighting mission.

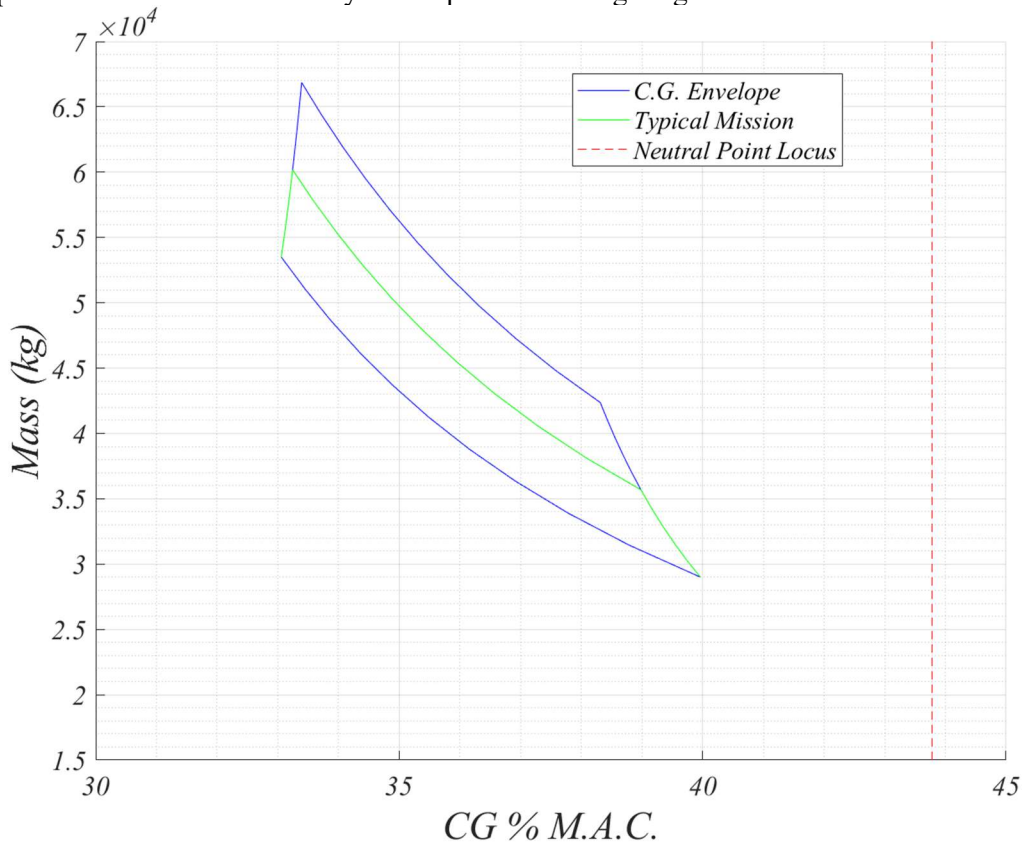


Figure 38: CG Excursion envelope.

Using the weights and C.G. locations outlined in Table 6 an overall C.G. of the aircraft can be determined and from this an envelope of C.G. shift can be drawn corresponding to the different loading configurations and fuel consumptions. The C.G. shift over a typical mission can also be plotted on the same graph.

As can be seen within Figure 38 throughout the entirety of the design envelope the aircraft's centre of gravity remains stable with a static margin varying from $\sim 5\%$ to $\sim 10\%$ MAC. This static margin allows for an aircraft that behaves predictably and stable, without over-stabilising and causing a lack of manoeuvrability. Within the typical mission on the chart the line that cuts through the centre of the envelope displays the C.G. shift for retardant drops at the design radius. It should be noted that the C.G. was designed to shift aft after dropping, as it is standard procedure for retardant drops to be conducted in level flight or in a slight dive at heights of $\sim 300\text{ft AGL}$, and therefore it is essential that when the payload is dropped the aircraft does not pitch downward towards the terrain.

After C.G. location was known, Raymer [12] was then used to calculate the longitudinal static stability derivatives of the aircraft which are shown in Table 22. Additionally, a plot of the aircraft in the trimmed condition at cruise was created using the XFLR5 software Figure 39 and confirms that the static stability of the aircraft is positive as (in agreement with the second requirement) the pitching moment is positive at $C_{L\alpha} = 0$ and the gradient of the line is negative.

Table 22: Nerodia static stability derivatives.

Stability	C_{l_a}	C_{m_a}	C_{m_Q}	C_{n_R}	SM	NP	C.G.
Derivative	(per Rad)	(per Rad)				(%MAC)	(%MAC)
Nerodia	5.61	-1.38	-20.61	-0.07	10.39	43.78	33.39

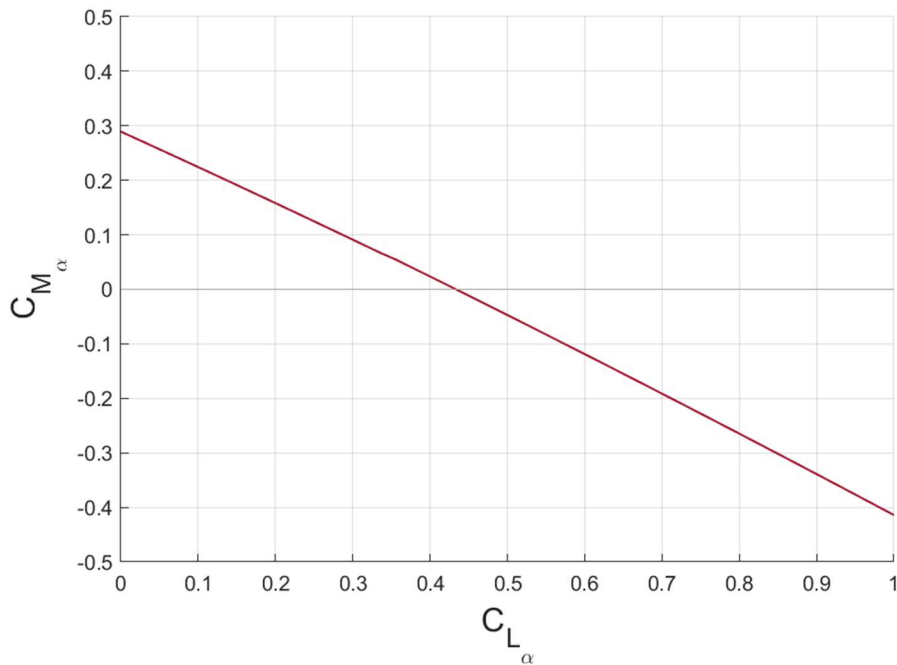


Figure 39: Lift curve vs moment curve.

6.4 Dynamic Stability Derivatives

To gain an understanding of the dynamics of the aircraft, a replica of the aircraft's geometry was created in the software XFLR5 (an XFOIL based analysis program) with corresponding point masses in the C.G. locations of all the components within the aircraft. This was then used to analyse the dynamic stability of the aircraft by simulating the aircraft's modal response to disturbances. The culmination of this analysis is shown in Table 23.

Table 23: *Nerodia* dynamic stability requirements and derivatives.

Dynamic Mode	MIL Standard	<i>Nerodia</i>
Short Period	$0.3 \leq \zeta_{SP} \leq 2.0$	0.3799
Phugoid	$\zeta_{SP} \geq 0.04$	0.0533
Roll Damping	$T_R \leq 1.4$	0.4715
Dutch Roll	$\zeta_d \geq 0.08$ $\omega_{dr} > 0.4$	0.1794 0.5446
Spiral	$T_{2s} \geq 20$	24.9209

Due to requirements of FAA 14 CFR Part 25 not being adequately quantifiably descriptive for the desired characteristics of the aircraft when experiencing the five different dynamic modes, the choice was made to use the requirements of the MIL-F-8785C [29] instead. MIL-F-8785C defines the requirements for differing nonterminal flight phases to differing levels of the flying qualities scale. The aircraft has been designed to level one of this flying quality scale and Category B of the nonterminal flight phases. The requirements for this selection either meet or exceed the stability requirements of CFR Part 25, meaning MIL-F-8785C can be comfortably used as a substitute.

The first two dynamic modes shown in Table 23 (Short Period & Phugoid Mode) are the longitudinal dynamic stability modes and both are necessarily damped to meet the requirement of being clearly adequate for the mission flight phase (level 1 flying quality). The last three dynamic modes in Table 23 (Roll Subsidence, Dutch Roll, and Spiral Mode) are the lateral dynamic stability modes and all exhibit values well within the requirements of the military standard. When plotted on complex axis the spiral mode was seen to have positive real roots suggesting instability, however the time period for this is so great (with the time period to double amplitude being: $T_{2s} = 24.9209$) that it is well within the standards of dynamic stability.

7 Payload

7.1 Mission Requirement

To achieve the payload of 6000 US-g without entering the VLAT category such as the recently retired Martin Mars, the payload team worked intensively on a solution to optimise the readily available volume in the fuselage. To avoid the lack of integration found in previous firefighting airtankers with spherical pressurised tanks that don't make efficient use of the fuselage space, the payload team opted for an elliptical cylinder-type design. This most effectively uses the interior space, as well as eliminating the extreme CG shifts experienced by incorporating a 3-tank design. The CG-shift predicament remains for the large cylindrical tank. An unbaffled tank of 7 m in length will exhibit a CG shift of greater than 32% tank length, which proves catastrophic for the static and dynamic stability of the aircraft. This unmitigated is far worse than that of the initial 3 spherical tank design. However, the current design has great potential when implementing an effective baffle design. The sub team working on baffle design encountered two distinct problems;

1. The instantaneous sloshing of water when a manoeuvre is performed
2. Gradual and continuous movement of water whilst in steady climb or decent.

The solution to both issues is through the implementation of baffles, however although existing baffle designs are effective in combating the problem, enclosed baffles give rise to the next issue of payload drop, as each baffle subsection traps a volume of water away from the exit pipe. Several solutions were suggested, where the chosen solution lies within the baffle design – with the inclusion of a one-way valve system.

The shape of the tank itself greatly influences the pressurisation capabilities. Pressure concentrations around sharp edges will apply higher loads on the tank material. Therefore, the final tank embodies an ellipsoid configuration to alleviate material selection and geometrical complexities. Furthermore, bleed air from one inboard PW150A turboprop engine contributes sufficient air to achieve 18 bar of pressure within the tank. However, with the numerous tank subsections subdivided by the baffles, even pressurisation is achieved through clever design of the baffles themselves. Having, a sliced top allows for pressurised air to pass throughout the tank allowing for an equilibrium of high pressure.

The baffles allow for filling of each cavity as the pressurised retardant enters and sloshes towards the outboard sections through the top gaps. The material selected for the baffles needed to withstand the forces of sloshing water as well as the forces exerted on each baffle when one segment contains a higher volume of water than that of the consecutive section, exerting an uneven pressure on the baffle. Furthermore, the baffles must remain light and have minimal contributions to the weight of the tank. DuPont Delrin [5] is an acetal resin with superior corrosion resistance and machineability when compared to other plastics/composite materials.

7.2 Baffle & Tank Design

As each drop is deployed, the level of retardant within the tank decreases and allows for a greater bulk movement / slosh of fluid. This will negatively affect the pitch, roll planes, lateral forces and longitudinal forces resulting in a dynamic load shift in those planes and further influencing the pitch and roll moments. Thus, affecting the partially filled tank after each drop, and mass moment of inertia affecting the stability limits. To suppress the retardant sloshing throughout the mission, it was decided a baffling system would be needed for a successful mission [30].

For space efficiency and to reduce complexity with mechanical devices, it was more appropriate to use a single tank compared to a 3 spherical tank system. The tank was selected to be an elliptical prism to allow for the wing strongbox to protrude into the fuselage. “Effect of Tank Cross-Section and Longitudinal Baffles on Transient Liquid Slosh in Partly-Filled Road Tankers” is a research paper [31] which goes into depth regarding the cross-sectional area of circular, elliptical and modified oval cross section. The results indicated strongly that wider elliptical and modified oval cross section yield higher roll mass moment of inertia of sloshing around 40% fill compared to 80%, while on the other hand under high fill and moderate levels these cross sections yield significantly lower rolls mass moment of inertia. The tank was also selected to be an elliptical prism to allow for the wing strongbox to protrude into the fuselage. Thus, coming to the chosen dimensions: 7 m long, 2 m high, and 2.25 m wide.

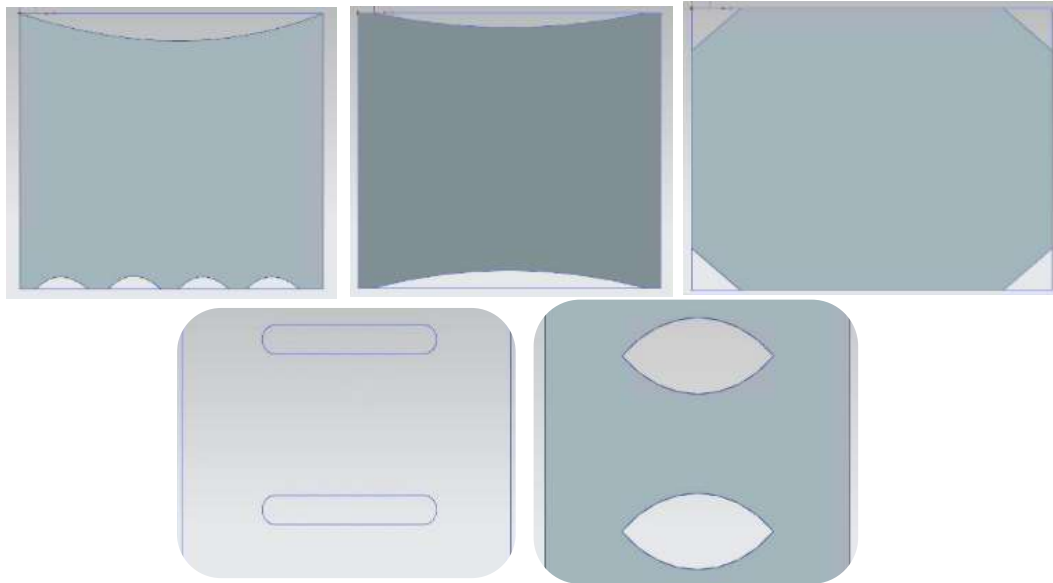


Figure 40: Early Baffle Concepts.

From Figure 40 above, some early concepts of the baffle design can be seen. Creating space for retardant and bleed air to flow inbetween sections whilst also allowing for ullage at the top was an important aspect. From the baffle optimisation code, it was estimated 14 baffles were needed, this will be further discussed in the optimisation code section. Though these designs were effective for

sloshing reduction, it affected the amount of retardant in the centre cavity - as the retardant would be flowing through the centre section of the tank into pintle nozzle for drop

To solve this issue, a set of one-way valves on each baffle face constrain the flow of retardant towards the centre section, limiting the fluid trapped in the outer sections. The designs for both the baffle and one-way valves can be seen in Figure 41. The one-way valves were set as an octagon shape to allow for a strategically offset pattern, and to allow enough space for the stopper and hinge geometry. The sides of the octagon apertures and gates have a 45-degree chamfer, to ensure the valves tightly closes and cannot return. A stopper was added to limit the valve rotation to 45°, facilitating a fast response time valve closure.

7.2.1 Outlet Pipe Sizing

The outlet pipe that bridges the payload tank and the pintle nozzle must be sized such that a large quantity of retardant is able to flow to the pintle nozzle to achieve the high flow rates expected of Nerodia. Firstly, the outlet velocity, v , needed to be defined and this was done by the following equation:

$$v = C_v (2gH \frac{p}{\rho})^{\frac{1}{2}}$$

where C_v is the velocity coefficient, g the gravity, H the maximum height of the retardant within the tank, p the pressurisation in the tank, and ρ represents the density of the Phoschek LC95 retardant. Taking the velocity coefficient as 0.94, gravity as 9.81 m/s², the height as 1.9 m, the pressure as 18 bar and density of retardant as 1077 kg/m³, the outlet velocity was calculated to be 54.6 m/s. Setting the inner diameter of the outlet pipe to be 0.4m, the cross-sectional area of the pipe was calculated to be 0.126 m². Multiplying the outlet velocity with the cross-sectional area yields the maximum volume flow rate as 6.869 m³/s. This equates to 6869 l/s and 1813 US-g/s.

7.2.2 One-Way Valve Sizing

As there is one baffle on either side of the centre cavity, only half the maximum volume flow is ever needed from a single set of one-way valves. To get the area to allow a flow rate of $3.435 \text{ m}^3/\text{s}$ (total volume flow rate /2), the below equation is used in a rearranged form

$$V = C_d A \left(2 \left(gH + \frac{P}{\rho} \right) \right)^{\frac{1}{2}}$$

where the discharge coefficient C_d is 0.6 to account for the sharp edge chamfers of the valves. Pressure was set to 0 as the pressure through each baffle from the outer edge to centre would be the same. Height was set at 1 m to find the optimum area needed for a half tank (worst case cg shift). This gave a total Area as 1.2924 m^2 for a complete set of one-way valves.

A sensible number of 20 individual valves was chosen through an iterative process to produce a set of valves with appropriate negative space between the valves, which also meant that the baffles could take the load and distributed force equally along the wall of the baffle to open when enough hydrostatic force was applied. This produced an area for individual one-way valves of 0.0646 m^2 , giving an incircle radius (apothem) of each octagon as 0.1396 m. The size and distribution of the one-way valves could have been optimised more for varied hydrostatic pressure if more time was given to research this. A 300mm distance centre to centre of each octagon was chosen to create this structure. The bottom 3 valves were placed strategically 5mm from the bottom baffle to capture all the retardant in the centre and increase the useable volume. Thus, the thickness of the baffle was an important decision, this will be discussed later in Baffle thickness section. The distribution and size of one-way valves can be seen in Figure 41. It's assumed that during the sloshing motion when the tank is halfway, the one-way valves will be forced to open due to the forces and motion, forcing retardant to go into the next baffle section but not backwards. Thus, locking the retardant in the centre until drop ready.



Figure 41: Baffle with one-way valves.

7.2.3 Payload Tank Baffle Sizing

The individual baffles that slot into the payload are sized with lower and upper bounds according to hydrostatic force and unstiffened baffle design methods from the Pressure Vessel Design Manual [32]. The lower bound (or minimum baffle thickness) of 4.7 mm is derived from estimating the max hydrostatic force on a given baffle by retardant in a single 'cavity' pulling up at 30° out of a drop, assuming a Delrin [5] baffle with shear strength of 66 MPa and circumference of 6.68 m. The

upper bound (maximum baffle thickness) of 17.7 mm is derived from Moss [32] assuming three simply supported edges with uniformly decreasing load to the free edge (top) with the equations

$$t_b = \sqrt{\frac{\beta_1 p b^2}{F_b}}, \quad p = \frac{62.4 a S_g}{144}$$

where β_1 is found from empirical data concerning the ratio of $\frac{a}{b}$ (a being the height to the top free edge and b being the width of baffle), p is the distributed load of the Phos-Chek [4] retardant, F_b is the max bending stress of Delrin, and S_g is the specific gravity of Phos-Chek. This simplified design method does not account for stiffened baffles, where the one-way valves and hinges would provide additional stiffness that is unquantifiable within the scope of the project. A conservative choice of 10 mm for the baffle thickness was taken as a sensible value due to the availability of Delrin in such a standard thickness, potentially lowering manufacturing costs and any replacement components in the future.

7.2.4 Optimisation

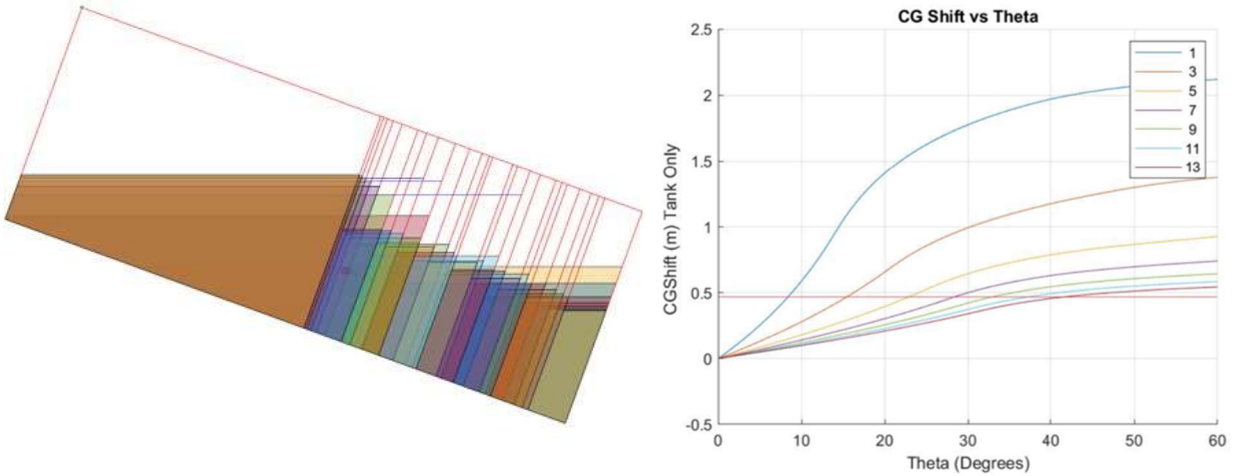


Figure 42: Optimisation at single state (left), full baffle range results (right).

To ensure the optimal number of baffles is selected to strike a balance between complexity and controllable CG shift, custom code was written to evaluate the effectiveness of baffles at reducing CG shift in the fixed pitch climb / dive scenario. A 2d representation was first made, the code treated valves behind the CG of the empty tank as fixed and ignored those in front, assuming retardant level had equalized.

The volume of each section was measured in level flight for the chosen fill level and value stored, then for each climb angle - the fluid level in each section was varied to match the original fill volume. The CG of the new shape was calculated and added to the overall fluid CG. This process was then looped for a range of both climb angles and baffle spacings.

An example of this is shown Figure 42 left, with all the states created for the 15 degrees climb scenario shown. The stability team then completed CFD slosh analysis to find a safety factor for

converting from 2d to 3d. They then provided a hard limit for maximum CG shift allowed. This is shown as the horizontal line in Figure 42 right. From this it was found the optimal baffle count for ensuring maximum possible sustained climb was 14 individual bulkhead sections. In addition to proving the optimal number of baffles were selected, this code shows the massive 75%+ drop in CG shift achieved by the addition of bulkheads.

7.3 Pressurisation

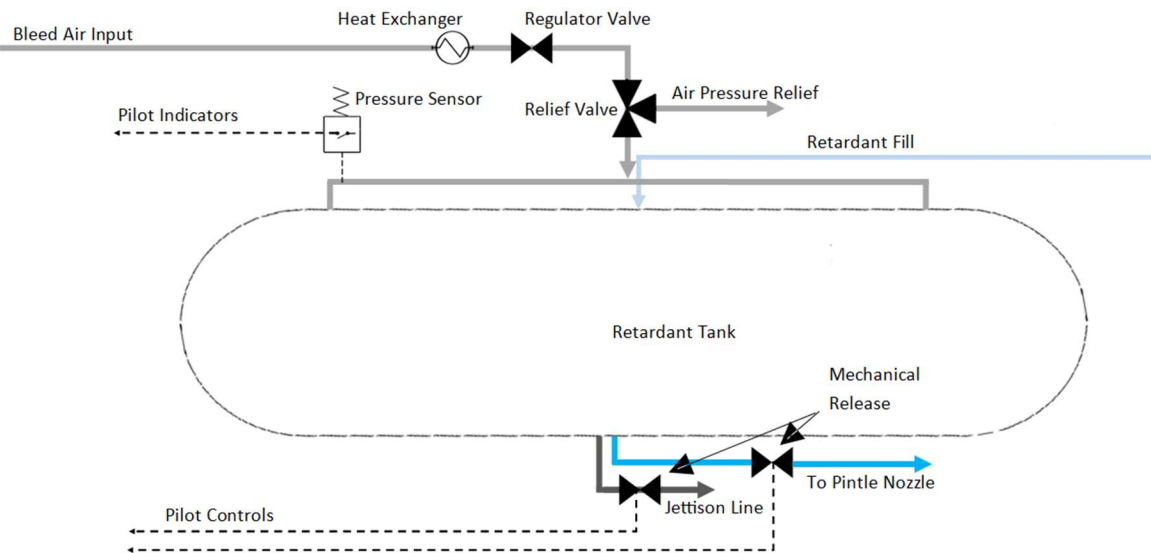


Figure 43: Payload system schematic.

To achieve a high drop accuracy and effectively suppress fire on a specified region, a constant high flow rate is required from the payload delivery system. Retrofitted competitor aircraft have opted to achieve this via compressors and air tanks kept onboard the aircraft, however the penalties for this in terms of weight and internal space is huge. Therefore, it was decided that bleed air from an inboard engine could be used to pressurise the payload tank, and this in combination with a pintle nozzle will prove the most effective way to achieve a constant flow rate.

Bleed air of mass flow rate of 1.44 kg/s is sourced from the final stage of the high-pressure compressor at a temperature of ~800 K and cooled down via the heat exchanger to a usable 380 K which is then routed through a regulator and pressure relief valve before being pushed into either end of the tank. The bleed air has a pressure of 18 bar and loses 1.5 bar of pressure from the drop in temperature through the heat exchanger. The bleed air pipe is sized at 23.8 mm (ID) using equations shown in the succeeding section. The pressure being fed to the tank is monitored by a pressure sensor and the pressure can be dumped via the air pressure relief valve by pilot input if necessary. As observed by the payload system schematic above in Figure 43, the retardant refill pipe is positioned in the middle of the tank so that retardant is spilled over to neighbouring cavities. Should the pintle nozzle fail closed, the retardant can still be dumped via the mechanical release within the primary disposal line. A jettison line which is activated with a mechanical release is also

incorporated so that should a failure of the outlet pipe occur in the form of a blockage, the retardant can still be dropped in a timely fashion to land the aircraft safely.

7.3.1 Bleed Air Pipe & Slot Gap Calculations

With engine bleed air being used to pressurise the payload tank, the sizing of the pipes to transport the bleed air to the tank is essential. It was concluded two inlet pipes would be necessary at either end of the tank to achieve the 16.5 bar of pressure in a short time span. A fair assumption was made that the area required for the bleed air pipe will be the same area required for the slot gap at the top of the baffle. Figure 44 shows the proposed slot gap at the top of the baffle.

The mass flow rate of the engine bleed air is 1.44kg/s for pressurisation. The air density at 16.5 bar

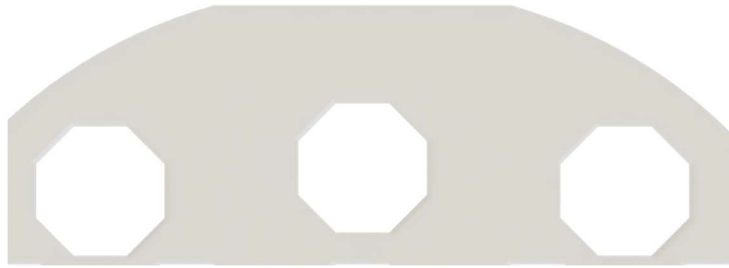


Figure 44: Baffle slot gap.

of pressure was calculated to be 7.8 kg/m^3 . The volume flow rate was then calculated to be $0.18 \text{ m}^3/\text{s}$. A minimum bleed air exit velocity, v , of 100m/s was assumed as a worst-case scenario and this was used to calculate the area of the bleed air pipe, A . The area of the bleed air pipe was calculated to be 0.00178 m^2 . Assuming for a circular pipe, the inner diameter was of the bleed air pipe was calculated to be 23.8mm . Hence the area of the slot gap was also determined as 0.00178 m^2 .

7.4 Pintle Nozzle (Dispersal System)

For the discharge system, it was important to have a reliable nozzle that has great dispersal properties and sprays up to 3000 US-g of retardant per drop, powered by compressed air. As such, the pintle nozzle was chosen for this operation due to its proven history in variable dispersion rates on the MAFFS [33]. The pintle nozzle design has a cone feature which forces the retardant to flow around the aperture perimeter, creating a straighter concentrated spread towards the targeted location. As the pintle tip is retracted into the body, the discharge coefficient is changed. The pintle nozzle is placed on the belly of the aircraft on the tank centreline to use gravity as well as the pressurisation to drive out the fluid. The pintle nozzle allows for a constant-rate-flow to combat the variable flow rate associated with decreasing pressure head. It also allows for safe closure of the nozzle to prevent hydraulic ram. The pintle nozzle has an emergency manual discharge capability in case the aircraft is not able to release the fluid. This is helped by the high-pressure differential between tank and nozzle [33].

A jettison line is used in case of pintle nozzle failure, to disperse any excess retardant before landing. This still allows a pressurized discharge of retardant from the main tank.

The pintle nozzle dimensions were calculated as follows.

$$A = \frac{\dot{m}}{Cd\sqrt{2 \times \rho \times \Delta P}}$$

where A is the area required for 6869 l/s flow discharge and \dot{m} is the mass flow rate – 7399 kg/s. The MFR was found by multiplying the volume flow 6.869 m³/s and density 1077 kg/m³ (Phos-check LC95). ΔP is the pressure difference from the outside atmosphere to the pintle nozzle which was set to 3bars. Density ρ was set to 1077 kg/m³ (Phos-check) to give an area of 0.4158 m².

$$h = \frac{A}{2 \times \pi \times r}$$

The height of the pintle is h, A is the previously calculated area, r was set a reasonable 0.3m. This gave the height of the pintle of 0.221m.

$$\pi(R^2 - r^2) = A$$

Making R the subject of the formula and substituting in the previously stated values, gave R the outer radius of the circle as 0.472m. This gave a finalised values of 0.472m for the outer radius of the nozzle and inner radius of 0.3m and pintle height of 0.221.

This design enables a maximum retardant flow rate of 6869 l/s, which is achieved consistently when changing the pintle area (with reduced pressure). The pintle nozzle geometry was validated in STARCCM+ with a freestream domain and Euler multiphase simulation (retardant->air).

The pintle nozzle geometry was imported into the STAR CCM+ CFD software within which the max flow rate was assessed.

The drop height is calculated using an equation from the USDA [34]

$$S = 101 + 0.0112L + 0.0202P + 50$$

Where: S = Drop height (ft)

L = Load size (gal)

P = Peak Flow Rate (gal/s)

P is 1511 gal/s, L is 6000gal, this gave a drop height of 248.72 ft, 75.8 m. This drops 2000 gal in 1.3 s, at an optimum height of 75.8 m. The efficiencies of the aerial drop of the retardant is extremely dependent the pilot skills and the communication received. As it's contingent on atmospheric conditions and on-board systems for assisted computer automated drops.

7.5 Payload Stability

The dynamics of the payload within the tank were studied using the CFD tool STARCCM+ to acquire a better understanding of how the payload will react to forces felt in flight and how this will impact the centre of gravity of the payload tank. A model of the payload tank in an unbaffled configuration was filled to the halfway point with fluid matching the dynamic properties of the

retardant Phos-Check LC95 using the Volume Of Fluid (VOF) solver. This was taken as the worst-case scenario for C.G. shift due to retardant slosh and was used for all CFD investigations. To carry out the simulation, the team used a roughly analogous aircraft (the C-130J) that was deployed in the software X-Plane 11 to conduct the manoeuvres required of Nerodia during a typical firefighting mission at the drop zone. A programme was used in the software to log the accelerations felt by the aircraft into a CSV file that could be entered into the CFD software to simulate how the payload would behave to these accelerations.

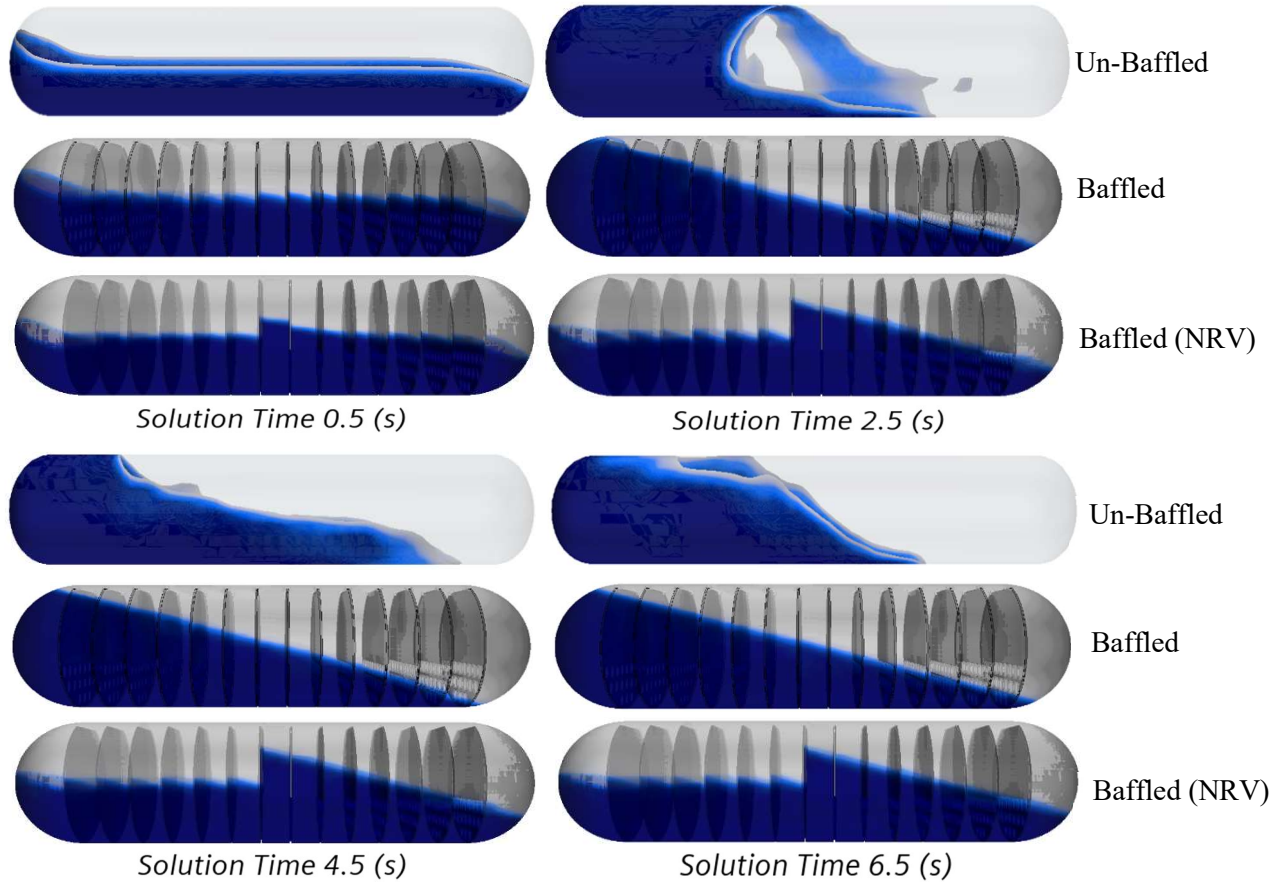


Figure 45: Payload slosh CFD time-history for un-baffled, baffled and baffled (NRV).

Initial simulations of the retardant's dynamics highlighted that the slosh of the retardant was not the largest cause for concern to the stability of the aircraft (through shift of C.G.) but the settling of the retardant during climb and descent was. A section of the results wherein the aircraft pitches to 15 degrees angle of climb and remains at that attitude for 30 seconds was plotted both in graphical form Figure 45 and as a diagram visualising the flow at different solution times Figure 45. Figure 46 shows that there is an indistinguishable difference between the overall centre of gravity shift of both the baffled and un-baffled configurations; the only difference being the damping of the fluid perturbations as a result of the baffles. Both configurations however are unacceptable as they position the C.G. of the aircraft aft of the neutral point and will subsequently cause the aircraft to become unstable and pitch further nose up exacerbating the instability.

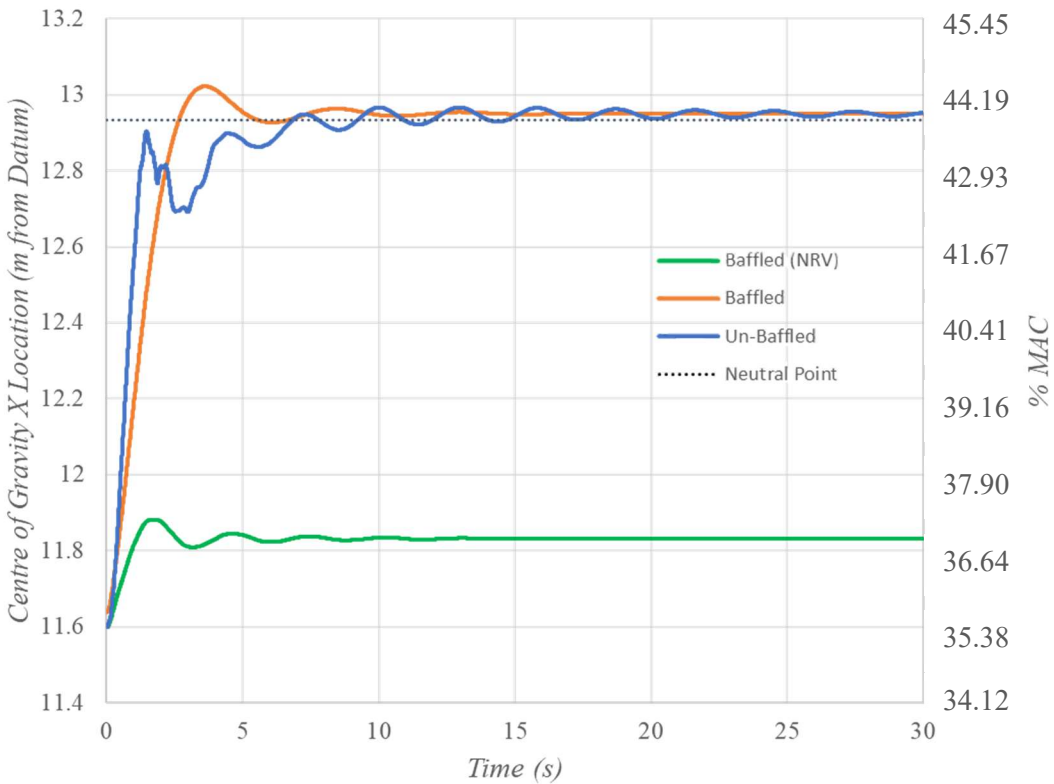


Figure 46: Payload CFD CG shift.

The extent of this payload-induced C.G. shift has been visualised in Figure 45. In this the un-baffled configuration allows free movement of the payload causing the fluid to form waves on the back wall of the payload tank that collapse on itself. This will cause instabilities in the C.G. location of the aircraft which can be seen in the 0 to 5 second range of Figure 46. The implementation of the baffle decreases the perturbations considerably however this does not solve the problem of the C.G. settling of the pay load if it has the freedom to move throughout the whole payload tank.

The solution to this problem came in the form of a system of no return valves (introduced in Section 7.2) which allows fluid flow into the centre of the tank but prevents flow entering the outer sections. This can be visualised in Figure 45 where the retardant from the right-hand side of the payload tank is seen to congregate in the central section's whilst the left-hand section's retardant stays within their discrete sections due to the one-way valve system. The effect this system has on the shift of the C.G. can be seen in Figure 46, where the C.G. shifts up to 1.4m (marginally aft of the neutral point of the aircraft) in the non-check valve configurations. However, when the NRV's are implemented the C.G. shifts only 0.2m to a %MAC of ~36.7% (which corresponds to a static margin of around 7%) - well within the stability requirements of the aircraft. With this configuration (Baffled with NRV) the tank has been confirmed (via simulations of retardant drop sorties) to always operate within the safety requirements of C.G. shift (0.5m).

7.6 Refill

The retardant refill pipe is mounted on the tail door and to meet the RFPs refill requirement of 500 US-g/min, a high flow rate fire pump is required. Crassus Aviation recommends using the Waterous CSUC20C single stage fire pump as it boasts a peak flow rate of 2000 US-g/m. Operation of pumps at peak flow rate can degrade the performance excessively, thus the ground team will operate the pump at 80% of peak flow rate to fill the tank in under 4 minutes. This leaves plenty of time for the ground team to uncouple the retardant and refuelling hoses safely before push back is required. A pressure regulator valve is present in the payload tank which will regulate the internal pressure of the tank as it is being filled up with retardant, so no pressure build-ups occur. Although implementing specialised retardant hoses and couplings offer improved performance, it would also require a far greater investment by operators to purchase additional ground equipment which would ultimately increase operational costs. Therefore, a conscious choice was made to design the refill pipe such that it will work best with standardised retardant hoses and couplings to appeal to all current operators.

7.7 Maintenance

With fire retardants being corrosive, it was concluded that a material that boasts good corrosion resistance should be used to construct the payload tank and hence Aluminium 5052 H32 was chosen. Considering the duration in which retardant will be on contact with the tank, as an added precaution the internal of the tank will be Alodine coated, as it promises to be an effective corrosion inhibitor. It also provides some resistance to abrasion so should miscellaneous debris end up in the tank and abrade the internals, there is a decent level of protection present that immediate maintenance would not be required. Fire retardant also has a risk of solidifying (at altitude) and in this form poses a far greater risk of corrosion, hence, to reduce the risk of this, the payload tank should be flushed with high pressure water every 20 operational hours to prevent the build-up of solidified retardant which will ultimately reduce the carrying capacity of liquid retardant.

The 58 mounting points of the payload tank can be fastened/unfastened via small hatch doors in the belly of the fuselage and the small hatch on the top of fuselage. Whilst the big hatch on the bottom of the fuselage is used to attach/detach the pintle nozzle and its associated fixtures. At least every 200 operational hours the payload tank should be unfastened from the mounting points and the pintle nozzle should be detached so that the tank can be removed via the tail door. Once removed the mounting bands, which wrap around the tank, can also be unfastened so that the tank opens due to its split casing design. Allowing a qualified maintenance engineer to inspect the internals of the tank, baffles, and one-way valves - repairing when deemed necessary. All fluid pipes should be inspected and serviced whilst all mechanical fittings and linkages should be lubricated to ensure the risk of the aircraft's payload system having operational failures is reduced.

8 Structures

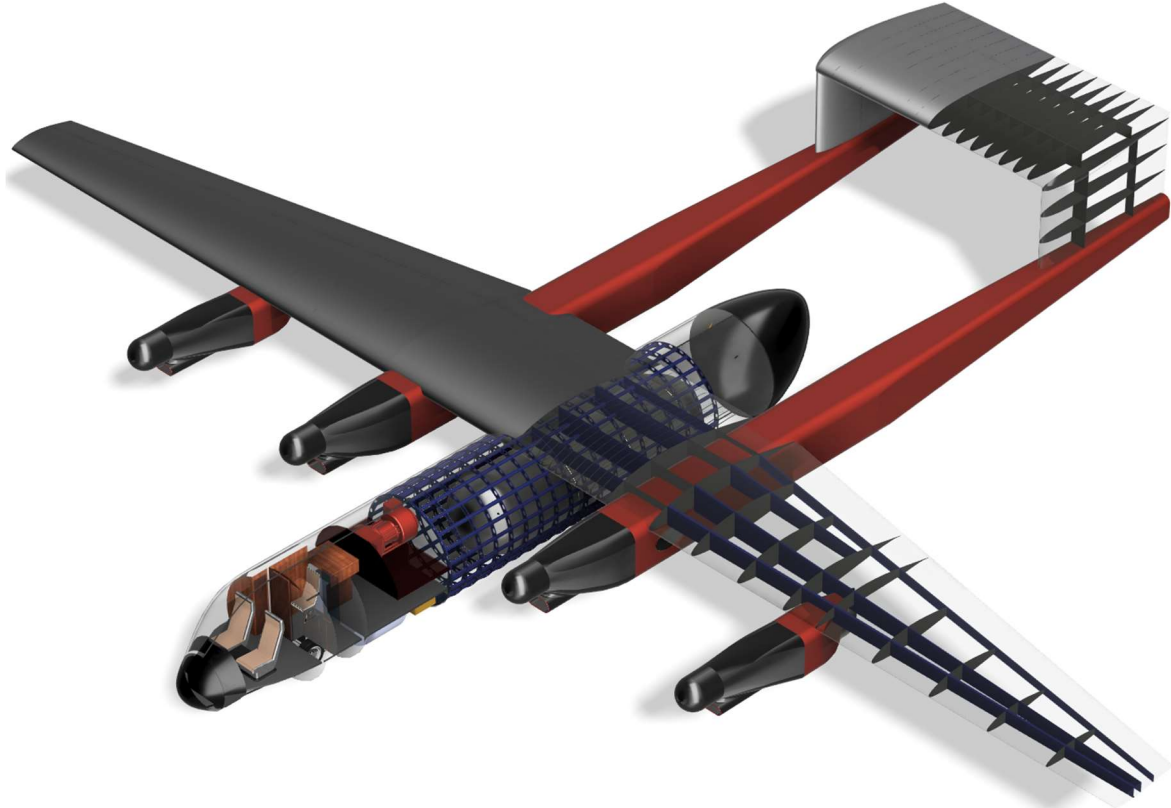


Figure 47: Structural X-Ray rendering of Nerodia.

8.1 Load Definition

The flight envelope represented in Figure 48 depicts the capability of the design at various airspeeds and load factors. The maximum load factor occurs at 3.25 and is in compliance with the upper limit of CS-25 requirements [36]. CS-25 was selected as it exceeded or matched all values in FAR-14 CFR Part 25 [22]. The gust loads depicted with the dotted lines are also compliant with CS-25 regulations. The upper limits of the aircraft is shown using the dive speed (V_D) at 412 kts and lower limit is shown as the stall speed with the flaps down (V_{S_Dirty}) of 97 kts. V_D represents the maximum speed of which the aircraft can operate without permanent structural deformation occurs. The stall speed with flaps down is critical for the aircraft to complete its mission with a drop speed (V_{Drop}) of 139 kts. The stall speed with the flaps up ($V_{S\ Clean}$) is only 127 kts and stall would occur before the aircraft could drop the payload at the desired speed. The speed of which the aircraft flaps would sustain damage when down (V_{FE}) is 210 knots. All key speeds and their exact values can be referenced Table 5.

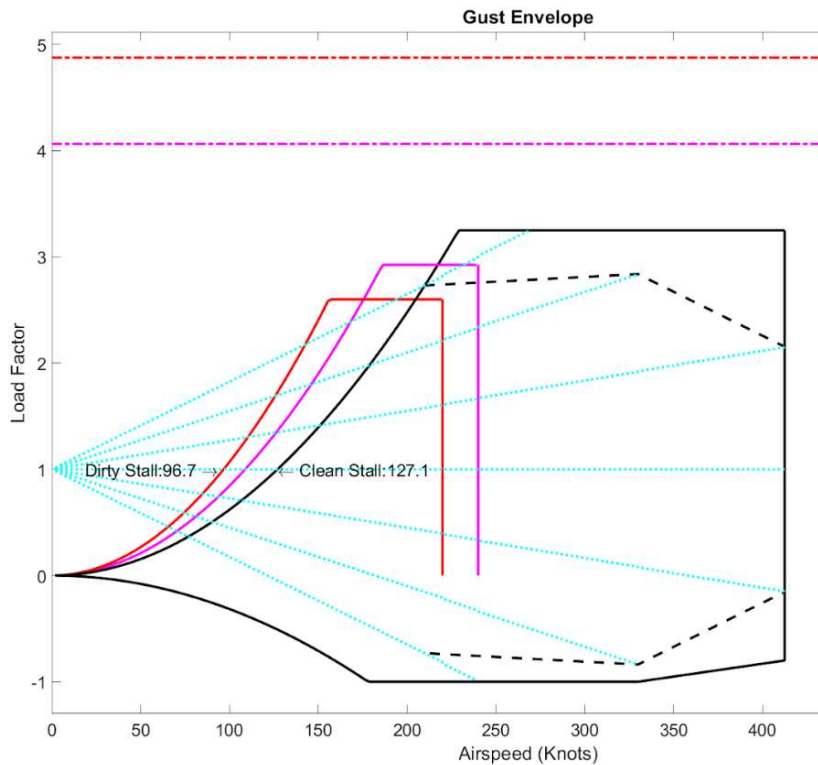


Figure 48: V-N / Gust Diagram.

Sufficient flap speed overlap has been designed to allow the aircraft to transition from Dirty to Clean configurations at any point in the flight dynamic, as well as allowing the FCS time to close the flaps as the aircraft accelerates to protect the structure from overspeed damage.

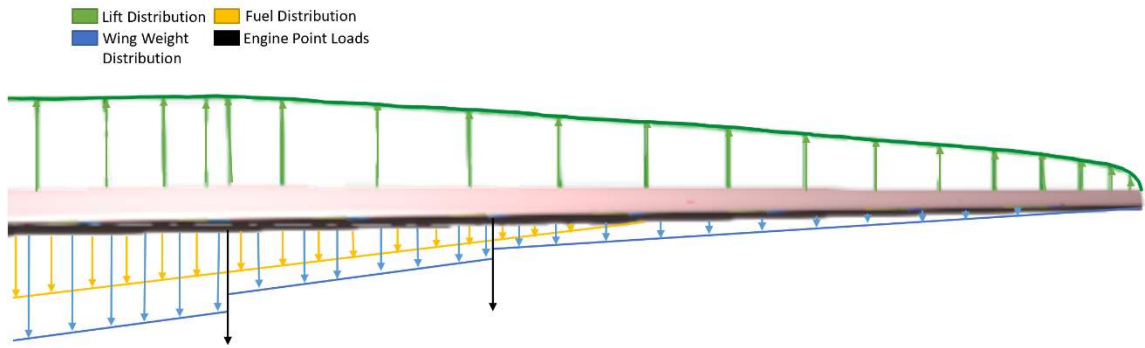


Figure 49: Wing loading distribution. N.B. Point loads not to scale.

The wing loading was calculated to evaluate an initial estimation of expected load and structural requirements. This was passed into a custom FEA code in MATLAB to evaluate loading and improve spar design estimation. The step increases in wing weight are due to increases to accommodate thrust loading, engine mass on ground, and primarily to assist in the resistance of boom induced torsional loads. Fuel distribution is shown for a typical MTOW liquid load.

8.2 Material Selection

Isotropic materials were primarily used to reduce structure complexity, as this allows more focus on an optimally designed geometry without the added complexity of material anisotropic behaviours. This allows a greater deal of accuracy to be achieved within the scope of the skillset of the structural team.

Two main areas are modelled/designed in detail:

- 1) The Inner wing box section
- 2) The Payload Tank.

Table 24: Typical high performance material examples.

Material	Density (kg/m ³)	Young's Modulus (GPa)	Specific Strength (kN.m/kg)	Corrosion Resistance	Isotropic	Workability	Failure mode
Carbon Epoxy	1580	110	785	Excellent	No	Complex	Instant
Magnesium Alloy	1740	80	158	Weak	Yes	Excellent	Smooth
Carbon Fibre (AS4)	1750	183	2454	Excellent	No	Complex	Instant
Aluminum 7075	2810	72	204	Good	Yes	Good	Smooth
Titanium Beta C	4810	107	260	Good	Yes	Bad	Smooth
Steel Bainite Rich	7870	246	321	Weak	Yes	Bad	Severe
Steel C350	8080	200	291	Weak	Yes	Bad	Severe
Steel EN24	7850	210	110	Weak	Yes	Good	Severe

Material selection was heavily influenced by the workability and smooth failure mode requirements, these are critical in ensuring low maintenance costs and increasing aircraft survivability in the event of an over G scenario. To avoid issues caused by Bi-Metallic corrosion/Poisson ratio differential stress and multi material welding, the iteration of structural design in this report will work under the assumption all analysed structural parts are to be made of one material. For this reason, Aluminium 7075 has been selected due to its average or better performance in all key fields. Minimum material thicknesses are also an important consideration. The specific temper of aluminium chosen will be Aluminium 7075-T73 for its additional resistance to stress corrosion due to its heat treatment and artificial ageing.

Table 25: Key selected materials.

Part	Material	Reason
Internal Structures/Wing	7075-T73	As above
Fuselage Skin	Carbon Fibre (AS4)	Corrosion resistance.
Landing Gear	Steel EN24	Higher Youngs modulus, good workability.

8.3 Initial Wing Sizing

$$T = \frac{1}{4} \rho V^2 S \bar{c} C_m + T_{Tail}$$

$$T_{skin} = \frac{abs(T)}{2A_{cell}\tau_{max}}, t_{web} = 3n_{ult} \frac{W}{4h\tau_{max}}, F_{bend} = \frac{n_{ult} W Y_{MGC}}{2h}, N_{ribs} = INT\left(\frac{b}{c_{avg}}\right) + 1$$

The initial sizing of the wing began with a simple analysis of a single spar located at 30% of the chord from the leading edge. The thickness of the skin was determined using torsion at the root plus the torsion from the tail loading which was approximated as -1.0621E7 N. This value was later refined as further analysis was conducted. The initial skin thickness was estimated to be 19 mm at the root, and 3 mm at the tip. The weight of the skin at this configuration was 2970 kg. While the shear thickness of the web was calculated using the ultimate load factor of 4.875. This is shown in Figure 48. The shear web thickness was approximated as 2.1 mm at the root and 0.51 mm at the tip with an approximated weight of 39.7 kg. Then the spar cap area was determined by finding the bending force and found to be 1.7131E6 and dividing this value by the tensile strength of the material selected resulted in a spar cap area of 0.0039 m² with the spar cap area at the tip estimated at 0.002 mm. 6 ribs were found required in this wing. Finally, the total wing weight was estimated as 3,640 kg. However, it would turn out that this initial design would not be enough to resist the extreme torsional loading and further analysis using FEA was critical in the final design of the wing structure.

8.4 Reinforcement Optimisation With LS-DYNA FEA-FEM

The simplified wing approximations completed up until this point are excellent at predicting the requirements of aircraft structure under a typical loading pattern. Notable about the Nerodia A/C is the twin boom design, as this introduces massive loads into the wing section that would normally not be present.

This initial analysis model used the standard spar size, cap thickness, shear area and skin thickness found from the simplified analysis. A model was then manually meshed with the initial model as a pure test of the torsional capabilities of a standard wing section. This initial stiffness evaluation

model is shown below, the wing is rigidly mounted to the fuselage via a rigid tail boom section. This allows simplified analysis of the initial torsional stiffness of the wing section.

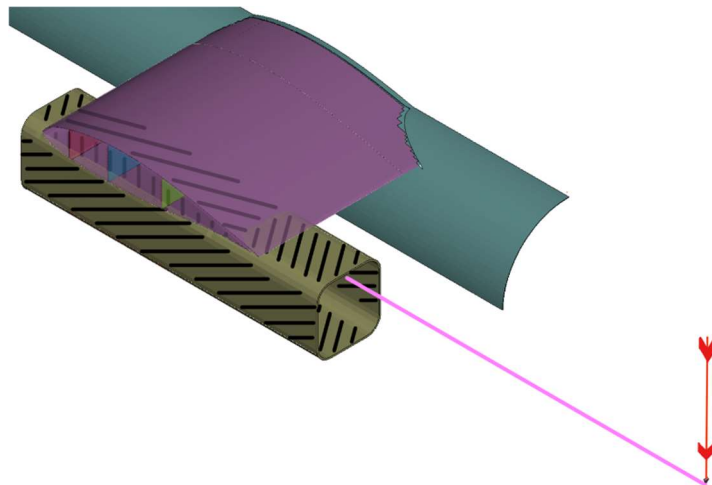


Figure 50: Model loading configuration for wing bending.

Load was applied at the aerodynamic centre of the tail section in line with the boom, the force for this was calculated using the following equation.

$$F = \frac{\text{Aerodynamic Torque}}{\text{Distance}} + W_{\text{Boom}} \frac{3.25}{2} + \frac{\text{Maximum Load from tail}}{L_{\text{Maximum}} + W_{\text{Tail}}}$$

This approximates the worst case load the structure could feasibly see in a high loading scenario.

The design requirement for this load was set based on minimal permanent deformation after the worst case of reaching it, and no fatigue introduced until at least 70% of this value. The total load requirement solves to be around 2.6 million Newton Meters of torque at the wing centre instantaneously.

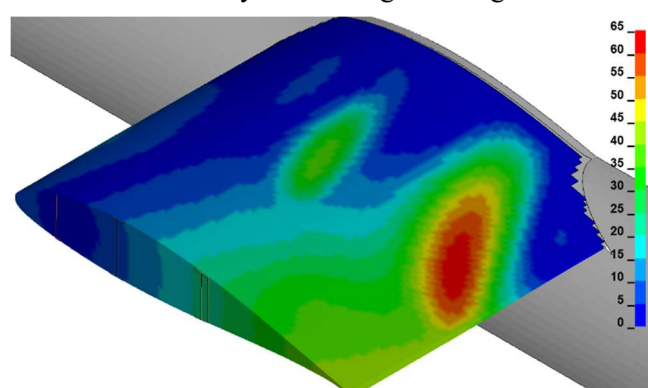


Figure 51: 40% Load displacement map (mm).

The initial simulation results are shown in Figure 51, with deformations shown in mm, shown at ~40% load. Beyond this, material failure occurs. Following on from this, a series of iterations of internal wing structure were tested, using a failure reinforcement optimisation method to inform the next designs.

These iterations resulted in a geometry as shown in Figure 52 below, capable of reaching full load with stresses peaking at 154MPa, 4MPa beyond the fatigue limit of the material, this only occurs at hot spots near rigid mounts, so likely is elevated beyond the “real” value slightly.

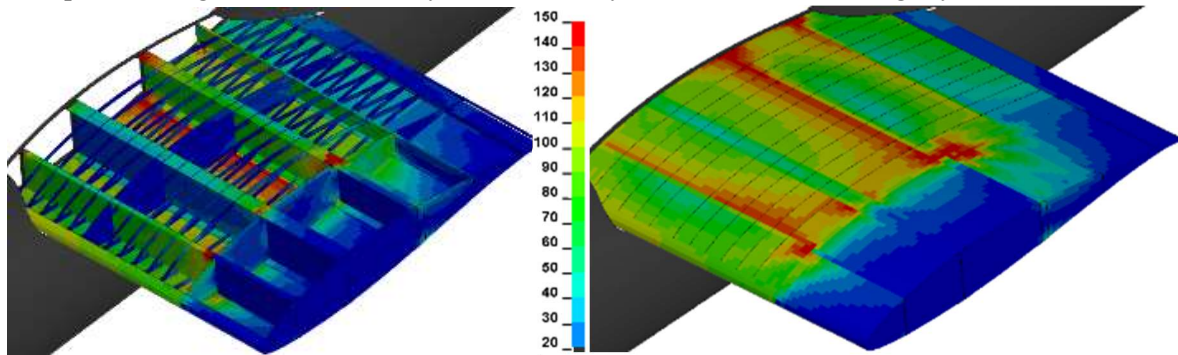


Figure 52: Wing Von Mises strain, internal and external at peak load (MPa)

150MPa design force limit was selected to ensure the structure performs below the fatigue limits of the aluminium. This is critical to ensuring the long fatigue life of the airframe, a critical risk of firefighting aircraft.

A benefit of aluminium’s large gap between yield and ultimate load is that any fatigued component will show obvious measurable permanent set well before failure, making it easier for ground crews to recognise signs of fatigue well in advance. Additionally, the structure can be taken beyond yield consistently over a flight, if absolutely necessary, without failure to ensure pilots can have the trust in the airframe they need to manoeuvre in close and precisely destroy fires, increasing effectiveness of the airframe.

This geometry is designed around creating a low mass solution for a wing section that surpasses all reasonable flight loads without fatigue, operates in all typical high loading dynamics that could be expected with no material strain and when it does strain, does so in a manner that is predictable to the pilots. Manageable and sufficiently controlled to allow the airframe to safe return to the original airfield without catastrophic failure. The stress strain graph in Figure 53 shows a typical pattern for this alloy type, with key load points for this aircraft plotted.

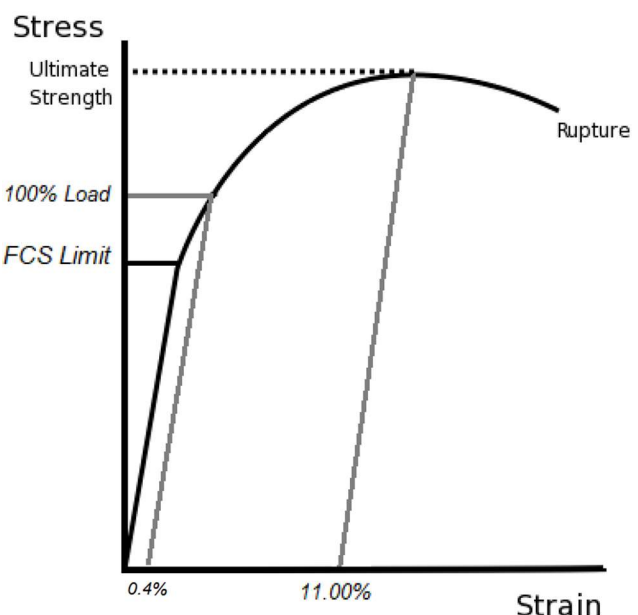


Figure 53: Structure overall stress strain.

8.5 Deformable Boom

Following on from the development of the wing structure, the model was enhanced with the addition of a deformable boom. Simple analysis was completed finding that under load the boom section skin buckled, this was reinforced with a doubling plate. The result of this reinforcement is shown below. Results shown at different load as unreinforced fails before 45% load.

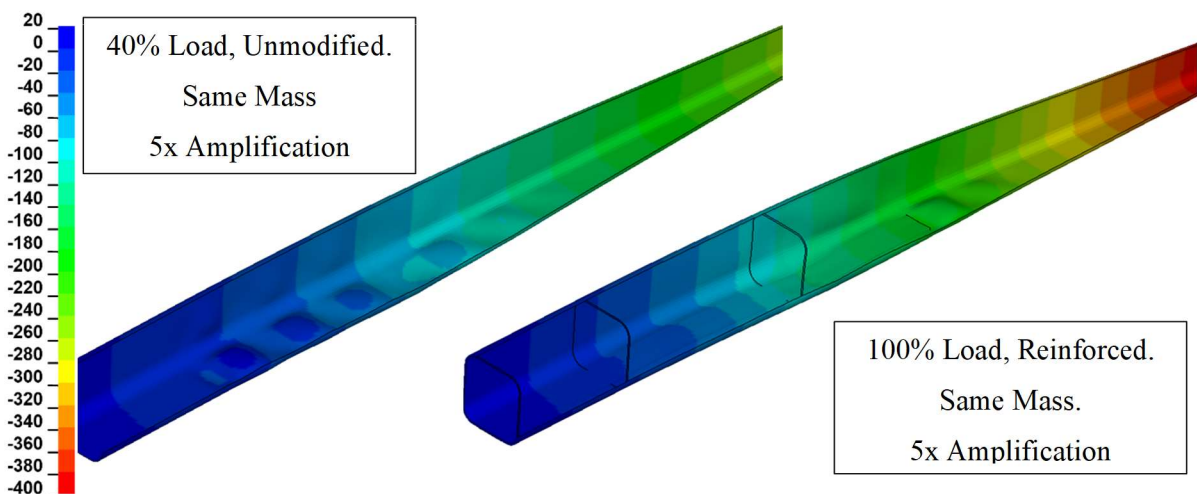


Figure 54: Amplified boom displacement (mm).

Colour maps show 5x amplified displacements and vertical displacements under load.

Reinforcement consists of some hoops and simple doubler plates on the top and bottom as below.

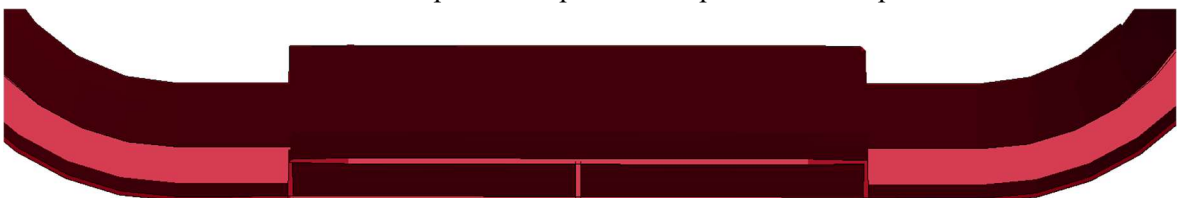


Figure 55: Boom reinforcement (front view).

8.6 Landing Gear Loading

Additionally, worst case landing gear loads were applied to the structure immediately after unloading the elevator torsion load finding peak Von-Mises stresses of 140MPa with no strain. Loading was increased to find a maximum value for landing gear load finding that the structure can resist a 600kN total force from the main gear without buckling. This allows a maximum vertical velocity in a vacuum on landing of 320 ft/min for single gear landing and 450 ft/min landing on both main gears. This value climbs substantially once effective weight reduction due to wing lift is factored in allowing the aircraft extremely high landing velocities if needed. This is sufficient that the aircraft would survive without flaring if needed, or even complete carrier landings, if only it had a tail hook. This structural load capability is not a design feature, but a side effect of the torsion box.

8.7 Tank Construction

The tank construction is comprised of a two main piece clamshell made of 5052-H32 aluminium with a spray coating inside. The clamshell design is built on the principle that during detailed servicing the tank is removed, split in two and the baffles / valve system are then completely accessible for maintenance. This also allows the baffles to be mounted into slots cut into the clamshell and slid into place, ensuring a secure, retardant tight, non-permanent bond between the aluminium and the acetyl baffles. A cut section of the clamshell with acetyl baffle in position is shown in Figure 56.

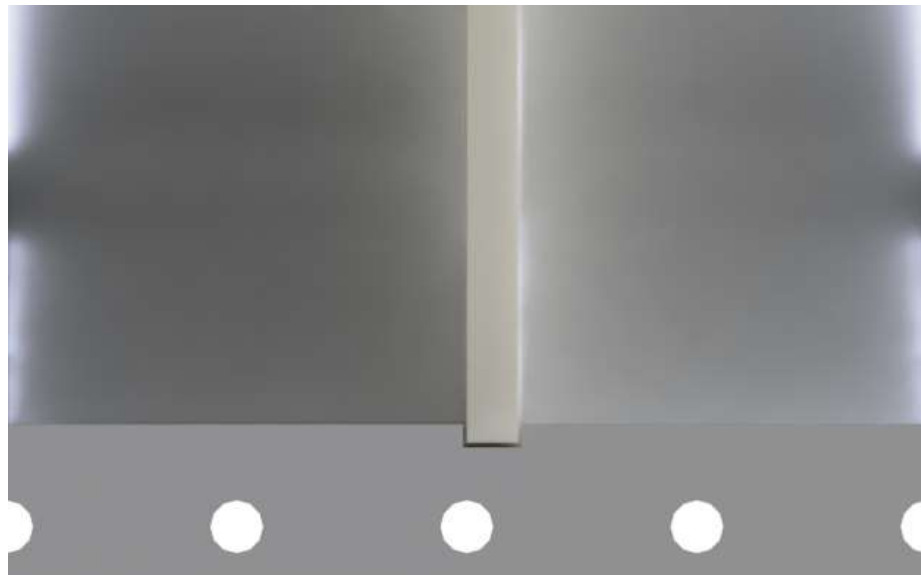


Figure 56: Acetyl baffle positioned in tank slot.

Baffles were selected to be acetyl (Delrin) following analysis of the load imparted by retardant mass. This was calculated to be relatively low, allowing a thin metal baffle to be used. However, the minimum thickness of the baffles was 10mm to allow the valve mechanism to be fitted. For this thickness of baffle, Acetyl provides sufficient strength at a lower mass penalty, whilst being

extremely corrosion resistant and easy to work. As this is a complex section, high replaceability / reparability is critical.

The baffles pictured right comprise of a honeycomb like structure. This pattern is selected as it allows reinforcing material to be present along hinge lines. Hinge lines are shown in red on Figure 57.

The fuselage has a series of stringer rails present connecting the fuselage hoops on the underside. These will be designed to resist the mass of the empty tank under 1g loading and exist to allow the tank to slide in and out. The primary mounting of the tank is discussed in the next section.

The one-way valves work very simply with a hinged sheet, filleted around the edge at 45° to prevent the valves opening in the wrong direction, with a stopper on the larger side positioned to prevent the valve opening past 45°. This mechanism is clearly visible from the perspective shown below in Figure 59.

This mechanism is repeated for each baffle. Before going into full production, it is advised that CFD be performed to evaluate the placement, and count of baffles, as it is expected less valves will be needed on baffles further from the centre and higher up due to reduced expected flow rate requirements.

Baffles are not bonded to the design to allow removal for inspection and maintenance during the off season.

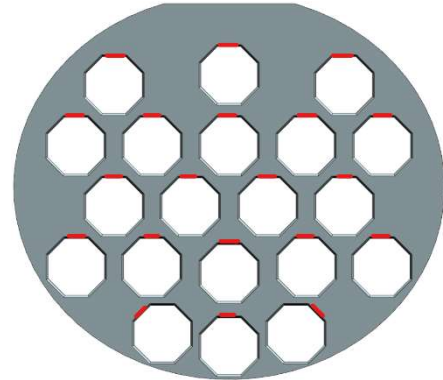


Figure 57: Baffle hinge locations..



Figure 59: NRV in situ.

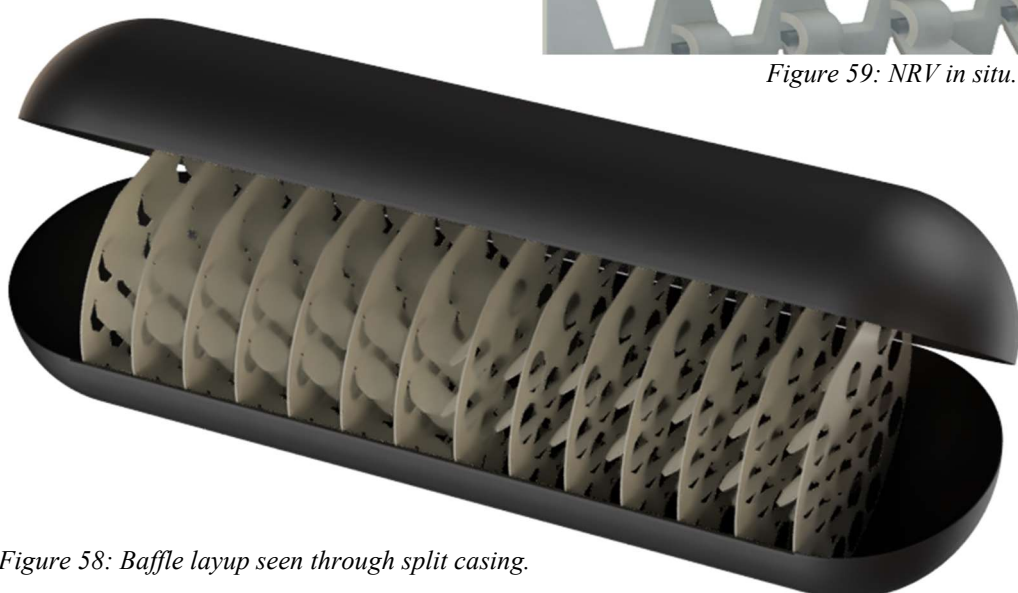


Figure 58: Baffle layup seen through split casing.

8.8 Tank Mounting

The tank needs a bolt-in removable mounting system. The mounting points were designated to match up with the internal hoops of the fuselage structure. To solve for the force seen by these

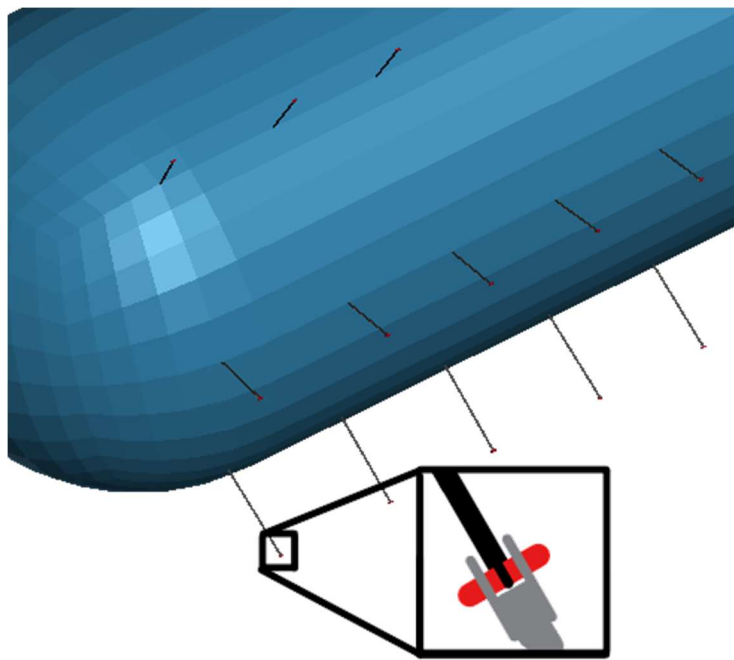


Figure 60: Bolt-double shear mounting technique.

bolts, a model was created of the tank with a solid core and shell outer layer matching that of the real tank, ensuring mass and moments of inertia matched. This model then uses a beam-to-beam mounting technique to transfer force to the bolts, this simulates a mounting section from the tank, being bolted into the hoops of the fuselage structure.

Seen in Figure 60, the tank mounting has been represented by bolts in double shear holding mounting bars. The bolts are then analysed using the NASA bolt failure criterion. The tank is loaded with an implicit 4.75g load with a full tank of retardant (ultimate load for airframe). For this load 58 x M14 grade, 12.9 standard pitch bolts achieve a peak failure criterion is 71%. This is below the typically accepted maximum safe value of 80%. This means the airframe will fail before the tank mounting bolts will shear.

Using many bolts like this is effective at distributing load for mounting, reducing stress imparted on the tank and the fuselage structure. Right shows axial force (N) distribution being applied to the mounting rods acting on the bolts at 3.25g.

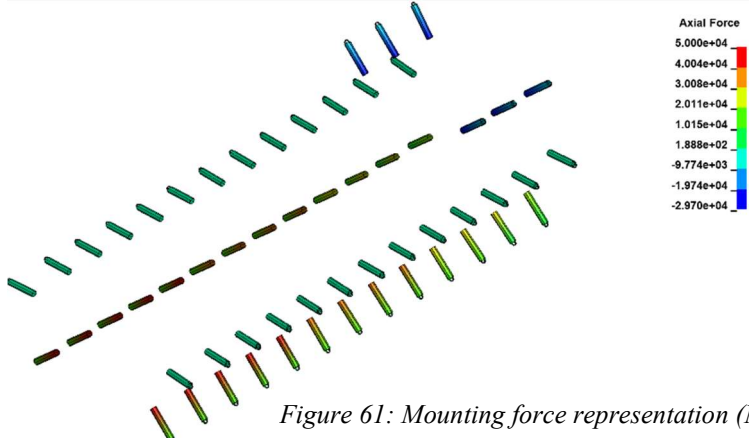


Figure 61: Mounting force representation (N).

9 Propulsion and Power

9.1 Functional Analysis And Design Requirement

Prior to any decisions being made about the propulsion system, a functional analysis was carried out to determine what Nerodia requires from its powerplants. The primary function is to propel the aircraft and at least overcome the drag at any given flight condition. The secondary function is to act as a power source for varying ancillaries and payloads. In the case of Nerodia, the unique requirement of a pressurised payload requires a pressurised source – which is targeted to be a secondary function of the propulsion system. An APU (outlined in subsystems section) provides power for most subsystems (avionics, hydraulics, de-icing, to name a few) and so the propulsion system has fewer accessory functions. Sadraey [35] provides a clear and well-constructed propulsion design process workflow, as seen in Figure 62, which has been followed for Nerodia's propulsion system. Constraints which kick-off the design process are outlined in the succeeding section. An assumption has been made that for an aircraft of this size, it is entirely unfeasible to design and manufacture a bespoke engine without grossly enlarging the budget.

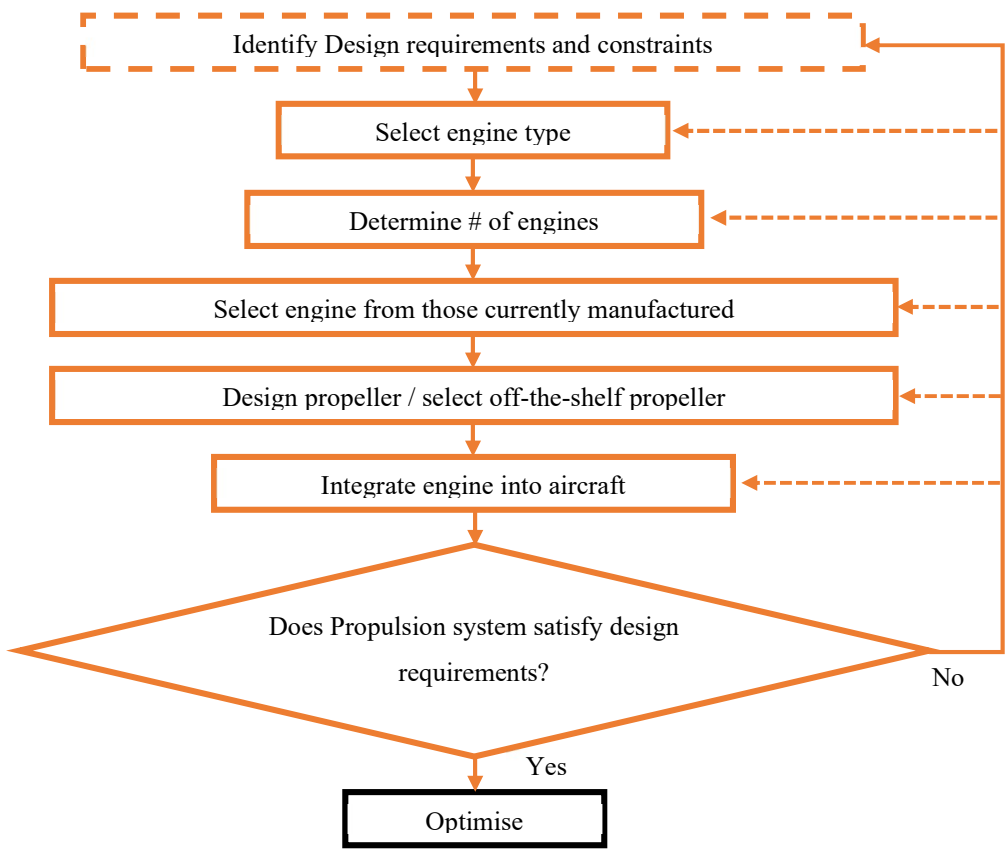


Figure 62: Propulsion system design process, adapted from Sadraey [35].

9.2 Engine Down Selection

9.2.1 Engine Type

The engine selection process first considers the type of engine, the required power, the number of, and then configuration/layout. To narrow down the type, the suitability of each is assessed based on its performance over Nerodia's flight conditions. Two ultimate criteria impact the selection most: absolute ceiling, and flight Mach number. The types of engines being selected from are only those that could feasibly work within Nerodia's flight conditions of Mach 0.57 and 10500 m ceiling. The lesser criteria are propulsive efficiency (weighted for the two ultimate criteria), specific weight, SFC, size, cost, maintainability, and noise. It is deemed that the packaging constraints (specific weight & size), and propulsive efficiency are more important than noise (Nerodia will operate mostly over mountains), cost (the airframe's cost is approaching that of cargo aircraft with all engine types), and maintainability (off-season maintenance schedules allow for reduced requirement). Thus, the 4 chosen engine types are evaluated in a down-selection matrix in Table 26, using weights for each attribute and Figures of Merit for each engine type.

Table 26: Down-selection matrix evaluating the 4 chosen engine types. 1: worst, 9: best.

Attribute and Weight /20	SFC	Engine cost	Noise	Specific weight	Propulsive efficiency	Maintainability	Size	Final score	Norm.
	5	5	2	9	7	4	8		
Engine		Figures of Merit /9							
Piston-prop	9	9	2	5	8	9	3	255	79.0%
Turboprop	8	7	6	8	7	4	7	280	100%
Turbojet	4	2	7	3	2	1	9	161	0%
Turbofan	5	4	9	4	5	2	8	206	37.8%

Turboprop and piston-prop engines standout as the likely candidates for the mission requirements.

As will be mentioned in the following subsection, the required power is roughly 11,180 kW and there is no piston-prop engine currently in production that would match the requirement in a reasonable configuration. Thus, turboprop engines are the obvious choice for propulsion.

9.2.2 Engine Selection

The constraints plot in Figure 20 determines the possible design space with respect to wing and power loading. The propulsion system itself is ultimately required to meet the total drag during steady level flight as a minimum, which is accounted for in the constraints plot by the below Equation [36].

$$\begin{aligned}
 T_{req} &= D, & P_{req} &= T_{req}V = DV \\
 P_{req} &= \frac{1}{2}\rho V^3 S C_{D_0} + \frac{W^2}{\frac{1}{2}\rho VS} \left(\frac{1}{\pi e AR} \right)
 \end{aligned} \tag{1}$$

The selected design point yields a power loading of 6.08 kg/kW, and with a MTOW of 66,859 kg – the required power is roughly 11,000 kW. To find a solution of engines that meets the required power, a select number of turboprop engines was assessed. The twin-boom nature of the Nerodia lends itself to integrating engines inside the booms for drag reduction. This biases the design towards an even number of engines, especially given there would have to be major design changes to incorporate an odd engine somewhere on the airframe/tail. The two configurations then are 2-engine and 4-engine layouts. Ultimately the engines capable of the 11,000 kW requirement in a 2 or 4 layout are limited, and at the time of writing there are currently 4 in use that provide reasonable specifications. Table 27 provides the max power, dry mass, and price per unit cost (where available) for the 4 engines.

Table 27: The 4 turboprop engines to be selected from [37]. DNA: Data Not Available.

Engine	Max Power (kW)	Dry Mass (kg)	Price/Unit Cost (mGBP)
EPI TP400-D6	8203	1795	DNA
PW150A	3781	718	1.19
RR AE2100D3	3458	790	2.47
Progress AI20M	2940	1040	DNA

The engines were then assessed for the 2-engine and 4-engine layouts, seen in Table 28.

Table 28: The 4 turboprop engines assessed in both 2-engine and 4-engine layouts for the 11,000 kW requirement. Chosen configuration shown in purple text. DNMR: Does Not Meet Requirement

Engine	2 Engine Layout		4 Engine Layout		P/W ratio (kW/kg)
	Power (kW)	Mass (kg)	Power (kW)	Mass (kg)	
EPI TP400-D6	16406	3590	32812	7180	4.57
PW150A	DNMR	DNMR	15124	2872	5.27
RR AE2100D3	DNMR	DNMR	13832	3160	4.38
Progress AI20M	DNMR	DNMR	11760	4160	2.83

The EPI engine is the only contender capable of performing in a 2-engine layout (of those assessed). The remaining engines are all capable of attaining the required power, however the Progress AI20M barely provides enough max power without considering parasitic ancillaries. The PW150A in a 4-engine layout is the standout solution; with the lightest dry mass, plenty of excess power, and a superior power-to-weight ratio. Pratt and Whitney engines of this type are also in much higher volume manufacturing than the other competitors and has known maintenance schedules & freely available information.

9.2.3 Engine Placement And Configuration

The choice of 4 engines somewhat limits potential, viable configurations. Nerodia's twin-boom design necessitates engines in the fore sections of the booms in a tractor configuration, to capitalise on the lower drag penalty of the setup (smaller wetted area when integrated as such). The

remaining 2 engines, then, could be placed either outboard of the booms, or in a out-of-the-box fuselage/tail configuration, in either a tractor or pusher layout. Considering the tail mount, the empennage would require a greater tail size to account for the loss of area, a reconfiguration of the control surfaces, and massive structural increases, which deems it not suitable. Thus, outboard of the booms is the only option. If the outboard engines were to be in a pusher configuration, new, complex structural loads would be introduced to the wing structure – which implies an overcomplicated design. The final configuration is 4 engines, with 2 integrated into the booms, and 2 outboard of the booms as far inboard as possible to reduce structural requirements.

Nerodia falls under 14 CFR part 25 regulations (Transport Category Airplanes) [22] which stipulates several clearances in 25.925. Of the ground, water, and structural, only the structural clearances require consideration during configuration (the current aircraft geometry eliminates the other clearance issues). In Layman's terms, the propeller blades must be at least one inch radially away from the structure and one-half inch longitudinally away from stationary parts, whilst having a positive clearance between other components of the rotating assembly and the structure. These clearances, along with the pre-defined boom spacing, guide the later propeller sizing and outboard engine placement.

9.3 Propulsion Performance

It is necessary to calculate the amount of power and thrust the aircraft needs to fly during different stages of the mission – such as take-off, cruise, and dash. The power available can be compared against the power necessary as a plot, which is unique for the turboprop style engine. As the shaft power of most turboprop engines has a modest reliance on airspeed, it can be assumed that the shaft power is constant with airspeed for general estimations. The amount of power available is usually expressed as

$$P_{av} = P_S \eta_p$$

where P_S is the shaft power, and η_p is the propeller efficiency. The efficiency of a fixed propeller is a strong function of speed; however, Nerodia incorporates variable-pitch, constant-speed props. So, for first approximations, the power available for a constant speed propeller is constant. The power required for the parabolic drag polar with constant parameters is found by multiplying the drag by the airspeed. The power required can thus be written as

$$P_{req} = \frac{1}{2} \rho V^3 S C_{d0} + \frac{W^2}{\frac{1}{2} \rho V S \pi A Re}$$

The take-off speed is set to 1.2 times the stall velocity, with both speeds expressed as

$$V_{stall} = \sqrt{\frac{W_{TO}}{\frac{1}{2} \rho S C_{Lmax}}}, \quad V_{TO} = 1.2 V_{stall}$$

The power required for each condition (take-off, cruise, dash) is then plotted as a function of velocity, alongside the available power, as shown below in Figure 63.

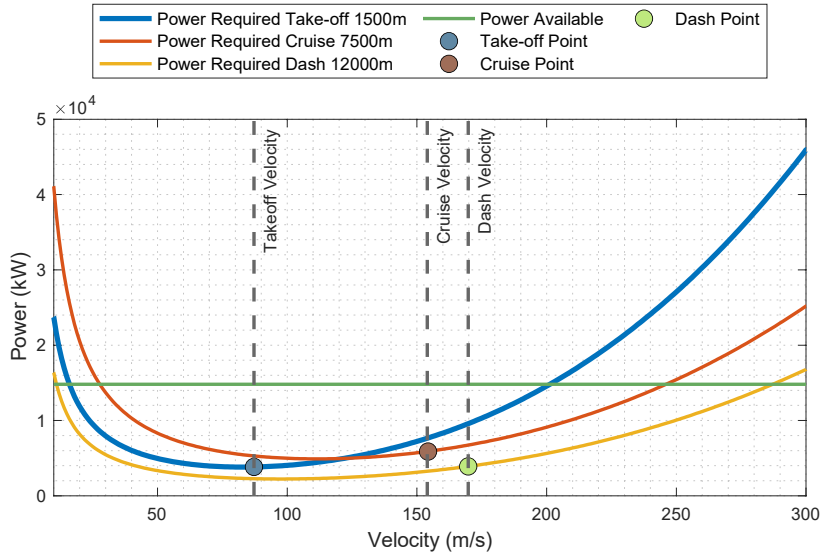


Figure 63: Required power curves for mission flight conditions varied with velocity. Operating points signified with dots.

The aircraft's required power drops dramatically as it transitions from stationary to forward flight for all phases due to a negative shift in lift-induced drag. Then, as the airspeed rises, the lift-induced drag subsides and the required power drops until speed reaches the “bucket”. This region is the highest difference between required power and available power, which can be converted to maximum rate of ascent or best power margin for manoeuvring flight. Beyond this speed, wind resistance increases, and parasitic drag takes over as the primary contributor from lift-induced drag for the necessary power increase. The total required power rises until it equals the available power. The velocity, total required power, and thrust at various stages of the mission profile can be found below in Table 29.

Table 29: Velocity, and total required power & thrust for varying flight conditions.

Phases	Velocity (m/s)	Total Power Required (kW)	Total Thrust Required (kN)
Take-off	65	3840	44.1
Cruise	154	5890	38.8
Dash	170	3560	21.2
Drop	72	3370	52.6

9.4 Propeller Design

A major decision had to be made prior to any propeller design could take place. The two options were to either purchase an off-the-shelf propeller from a known volume manufacturer or design a bespoke propeller and then outsource the R&D and manufacturing to an engineering company such as MT-Propellers or Dowty Rotol. Given the scale of design effort for the entire aircraft, and the potential for efficiency gains with a bespoke mission-focused design, Crassus opted to go for the

long route with a bespoke propeller in the hopes of saving money on fuel over a long period of time.

Regarding overall design methodology, the propeller was first sized and parameterised via hand calculations using equations from Sadraey [35], then optimised in an open-source MATLAB code called OpenProp [38], and finally further optimised and assessed within another open-source prop design code called JBLADE [39] at a range of different airspeeds, altitudes, and pitch angles to achieve efficiency, power requirements, and thrust values.

The propeller design process started with material selection. To enable thin, efficient aerofoils with directionally varying stiffness & strength, carbon fibre composite blades were chosen. The recommended propeller tip speed limit for composite is roughly 250 m/s [35]. Using this tip speed limit, general aircraft parameters, and idealised propeller parameters – the propeller diameter and rotational speed was calculated using

$$D_p = K_{np} \sqrt{\frac{2P\eta_p AR_p}{\rho(0.7V_{tip\,cruise})^2 C_{Lp} V_c}}$$

$$n = \frac{60}{2\pi} \left(\frac{2\sqrt{V_{tip\,cruise}^2 - V_c^2}}{D_p} \right)$$

The activity factor was then rearranged to calculate the average blade chord length for the propeller. An appropriate AF range for aircraft propellers is between 100 and 150, with higher values being associated with turboprop engines. An AF of 150 was selected to boost blade thrust output, giving us an average blade chord length via

$$AF = 10^5 \int_{0.2}^1 \left(\frac{c}{D_p} \right) \left(\frac{r}{R_p} \right)^3 d \left(\frac{r}{R_p} \right) \approx 1563 \left(\frac{\bar{c}}{D_p} \right)$$

$$\bar{c} \approx \frac{AF D_p}{1563}$$

The propeller and aircraft parameters were then collated for OpenProp input, as seen in Table 30.

Blade Count	Rotation Speed (RPM)	Rotor Diameter (m)	Hub Diameter (m)	Required Thrust (kN)	Air Speed (m/s)	Fluid Density (kg/m³)	Average Chord Length (m)
6	826	4.55	0.94	10.1	154.3	0.549	0.430

Table 30: OpenProp input values.

Once inputted into OpenProp, propeller blade geometry parameterised by chord length, maximum thickness, pitch, twist angle, and skew angle at various radial locations was spat out. The geometry was then fed into JBLADE to optimise and evaluate efficiency, power requirements, and thrust outputs at various pitch angles and airspeeds. Further optimisation consisted of amending the Blade Element Momentum Theory (BEMT) component of the code to account for root and tip loss factor,

foil interpolation, and 3D corrections. To compare and validate this newly optimised propeller, two propellers with known technical information [40] and parameters were similarly parameterised in JBLADE and assessed. N.B. Genuine propeller information concerning parameters is scarce, and so this information source is not representative of competitor propellers. Figure 64 below shows efficiency, thrust, and power over a range of airspeeds, and shows the required power and thrust at steady level flight (cruise).

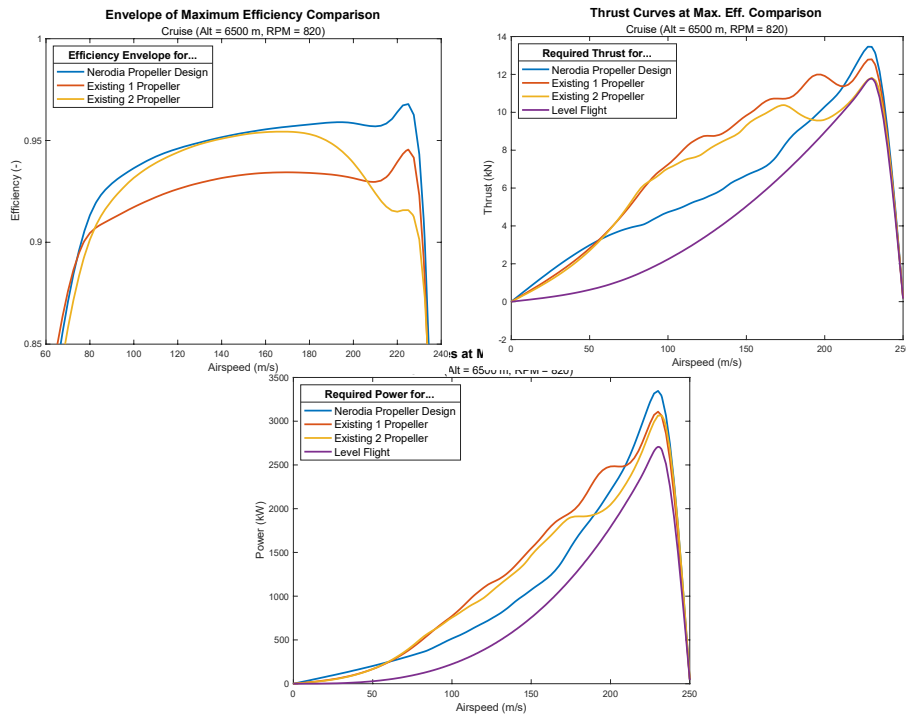


Figure 64: Bespoke-designed propeller performance versus NACA propellers.

The Nerodia designed propeller has a greater overall efficiency than the two existing NACA propellers, whilst also needing less power to spin at the ideal constant speed of 826 RPM while generating more thrust than is required for steady level flight. From this data, the proper pitch angle setup, thrust, and power at the maximum efficiency were identified at varying flight stages – as seen in Table 31.

Table 31: Propeller design specification at varying flight conditions.

Phase	Velocity (m/s)	Power Required (kW)	Thrust Required (kN)	Pitch Angle Required (deg)	Efficiency (%)
Take-off	65	1180	12.0	85	90.62
Cruise	154	1630	14.7	90	93.02
Dash	170	1170	6.39	92	93.35
Drop	72	1180	15.4	70	86.19

With known pitch angles and design parameters, the JBLADE model was exported and surfaced in SOLIDWORKS to be mated to mounting flanges and a central hub. The propeller blades were mirrored to produce a set of x4 propellers which counter-rotate (x1 clockwise and x1 anticlockwise on each side of the wing). The variation with radial position of chord length, coefficient of lift, and twist can be seen in Figure 65, highlighting the swept tip optimised by the JBLADE code to ensure a constant effective Mach number over the swept region [41].

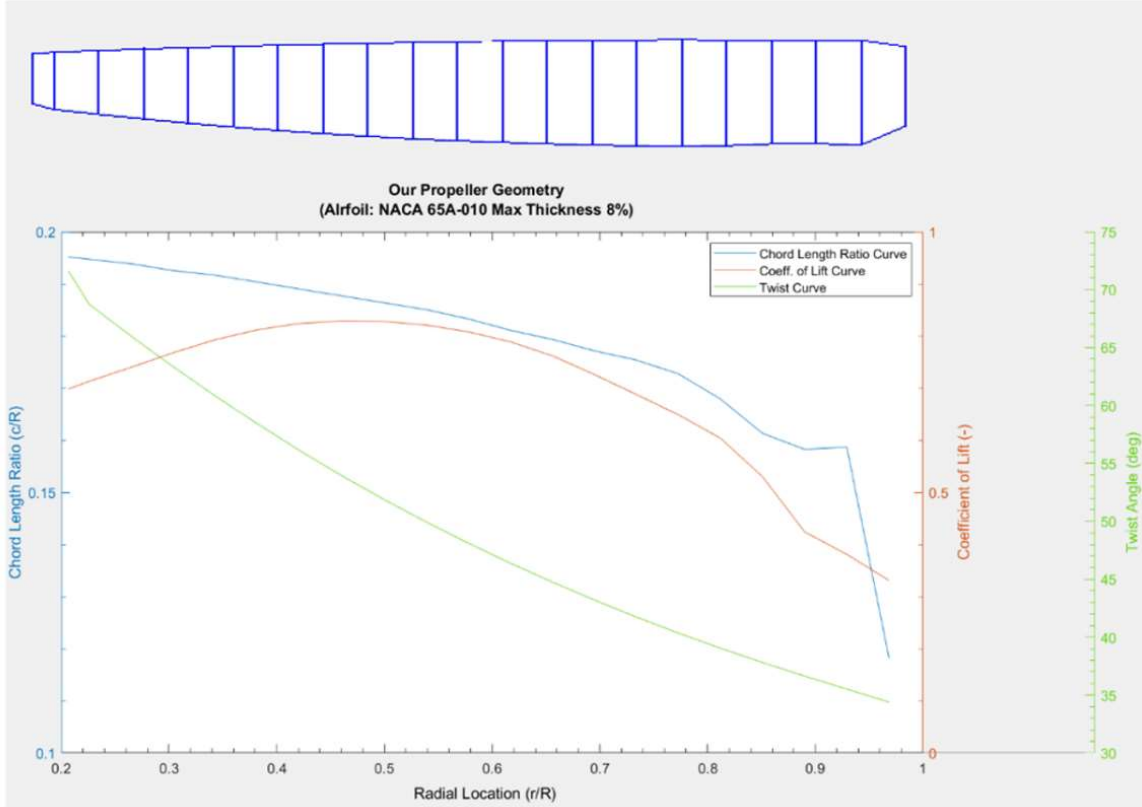


Figure 65: Radial variation of chord length, coefficient of lift, and twist of Nerodia's propeller blades.

9.5 Airframe Integration

As a contributing function, bleed air is tapped off from the high-pressure compressor (HPC) of the inboard engines for use in pressurising the payload (higher altitude dispersion) and for cabin air conditioning. The bleed air exits the final stage of the HPC at a temperature of around 800 K, which requires significant cooling to be of use. Heat exchangers are positioned inboard of the booms within the wing structure (scalloped out of the fuel tank). Typically, NACA ducts are embedded in the fuselage belly to feed aircraft heat exchangers, however the routing of air for inlet/outlet would be tricky given the fuselage is shrink-wrapped around the payload, and the payload pressurisation is done from the top of the tank. The inboard wing location provides maximum routing and packaging efficiency, and the inboard engine air inlets are oversized to also intake heat exchanger cold air. Spent hot air from the heat exchanger is conveniently routed to

blow the inboard flaps which aids in increasing the stall angle of attack and maximum lift coefficient. These aerodynamic benefits are not quantified in this project.

The heat exchanger area [42] is found by calculating the required heat flux from the cold side (or hot side) at cruise conditions (7500 m) using

$$\Phi = \dot{m}_c C_{P_c} (T_{co} - T_{ci}), \quad S = \frac{\Phi}{H \Delta T_{ml}}$$

where Φ is the heat flux, \dot{m}_c is the cold side mass flow rate, C_{P_c} is the cold side specific heat, T_{co} is the cold side outlet temperature, T_{ci} is the cold side inlet temperature, S is the heat exchanger area, H is the overall heat exchange coefficient ($3 \text{ kW m}^{-2} \text{ K}^{-1}$), and ΔT_{ml} is the logarithmic mean temperature difference (defined as $\Delta T_{ml} = \frac{\Delta T_2 - \Delta T_1}{\ln(\frac{\Delta T_2}{\Delta T_1})}$). Figure 66 illustrates the inlet and outlet temperatures of both the hot (bleed air) and cold side. Using individual plates of dimensions 0.8 m x 1.4 m (to fit within the inboard wing structure cavity), a total of 410 plates is required to achieve the heat flux necessary to cool the bleed air to 107°C (380 K on diagram) which is an adequate temperature for routing and pressurising the retardant.

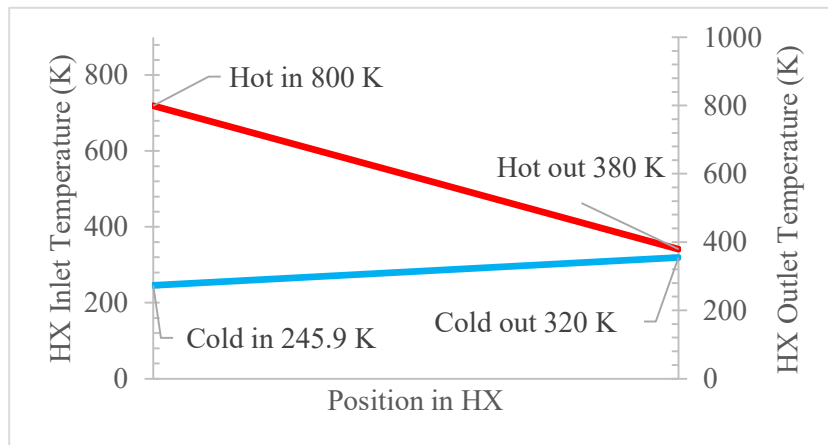


Figure 66: Simplified heat exchanger temperature profile.

As mentioned, the inboard air inlets are oversized to account for additional airflow to the heat exchanger for cooling purposes. Figure 67 illustrates the layout within the boom for ingestion of cold air to the engine, oil cooler, and heat exchanger.

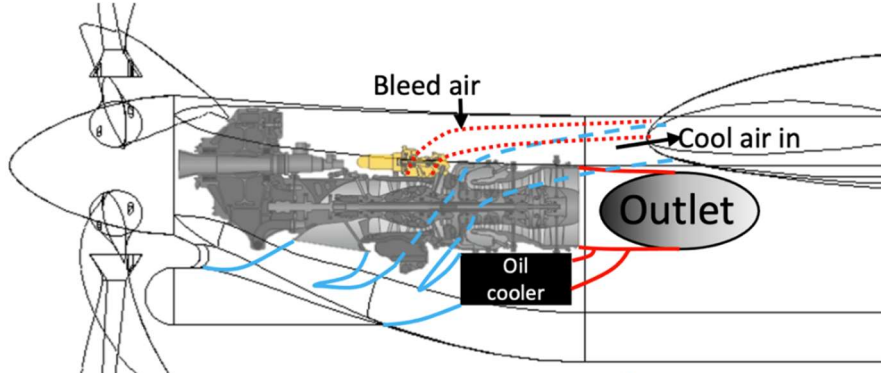


Figure 67: Internal layout of boom fore section, showing engine position, air intake & passages, and bleed air tapping.

10 Avionics and Systems

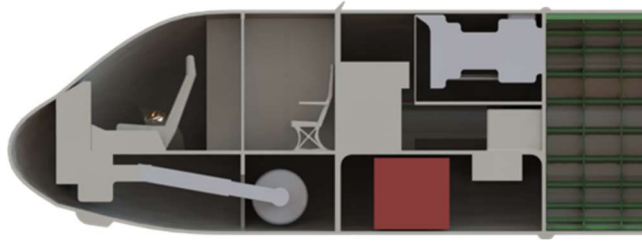


Figure 68: Avionics and cockpit cross section.

10.1 Avionics And Flight Deck

Key elements of the aircraft's avionics and flight deck are tabulated below. Design of these operator-oriented elements of the aircraft was tailored towards convenience, navigation, and ergonomics. Many of the implemented features have been selected to ensure the aircraft offers greater capabilities than other comparable firefighting aircraft. Flight deck convenience features benefit the comfort of operators during longer journeys or ferrying. Ergonomic features improve the ease and efficiency with which operators can utilise the aircraft – including by widening the conditions in which aerial firefighting may take place effectively. Crucially, safety features are included to give peace of mind to operators and give them confidence to perform their roles in a high-stress environment.

Table 32: Subsystem elements.

Flight Deck Elements		Avionics Elements	
Option	Reason	Option	Reason
Analog Display	Redundancy	GNSS	Navigation
Coat Locker	Convenience	Flight Recorder	Certification
Force-feedback	Ergonomics	Direction Finder	Navigation
HUD	Ergonomics	Communication suite	Safety, Navigation, Mission planning
Keyboard/Cursor	Ergonomics	Datalink	Navigation, Mission planning
Glass Windscreen	Safety, convenience	Weather Radar	Safety, Navigation
"Khazi"/Toilet	Convenience	EFVS	Safety, Navigation
Cupholders	Convenience	Autonomous systems	Convenience
3x14" Touchscreen	Ergonomics	Radar Altimeter	Safety, Navigation
Accommodation Station	Convenience	Traffic/Collision Avoidance	Safety
		Ballistic Payload Aid	Convenience, Safety, Ergonomics
		Night Flying Kit	Convenience, Safety, Ergonomics
		FMS	Navigation
		FADEC	Convenience
		FBW	Convenience, Weight

Avionics on the Nerodia have been tailored for operator convenience, particularly within the high-stress environment of aerial firefighting. Novel avionics suites planned for the aircraft allow safer, more frequent operation when compared to comparable aircraft of the same role. For example, night flying devices such as spotlights, radar altimeters, FLIR cameras, and Enhanced Flight Vision Systems permit the aircraft to continue effective low-altitude operation in poor visibility and low-light conditions (see Figure 70).

Flight control systems such as FBW and FADEC reduce operator workload, permitting more effective task prioritisation in stressful environments. FBW integrates seamlessly with the EHA actuators on control surfaces to permit rapid corrections to control inputs. This system forms the basis of the vehicle's autonomous flight capabilities.

The avionics system includes a bespoke “ballistic aid” suite. From the operator’s perspective this is represented by a “smart” ballistic sight for augmentation of payload drops. This system makes use of inertia sensors, altitude, wind conditions, and visual cues to give operators a real-time preview of where the payload drops will impact on the landscape. Such a system will considerably improve airdrop precision – and hence promote the safety of ground-based personnel at each incident.

The baseline avionics suite chosen for the aircraft is the Rockwell Collins Proline Fusion system (see Figure 69) Additional avionics capabilities and modules are added on top of this baseline suite to bolster its abilities. The Collins Proline Fusion avionics suite was selected for three key reasons: futureproofing, capability, and familiarity.

Being a very reputable supplier for avionics systems, Rockwell Collins is seen as a trustworthy source for the aircraft’s baseline avionic system; ongoing support and servicing of the avionics systems is expected to persist throughout the lifespan of the aircraft. The suite itself is also widely configurable for future uses, having numerous options to add new modules and third-party bespoke suites. This feature is especially prescient considering the ballistic suite capabilities of the aircraft. The capabilities of this avionics suite are also proven; the Rockwell Collins Proline Fusion holds Part 25 certification, qualifying it for use on the Nerodia. It offers interconnectivity capabilities with other aircraft or ground stations – enabling operators to update flight plans remotely. The three multi-function displays shown in Figure 69 can be operated using touchscreen control as well as keyboard and cursor control. Touch screen capability is effective in a low-workload environment, enabling quick and easy flight planning. Cursor and keyboard control is desirable in high-workload environments due to the tactile nature offering positive feedback and assurance to the flight crew.

Lastly is the key point of familiarity. The Rockwell Collins Proline Fusion has already been used on the Viking Air CL-415 and DHC-515 firefighting aircraft. Given the specialised nature of aerial firefighting, it is very likely that many pilots tasked with operating the Nerodia would have experience operating either of the two aforementioned types. Making use of the same baseline

avionics suite best enables these pilots to grow familiar with this new aircraft – streamlining the process of bringing the new aircraft into peak operating efficiency.



Figure 69: Rockwell Collins Pro Line Fusion avionics flight deck.

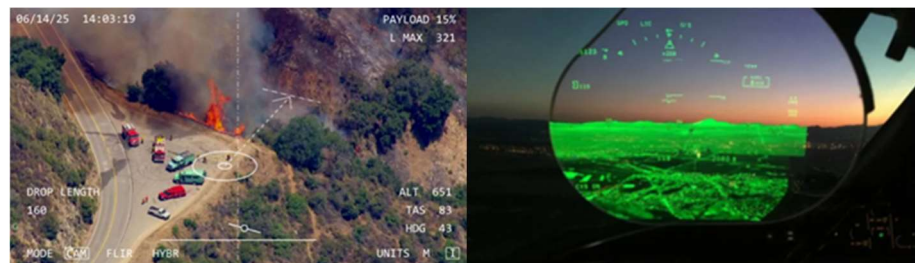


Figure 70: Payload Targeting System view (left) and Rockwell Collins Enhanced Synthetic Vision System integrated into the heads-up display (right).

Design of the flight deck is tailored towards convenience and ergonomics. Dual controls for both captain and officer, tactile touchscreens combined with keyboard-based alternatives enable seamless effective operation of the aircraft. Additional features such as the coat locker,” Khazi”, and accommodations station decrease stress placed on operators – especially during longer flights. The layout is planned to be similar to that displayed below in Figure 71.

- ① Captain Seat
- ② First Officer Seat
- ③ Captain Sidestick
- ④ First Officer Sidestick
- ⑤ Cockpit Center Pylon
- ⑥ Rockwell-Collins Proline Fusion Flight Deck
- ⑦ Cockpit Coat Locker
- ⑧ Crew Entry Door
- ⑨ Khazi
- ⑩ Crew Accommodations Station

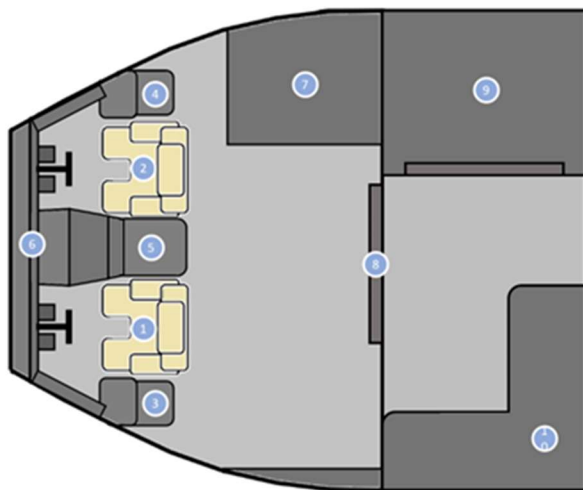


Figure 71: Cockpit layout.

The windscreens layout was designed according to 14 CFR 25.773-1 crew visibility requirements (see Figure 72). The windscreens illustrated is the minimum windscreens size permitted under the aforementioned requirement. An investigation into increasing windscreen design will be conducted

in the detailed design phase; instrument flight capabilities and the desire to pressurize the cockpit to higher levels drove the design of a smaller windscreens.

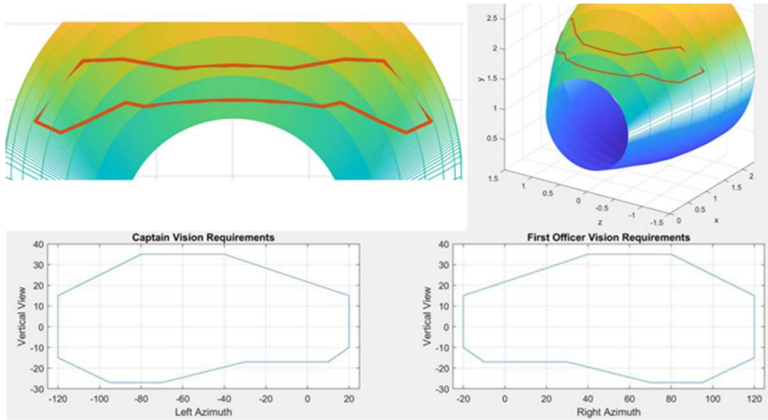


Figure 72: Windscreen geometry.

10.2 Autonomous Operation

Architecture for autonomous operation were included on the Nerodia. This capability was a design objective by the customer; however, there are many other reasons why this was included. By designing an autonomous variant of the Nerodia, any crew accommodations can be eliminated, saving the customer millions in pilot training programs. With an autonomous system, night-time missions become more realistic, as does extended high-stress manoeuvres. Finally, a catastrophic incident will never incur the loss of a pilot.

A very basic model of the autonomous architecture found on the Nerodia can be seen in Figure 73. According to this model, mission waypoints are provided to the Autonomous Flight System through satellite linkage. These waypoints are then optimized using a low-fidelity 3-degree-of-freedom “least-effort” simulation to generate an efficient mission trajectory. The trajectory is then fed into a proportional controller that works to maintain Nerodia on the desired trajectory. Sensor data from each of the engine’s Full Authority Digital Engine Control (FADEC), pitot probes, barometer, attack and sideslip angle vanes, and GPS are used to gather information about the conditions surrounding the Nerodia; engine thrust is monitored and controlled using the Engine FADECs, airspeed is measured using the pitot probes and a barometer, attitude angle is measured using the attack and sideslip vanes, and ground speed is measured using GPS and a statistical filter. Using the position and velocity relative to the ground, the force required to maintain the desired trajectory is calculated. This force is then translated into required control surface deflections using the attitude angle, airspeed, non-linear dynamics, and a gain table. The required deflections are then inputted into the fly-by-wire system as pilot controls and the proportional control loop is restarted. Inside the loop, a payload drop condition is included. In its most basic form, the payload drop condition can take the form of a slant-range to drop site check; if the Nerodia falls within a certain radius of the drop site, the payload is dropped.

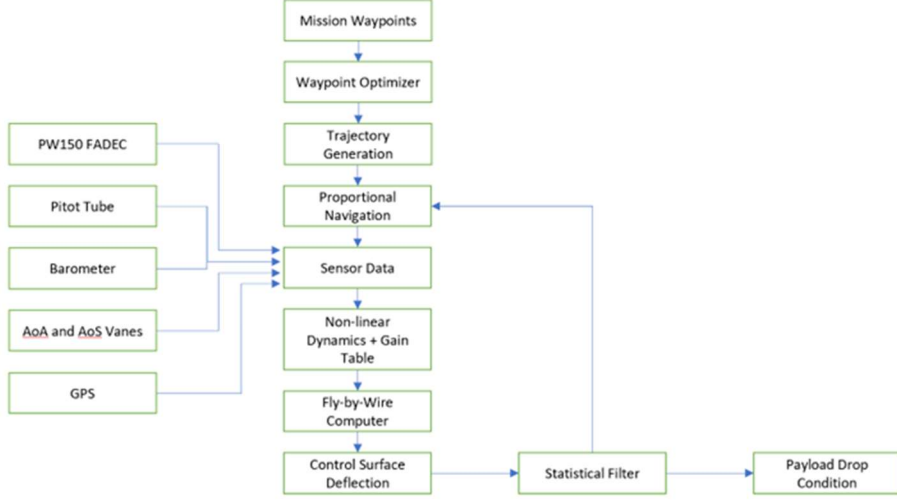


Figure 73: Autonomous flight system diagram.

It is difficult to determine whether this exact system is more of an automated system due to there being well defined mission waypoints with no details on how the trajectory updates. The current logic runs a nested 3-degree-of-freedom simulation that computes the “least-effort” trajectory that captures the pre-defined waypoints. Depending on how high the fidelity of this nested simulation is, the computational power and time required to update the desired mission trajectory may be small enough to be performed at any stage of the mission – except during high-risk manoeuvres, such as drops. As is, the current system would be between level 3 and level 4 on the society of automotive engineers’ six levels of autonomy

10.3 Power Systems

Power Systems encompasses two main domains: Electric power and Hydraulic power. Due to the focus on producing an aircraft in-line with the MEA concept, the bulk of power systems are geared towards generation and distribution of electrical power. Hydraulic power is required for the landing gear's steering and brakes only. Once the aircraft is airborne hydraulic power is no longer needed for operation.

Aircraft power requirements at cruise are estimated to be quite modest, at just over 211kW. The main drain on power is actuation, accounting for almost the entire power requirement alone. This relatively small power requirement has been achieved partly through effective dedication of alternative power sources to key functions – namely bleed air from the engines is employed for pressurisation of the payload tank, eliminating the need for a dedicated powered compressor system.

Table 33: Aircraft power requirements.

Item	Power Consumed (kW)
Rockwell Collins Proline Fusion Avionics	0.8
Thales FCC + REU	0.2 (estimate)
Actuators (full bore)	200 (estimate)
Lighting + Stratus 1kW LED (spotlight x2)	2
Anti-Ice	9
Autonomous Ops Flight Computer (x4)	Negligible
Swiss Air-Data HPS-1 (Heated Pitot Tube) (x6)	0.2
Swiss Air-Data SMV-1 (Attack Angle Vane) (x6)	Negligible
Curtis-Wright MPFR (Flight Data Recorder) (x2)	Negligible
Total:	211.4

The aircraft's maximum power generation is much larger than the expected power requirement of 211kW. At full power the aircraft is estimated to generate around 4.84MW of electrical power. Almost all of this is generated by the four PW150a engines, selected due to their thrust-to-weight capabilities. Due to the great potency of the aircraft's engines, one engine alone would be fully capable of providing all electrical power needed at any given time. This is unlikely to be of any consolation to the operators were three engines all to fail – however it would mean that they retain power over control surfaces, as opposed to simply spiralling into the ground.

An additional PW APS2300 unit serves as an onboard APU. This unit was also selected due to its reasonably low weight, small footprint, and good power generation capability. The APU's primary purpose is for generation of hydraulic power, which it does by directing pneumatic pressure to a compressor. The APU also provides start-up power when on the ground and can be used as a backup in the event of multiple engine failures. The APU generates up to 194 lb/min of pneumatic power.

Table 34: Aircraft power sources.

Item	Power Supplied (kW)
PW150A Engine (x4 full bore)	4800
PW APS2300	38

Three types of electrical power are provided by the power system: 230VAC, 115VAC, and 28VDC. 230VAC is required for the largest, most power-intensive components on the aircraft. This includes power to actuators for landing gear and aerodynamic devices, radar, and other such components. 115VAC is required for many intermediate avionics loads such as radar altimeters, FLIR, and communication equipment. Lastly, 28VDC is required for low power devices on the aircraft such as internal lights, displays, and computing components.

Each of these power loads has its own dedicated bus on the aircraft, with an additional 230VAC backup bus provided for emergency use – with a RAT as a last-resort power source.

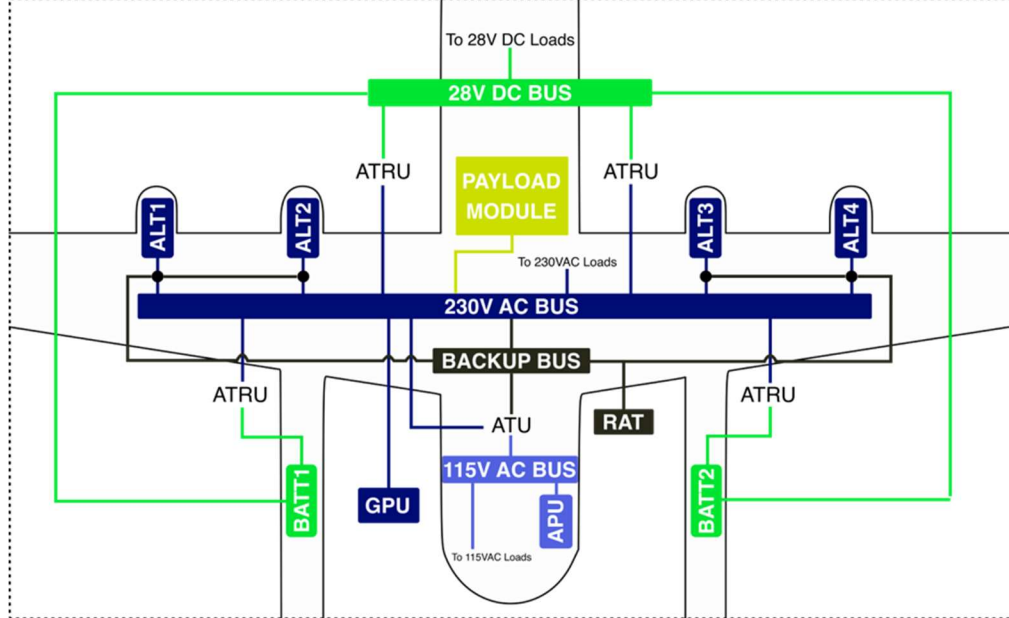


Figure 74: Aircraft power schematic.

Various payload modules are expected to have different power requirements. Instead of each module having to generate its own power, the module simply connects to the aircraft's 230VAC circuit. It is assumed that if the module requires power in alternative formats (DC or low voltage AC) it would have internal components for conversion from 230VAC.

10.4 Fuel

The fuel distribution system is comprised of multiple grouped fuel tanks, and their associated pumps, filters, and reservoirs for trimming about the airframe. The fuel tank groups consist of the ‘core’ tanks for fulfilling main mission range requirements; trim tanks in the fore and aft of the fuselage; Extra capacity tanks for longer endurance missions/ferrying; and small surge tanks towards the wing tips primarily intended for pressure expansion, fuel jettison, or trimming if needed. Tanks are compressed using Nitrogen gas, impeding fuel evaporation and ignition.

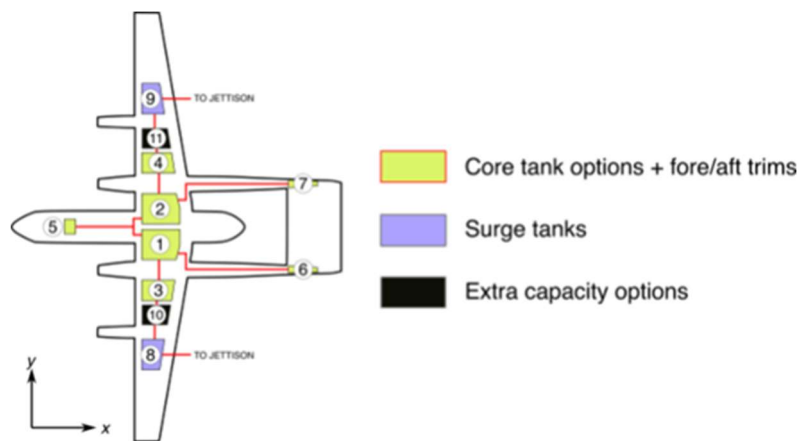


Figure 75: Aircraft fuel tank layout.

Table 35: Aircraft fuel tank quantities.

Fuel Volumes:	Volume (m ³)	Tank Numbers	Max Permitted range (km)
Core Tanks Only	15.2	1,2,3,4	3,965
Trim Tanks	2.3	5,6,7	602
Core + Trim Tanks	17.5	1,2,3,4,5,6,7	4,586
Surge Tanks Only	3.4	8,9	891
Extra Capacity Option	3.9	10,11	1,022
Maximum Permissible	24.8	All tanks	6,512

The core fuel tanks cater for the minimum fuel need of 15 m³ of storage. Due to the potential instability caused by mass changes after dropping of retardant, trim tanks have been placed in fore and aft locations as far away from the centre of mass as possible. The extra capacity tanks permit longer missions or transcontinental transit, though are not expected to be required during standard operations. Surge and trim tanks may be filled to increase endurance – although this is not recommended.

With all tanks brimmed, maximum range is estimated at just over 6,500km. This makes the aircraft fully capable of autonomous travel across the Atlantic, meaning it is possible to deliver the aircraft to a customer almost anywhere in the world. However, for normal operation it is not expected that the surge tanks and trim tanks would be fully filled.

Maximum range with the core tanks is still an impressive 3,965 km. The Extra-capacity tanks increase that range by a further 1,000 km. This means that a realistic maximum range (I.e., only the

core tanks and extra capacity tanks filled) is around 4,980 km. Note that all quoted ranges are for a one-way trip.

10.5 Landing Gear

The aircraft's landing gear is of a typical tricycle layout, with the nose landing gear stored under the pilot and the main landing gear stored in the booms, aft of the inboard engines. Information from D.P Raymer [1] was used to inform the configuration and design of the gear to ensure good steering and take-off roll performance. The landing gear height is configured to be greater than 90 percent of the aerodynamic stall angle, with tire spacing sufficient to reduce the turnover angle to less than 54 degrees. Gear specifications are listed below.

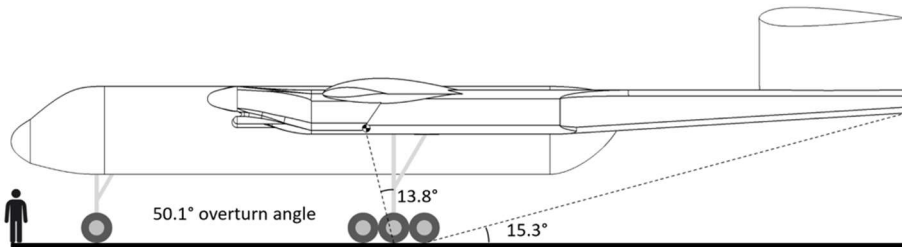


Figure 76: Aircraft landing gear angles.

Table 36: Aircraft landing gear specs.

Parameter	Value
Distance Between CG and Nose Gear (m)	9.1
Distance Between CG and Main Gear (m)	0.94
Distance Between Main Gear Struts (m)	7.74
Gear Height (m)	2.35
Overtake Angle (deg)	50.1
Tailstrike Angle (deg)	15.3
Main Gear Maximum Static Load (kN)	667
Main Gear Minimum Static Load (kN)	75.6
Nose Gear Minimum Static Load (kN)	57.8
Nose Gear Dynamic Braking Load (kN)	284.7
Tire Diameter (m)	1.04
Tire Width (m)	0.3

Landing gear struts are pressurised to 1200psi with a 300mm travel. The compression under a 3G load is around 200mm, which makes for a very hard landing. It is worth noting that finite element analysis done on the wing structure between the fuselage and the inboard boom shows that the aircraft can withstand a 3G landing with this strut design without issue.

Table 37: Aircraft landing gear specs II.

Parameter	Value
Piston Pressure (psi)	1200
Piston Diameter (mm)	119.4
Extended Gear Height (mm)	2651.8
Piston Travel (in)	304.8
1-Gee Load Compression Height (in)	10.2
3-Gee Load Compression Height (in)	200.7

10.6 Actuation

The aircraft uses 3 main types of actuation: Hydraulic, EHA, and EMA.

Design on the aircraft has been geared towards embracing the MEA concept. Selection of actuation methods reflects this. EHA and EMA actuation methods present numerous advantages over mechanical and pure-hydraulic actuation methods found on traditional aircraft. These novel actuation technologies are considerably more compact, require fewer components, and are typically much easier to maintain over the aircraft's lifespan. They also carry weight reduction benefits and remove the need for hydraulic lines passing throughout the aircraft's fuselage – enabling more efficient use of internal spaces either for alternative subsystems or structures.

Despite leaning towards EHA/EMA actuation, classic hydraulics remain part of the aircraft's design for two key purposes: landing gear steering & brakes. Alternative actuation methods remain unsuitable for these purposes at present. Power for these hydraulic functions is drawn from the onboard APU.

EHA actuators are employed for actuation of the main control surfaces (ailerons, rudders and elevator). EHA have their own self-contained hydraulic reservoirs and pumps. This avoids the need to have hydraulic lines running from a central part of the aircraft all the way to actuator locations. This reduces aircraft weight and complexity. Given the aircraft's twin-boom configuration, this is especially advantageous for limiting the stresses due to weight experienced by the booms. EHA also offers rapid response times compared to alternative electronic-derived actuation. The inclusion of self-measuring devices in some actuators can also be used to simulate force-feedback for the operator to improve sense of flight and safety.

Lastly, EMA actuators are employed for use on landing gear and High-Lift Devices (slats and Flaps). EMA was selected due to their low mass, high load tolerances, and minimal complexity. These actuators are slower than hydraulic or EHA alternatives, however this does not present an issue for these use cases.

Each control surface or High-Lift Device has more than one actuator to allow redundancy in the event of mechanical failure. It also permits selection of slightly weaker (hence more compact)

actuators in key locations. Most control surfaces and HLD's have three actuators, except for the inboard flaps which only have two.

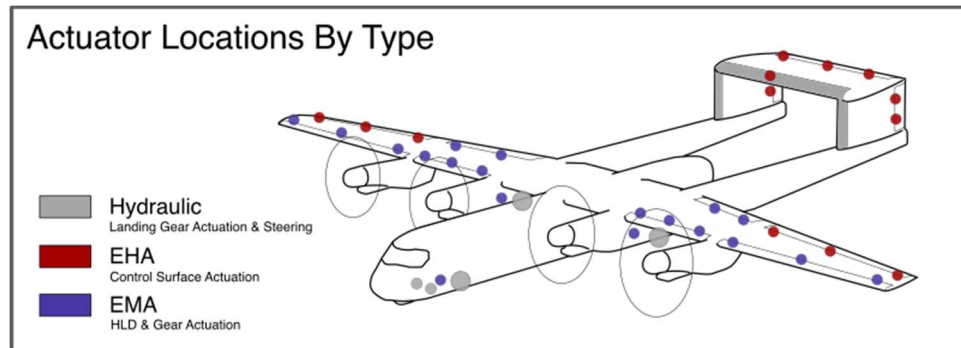


Figure 77: Aircraft actuator locations.

10.7 De-Icing

De-icing strips are present on the leading edges of the main wing and vertical & horizontal stabilisers. These are purely electrically powered, as feeding lines for antifreeze or bleed air would add unnecessary complexity to the design of the leading-edge salts. The De-icing machinery consist of large conductive surfaces (heating patches) separated into blocks by conductive wires (parting strips). Constant power to the wires causes any ice formations to be split into smaller blocks, whilst power is cycled through the conductive surfaces periodically to melt and remove ice build-up.

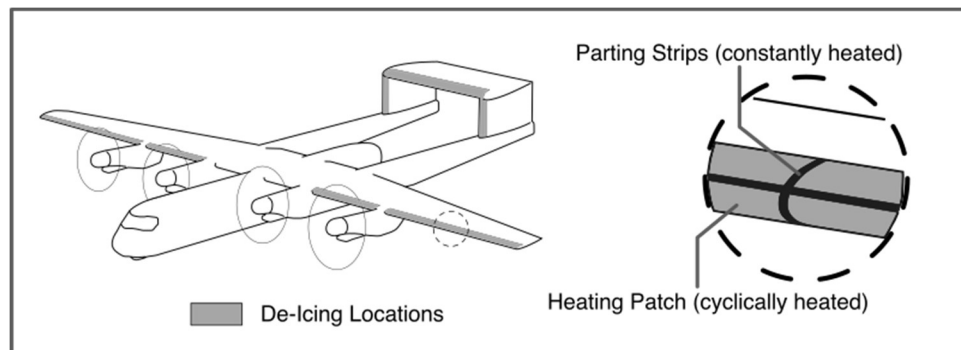


Figure 78: Aircraft De-icing locations.

11 Cost and Manufacturing

A key requirement was to minimise the acquisition and operations costs of the proposed FFA, and hence a decision matrix was set up with various estimation models and performance was compared with a range of parameters including accuracy of estimation, complexity, applicability etc.

Raymer's [11] model was chosen to approximate the Research, Test, Development and Evaluation (RTD&E) and Flyaway Cost. Whilst Robert Liebeck's [43] model was chosen for the estimation of Direct Operating Costs (DOC). As the FFA is required to enter service in 2030, all values below have been adjusted for 2030 U.S dollars, assuming a constant 3% inflation rate/annum.

11.1 Production Rates

Conducting current FFA market analysis and estimating future FFA market growth at 6.5% Compound Annual Growth Rate (CAGR) between 2021 to 2030 [44], whilst also making a cautious assumption that the aircraft will only be in demand for the first 10 years of its conservative 20-year lifespan, a production quantity of 85 aircraft was derived. 4 of the 85 aircraft will be flight test aircraft that will be initially owned by Crassus Aviation. Once flight test and certifications are complete, the 4 aircraft will be refurbished and sold to customers at reduced cost. Table 38 below shows the anticipated aircraft production rate across the 10-year manufacturing phase.

Table 38: Estimated aircraft production rate.

Year	1	2	3	4	5	6	7	8	9	10	Total
Production Rate	6	7	8	9	9	9	9	9	9	10	85
Days to build an A/C	60	51	45	40	40	40	40	40	40	36	

11.2 Rtd&E Cost

Using Raymer's approach, the RTD&E cost for the Nerodia program was estimated at ~\$8.9 billion for a production quantity of 85 aircraft. For reference that is ~\$7.0 billion in 2022 U.S dollars. The RDT&E cost breakdown is shown below in Figure 79.

RDT&E Cost Breakdown

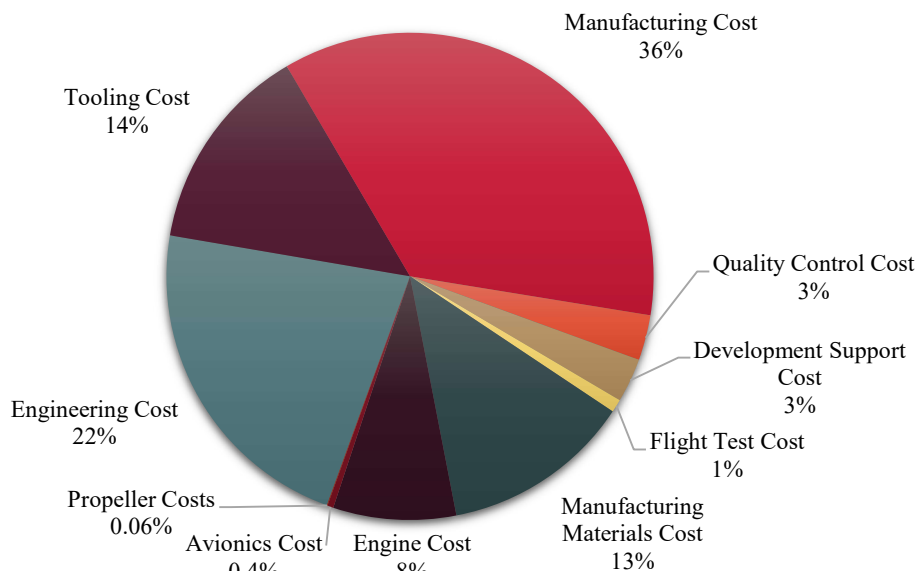


Figure 79: RDT&E cost breakdown of the Nerodia program.

11.3 Flyaway Cost

Flyaway or Acquisition cost is calculated by dividing the total RDT&E cost of the program by the production quantity and then marking this up by a given percentage to yield profits. Accounting for a 15% markup, the flyaway cost is set to \$119.9 million (\$94.6 million in 2022 U.S dollars). The 4-test aircraft will be sold at 80% of full acquisition cost, \$95.9 million. (\$75.7 million 2022 U.S dollars). Figure 80 below shows the production breakeven graph which depicts that the breakeven point is at 62 aircraft.

Production Break Even Point Graph

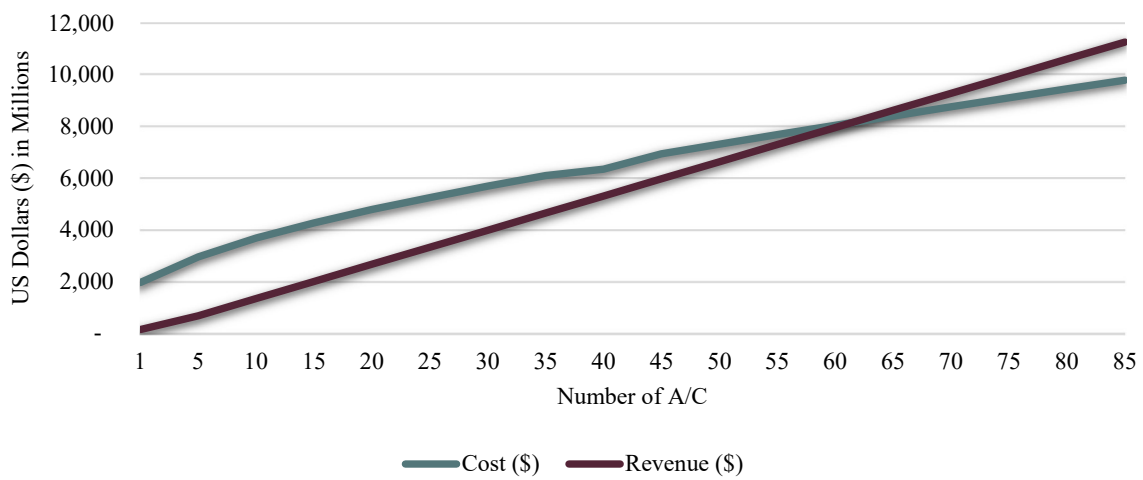


Figure 80: Production break even graph used to identify the production breakeven point.

11.4 Direct Operating Costs

Operating costs are what the owner/operator would have to pay on a mission basis to deploy the aircraft. The operating cost for a private entity to operate Nerodia was calculated to be \$43,400/mission. As seen by Figure 81 below, the most prominent costs are fuel and retardant costs. Crassus Aviation understand most of its customers will be government entities and hence deducting retardant, insurance and landing fees, the cost/mission for government entities was calculated to be \$22,300.

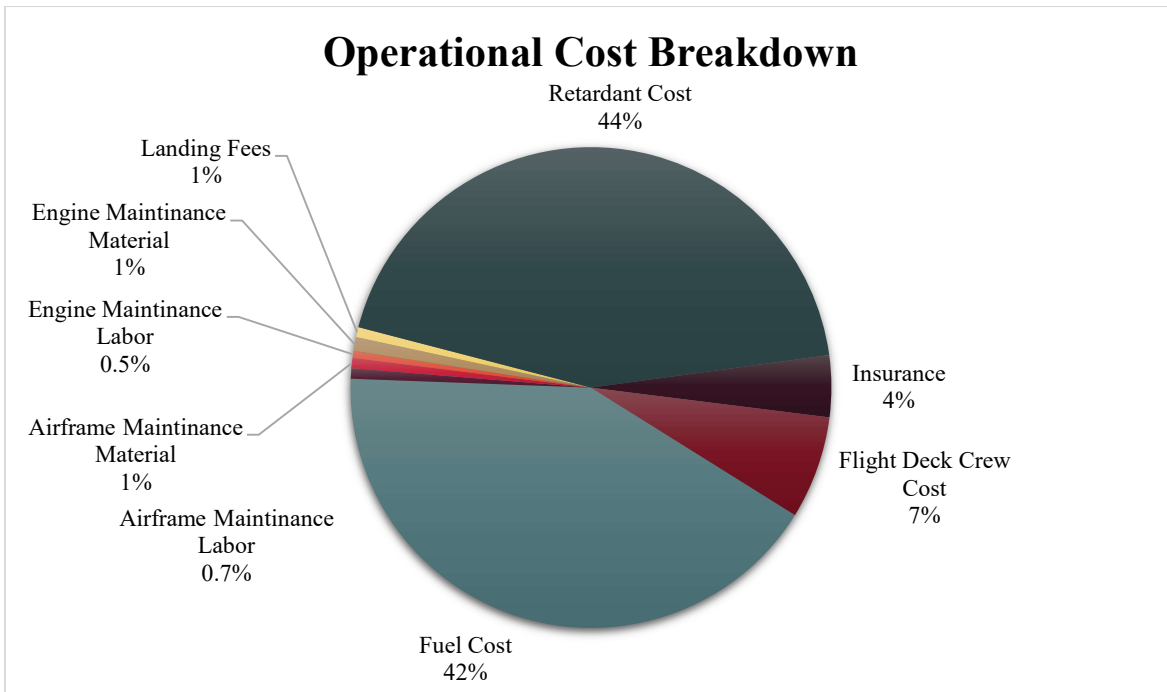


Figure 81: Operational cost breakdown of Nerodia for private entities.

11.5 Ffa Cost Comparison

Competitor cost analysis was conducted to determine how the Nerodia fared in terms of operational costs compared to existing FFA. The 4-competitor aircraft shown in Table 39 below are amongst the most prominent in aerial firefighting: the DC-10, BAE 146 and C-130 have been included as they have similar payload capacity to that of Nerodia, whilst the CL-415 was included due to its purpose-built nature, also like that of Nerodia. The total cost/drop is assuming the aircraft is owned by the operator and hence no availability rates are accounted for. The CL-415 costs are assuming it's dropping water, while the rest are accounting for dropping retardant (Phos-Check LC95). The acquisition costs for the DC-10, BAE 146 and C-130 are solely for the airframe itself, the cost of retrofitting payload system have not been included. A key requirement being to minimise operational costs for the operator, Nerodia has the lowest cost in 2030 U.S. dollars/US-g dropped of the competitors aircrafts, as shown by Figure 82 below.

Table 39: Cost breakdown of existing FFA, and Nerodia.

	Aircraft				
	Nerodia	DC-10	CL-415	BAE 146	C-130
Total Drop Capacity (usg)	6,000	9,400	1,600	3,000	3,000
Total Cost/Drop (\$)*	43,400	78,800	17,100	28,300	31,100
Cost for ~18,000 usg (\$)	130,200	157,600	188,100	169,800	186,600
% diff. in DOC from Nerodia	-	16	48	30	43
Cost/Flight Hour (\$)	18,100	35,200	17,100	18,800	21,600
Acquisition Cost (\$)	119,900,000	>172,000,000	44,600,000	>69,000,000	>44,100,000

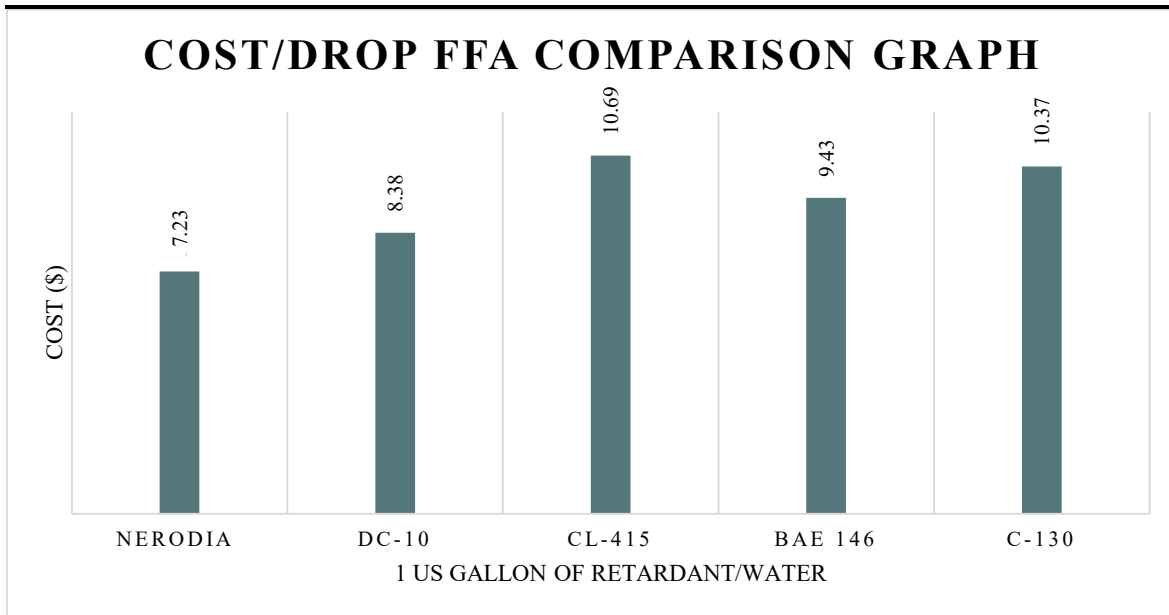


Figure 82: Cost/drop comparison of 1 US-g of existing FFA with Nerodia.

11.6 Loan & Lease Schemes

Crassus Aviation understands some potential customers will lack the initial capital to buy Nerodia outright and hence loan and lease schemes will be introduced to aid those customers. The loan will require customers to put forward 20% deposit and the remaining 80% can be paid as monthly/annual instalments with the interest rate set at 2.5% and the loan duration ranging from 10 to 15 years. The lease scheme will work by limiting the customer to roughly 1200 operational hours/annum with a daily availability rate of \$26,400 and a flight hour rate of \$9,200. The lease will cover costs for maintenance, insurance, and depreciation of aircraft. The associated cost/annum for customer and profits for Crassus Aviation for both schemes are shown in Table 40 below.

Table 40: Cost breakdown of loan and lease schemes.

Scheme	Parameter	Value	Cost (\$)/annum for Customer	Profit (\$) for Crassus Aviation
Loan	Deposit Value (%)	20		
	Loan Value (%)	80		12,590,000 to 19,210,000
	Duration (Yrs)	10 to 15	10,850,000 to 7,680,000	per A/C
	Interest Rate (%)	2.5		
Lease	Daily Availability	26,400		
	Cost (\$)			
	Flight Hour Cost (\$)	9,200		3,960,000 per A/C per
	Avg. Operational Days/Yr	150	15,000,000	annum
	Avg. Operational Hrs/Day	8		

12 Business Operations

12.1 Business Operations Plan

To meet the entry into service (EIS) scheduling requirement stated in the RFP, a project timeline was produced as shown below by Figure 83. The technology freeze for the initial design was scheduled for the end of 2020, this date will allow for the use of modern methods and materials for the design. Two years have been allotted for testing and certification, with the design LAT reaching initial operational capability at the end of 2030. Full operational capability is expected at the beginning of 2032 and planned system updates are scheduled until 2065.



Figure 83: Project timeline and EIS.

In order to achieve smooth running of the timeline as stated above, Crassus Aviation alongside Omega Technologies have devised a 4-stage initial business plan; Design Phase, Marketing Phase; Manufacturing Phase and Sales Phase.

12.2 Stage 1: Design Phase

The design phase will consist of utilising a small team of design professionals who are hired to operate in conjunction with Crassus Aviation and Omega Tech. and ensure the detailed design carried out by the two companies is of a viable one. Coulson Aviation is a perfect example of a modern company with professionals who are recognised as global leaders in aerial firefighting [45]. Coulson is a US based company, whose expertise Crassus Aviation will greatly benefit from. Through communication with Coulson as well as continuous outreach to other FFA operators Crassus aviation aims to develop a rapport and work to better Nerodia to surpass the effectiveness of current operators.

12.3 Stage 2: Marketing Phase

The marketing phase focuses on raising awareness of Crassus Aviation and its impact on wildfires. Awareness can be largely achieved through social media interaction, such as a website and public outreach, promoting popularity in the public eye. *Crassus Aviation hopes to shine a new light on aerial firefighting which will lead to target markets being excited when the name Nerodia is uttered.*

Further marketing strategies will include:

1. Pitch ideas to investors and venture capitalists to promote funding for the program.
2. Directly engage government entities and current FFA operators and explain operational cost benefits and the improved effectiveness in suppressing fires due to the bespoke nature of Nerodia.
3. Visual Advertising: such as a visual poster to entice public interaction (see Figure 84)

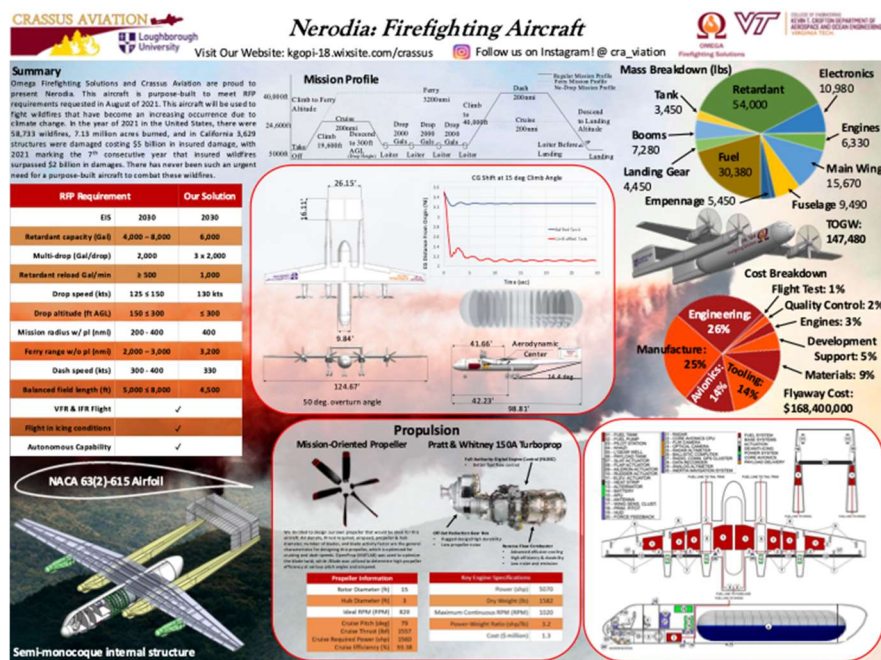


Figure 84: Poster for public engagement and awareness.

12.4 Stage 3: Manufacturing Phase

Crassus Aviation intends to use a combination of outsourced and built-in-house structures/systems to manufacture the Nerodia. Structures/systems such as the landing gear, engines, and avionics will be outsourced to subcontractors to reduce overall program costs. Subcontractors will be chosen based on promised quality of structures/systems, transportation costs, and costs of manufacturing the structure/system itself. To facilitate for the manufacture of bespoke structures/systems, such as wings, booms, tails and propellers, Crassus Aviation intends to build its own manufacturing facility. The manufacturing facility shown in Figure 85 below resembles an assembly line in which,

in house-built structures/systems are manufactured, tested and quality checked before being fitted to the aircraft at placement zones. Test and quality control checks of such structures/systems are performed at their respective manufacturing zones to identify issues as early as possible to prevent complex, expensive repairs later in the manufacturing process. The Nerodia program is a low production volume project and hence only a small team of highly versatile professionals will be employed to keep costs down.

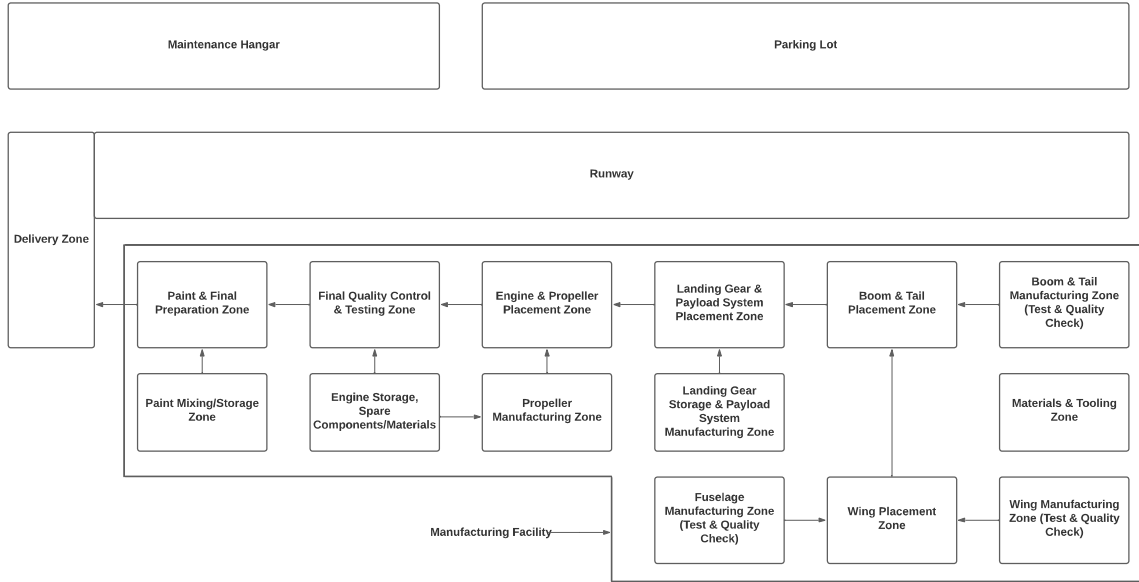


Figure 85: Crassus Aviation's manufacturing & maintenance facility.

Adjacent to the manufacturing facility is a runway so that in-flight test runs can be conducted. A maintenance hangar will also be present on site to perform maintenance on leased aircrafts. Finally, a parking lot to store completed aircraft awaiting collection from customers. Crassus Aviation believes this manufacturing ideology will allow for a streamlined production process in which the number of aircraft produced annually can be increased from 6 in the 1st year to 10 in the 10th year.

12.5 Stage 4: Sales Phase

During the sales phase of the business plan, Crassus Aviation will be initially targeting the largest markets for FFA. These being the locations where forest fires and grassland fires are most prominent: USA, Australia, Canada, and Indonesia.

The 2021/2022 US federal budget included \$192m for forest service. This encompasses wildland preparedness including investment in equipment and aviation, with investments in up to 18 next gen airtankers [46]. The US also operates on a surplus funding from each state with their own firefighting budget. The state of Colorado has a state budget of \$78m which includes one-off payments for FFA [47]. Cal-Fire being US largest firefighting company has state funding of \$48m with an additional US Air Force federal funding of \$150m. Which has been used in the purchase of 7 LAT (C-130H) for 2021-2022 year [46].

Australia has a yearly budget for fighting forest and grassland fires of \$14.8m with the potential of rising to \$28m with the increase in severity of wildfires. Australia has made also available \$20m to lease 4 additional LATs as a means of contingency [48]. Canada has no national fixed budget for firefighting investment. The provincial budgets vary hugely, however there is a market available as Conair have a fleet of 20 air tankers currently in operation with room to improve [49]. Indonesia, like Canada, has no national budget, but has recently purchased 6 new CL-415 with an emerging market for FFA [50].

The lease and loan schemes can be optimised to reach out to customers in different regions making most use of tax laws in place at different market locations. Crassus Aviation aims to gradually boost sales and become greatly profitable whilst being operationally effective.

13 Risk and Reliability

General risks present on most aircraft are omitted to focus on those specific for an FFA. Risk analysis was done by the team which involved using a risk matrix bespoke to the design of the aircraft, as well as the project mission and business aspect. This involved rating each Risk/Hazard for probability (Prob) and severity (Sev). Table 41 shows the Risk/Hazard and outcome on the left-hand side with Probability and severity of this occurring. Probability and severity were each given a score from 1 to 5. Probability being the likelihood of it occurring and severity expanding on the potential loss or consequences. Probability is calculated through a combination of the likelihood of mechanical failure and likelihood of the event occurring, 5 resulting in a high certainty of occurrence / high risk event, whilst 1 results in a very low likelihood / low risk event. Severity is calculated as the effect on aircraft mission capability, 5 being complete permanent inability of mission completion until repair, and 1 being minimal effect on mission completion. These two scores were then multiplied to get a comprehensive risk score. The team then identified the most critical risks and produced a strategy to mitigate the impact of these Risks/Hazard to reduce the probability of the event occurring.



Table 41: Risk matrix.

Hazard	Outcome	Prob	Sev	Risk	Mitigation
Payload					
Unable to close nozzle	Secondary drops ineffective	2	3	6	Land aircraft safety, fix nozzle, refill and attempt mission
Unable to open nozzle	Unable to discharge retardant on desired location, mission not accomplished	1	2	2	Secondary Discharge channel
Nozzle and secondary valve fail closed	High Mass landing, structural fatigue risk.	1	3	3	Burn / dump excess fuel, land smoothly then inspect structure.
Relief valve fails closed	Excess pressure leaks through Pintle nozzle	1	3	3	Release the pressure and retardant using the nozzle, until tank stabilises
Relief valve fails open	Fails to pressurise	1	1	1	Use computer aided system to re target the drop area with regulated speed
NRV remains open	Inaccurate flow of retardant between baffle sections – imbalanced CG shift and retardant drop	4	2	8	If one fails there will still be an effective flow rate into the centre baffles, as there will be 19 one way valves left in operation, repairs can be performed upon returning to the ground
NRV remains closed	Reduced Retardant flow rate on drop	2	3	6	Reduce speed to keep up with the retardant flow rate
Tank has not fully pressurized before drop.	Poor drop distribution	2	2	4	Sensors are built into to check for pressurisation, so pilot will have to control speed to effectively drop in desired area.
Retardant fails to fill central section	Central section not refreshed. Maximum drop quantity diminished.	3	2	6	Perform dive / turn to assist flow, if still failing, emergency drop and refer to failed NRV
Retardant coats non corrosion resistant materials	Long term material damage if unnoticed	3	1	3	minimal exposed materials are non corrosion resistant, a/c designed to reduce chance of retardant contact.
Fill line failure	Mission delayed until repaired.	2	1	2	
Aerodynamics					
Deep Stall	Aircraft stuck in stall until terrain impact.	1	4	4	FCS to prevent pilot pulling into a deep stall.
Structures					
Excessive use of Obstacle avoidance mode	Accelerated Structural fatigue	3	4	12	Proper training and warning messages for pilot warning of risks
Power system failure	Landing Gear actuators fail, reliant on mechanical backup.	2	3	6	A secondary power supply for landing gear as a surplus to the APU
Undiscovered structural Fatigue	A/c structural failure in flight	3	4	12	Regular maintenance and frequent repairs will alleviate the influence of fatigue
Subsystems					
Night vision system failure in use	Loss of vision	1	3	3	LEDs, RADAR and IFR systems can be used to safely return
Ballistic computer failed	Drop accuracy reduced	2	2	4	Pilot experience to drop manually
Miscellaneous					
Wildfires reduce in severity and probability	Reduces the need for FFA's, affecting YoY revenue	2	3	6	Alter the target location to where forest fires occur more frequently as well as Improving marketing tactics
Due to multiple outsourced R/D, subcontractors unable to deliver timely orders	Affects the deployment time, unable to meet needs	3	3	9	Extensive communication with contractors to avoid this situation
Loss of power to subsystems for communication on the ground	Unable to contact with ground team to support	2	3	6	A secondary system is also installed as a backup, using a different communication channel

14 Conclusion

14.1 Viability

Unfortunately, it appears that given the large costs that operating a fleet of *Nerodia FFA*'s would entail, the name "*Crassus Aviation*" (given the historical namesake) is a little more on-the-nose than would be desirable. Our aircraft would certainly be excellent for combatting wildfires – but could the customers stomach the cost?

14.2 Future Work

As has been expressed within this report, the payload is of critical importance to mission success – and constant iterative design is paramount to a complete solution. Ultimately there is far more work that could be carried out to enhance the design – including non-constant baffle spacing offset, one-way valve size variation with height, CFD of moving one-way valves to calculate loads (and minimise mass), CFD of nozzle dispersal to optimise nozzle geometry/angle/drop rate, and CFD of high-lift devices.

The PSC could also be adapted to expand the mission profile to encompass fish dropping for repopulation of lakes, however the bespoke payload design is not drafted to allow fish greater than a few mm to effectively be distributed over a drop-zone.



References

- [1] CAL FIRE, “Aviation Program,” 2021. [Online]. Available: <https://www.fire.ca.gov/programs/fire-protection/aviation-program/>.
- [2] J. Burnside, “Aviation Safety,” 25 November 2014. [Online]. Available: <https://www.aviationsafetymagazine.com/features/extreme-maneuvering/>.
- [3] USDA Forest Service, “Drop Testing Airtankers,” USDA Forest Service, Missoula, 2000.
- [4] Perimeter Solutions , “PHOS-CHEK LC95 Series,” 2022. [Online]. Available: <https://www.perimeter-solutions.com/en/fire-safety-fire-retardants/phos-chek-lc95-series/>.
- [5] DuPont, “Delrin Acetal Resin Design Guide,” [Online]. Available: https://www.distrupol.com/Delrin_Design_Guide_Mod_3.pdf.
- [6] Waterous Co, “CSC20 / CSUC20,” 2017. [Online]. Available: <https://www.waterousco.com/csc20-csuc20-1.html>.
- [7] European Aviation Safety Agency, “PW150 Series Data Sheet,” EASA, 2014.
- [8] Federal Aviation Administration, AC 150/5300-13B, Washington D.C.: National Archives, 2022.
- [9] AOE Department, “Range and Endurance Performance,” [Online]. Available: <http://www.dept.aoe.vt.edu/~lutze/AOE3104/range&endurance.pdf>.
- [10] AOE Department, “Climbing Flight Performance,” [Online]. Available: <http://www.dept.aoe.vt.edu/~lutze/AOE3104/climb.pdf>.
- [11] D. Raymer, Aircraft Design: A Conceptual Approach, Reston: AIAA, 2006.
- [12] D. P. Raymer, Aircraft Design: A Conceptual Approach, Washington, DC: American Institute of Aeronautics and Astronautics, Inc., 1989.
- [13] J. Laurence K. Loftin, Subsonic Aircraft: Evolution and the Matching of Size to Performance, Virginia: NASA Scientific and Technical Information Branch, 1980.
- [14] I. H. Guzelbery, Y. Eraslan and M. H. Doğru, “Effects of Taper Ratio on Aircraft Wing Aerodynamic Parameters: A Comparative Study,” European Mechanical Science, Gaziantep, 2019.
- [15] M. Sandraey, Wing Design, Daniel Webster College, 2012.
- [16] R. Finck, “USAF STABILITY AND CONTROL DATCOM,” Flight Dynamics Laboratory, 1978.

- [17] T. SIBILLI, “MODELLING THE AERODYNAMICS OF PROPULSIVE SYSTEM INTEGRATION AT CRUISE AND HIGH-LIFT CONDITIONS,” CRANFIELD UNIVERSITY, 2012.
- [18] S. Markert, “Aerospace CFD High-Lift Assignment,” Loughborough University, 2022.
- [19] C. Gologam, “Semantic Scholar,” 2010. [Online]. Available:
<https://www.semanticscholar.org/paper/A-Method-for-the-Comparison-of-Transport-Aircraft-Gologam/d0262dcd54a9e08f5132f8c09ae34a9859f16891>. [Accessed May 2022].
- [20] Z. Y. Yin Yuhui, “ARC,” AIAA, 30 September 2019. [Online]. Available:
<https://arc.aiaa.org/doi/abs/10.2514/1.C035514?journalCode=ja>. [Accessed May 2022].
- [21] E. Torenbeek, Synthesis of Subsonic Airplane Design, Delft University Press, 1988.
- [22] Federal Aviation Administration, FAA 14 CFR Part 25, Washington D.C.: National Archives, 2022.
- [23] J. Roskam, Airplane Design : Part II: Preliminary Configuration Design and Integration of the Propulsion System, Ottawa: Roskam Aviation and Engineering Corporation, 1985.
- [24] E. Torenbeek, Synthesis of Subsonic Airplane Design, Dordrecht: Kluwer Academic Publishers, 1987.
- [25] A. Hays, “16.3.1 Pitching-Moment Equation and Trim Calculation,” 2013. [Online]. Available:
https://www.adac.aero/_files/ugd/c40aeb_200b0583a1944974a57f26ad01c6bc71.pdf. [Accessed 11 03 2022].
- [26] A. Hays, “16.4.2 Lateral-Trim Analysis,” 2016. [Online]. Available:
https://www.adac.aero/_files/ugd/c40aeb_df9ee1ee280e44b2b2954ceb3e1b09ab.pdf. [Accessed 11 03 2022].
- [27] A. Hays, “16.3.2 Pitch Static Stability,” 2016. [Online]. Available:
https://www.adac.aero/_files/ugd/c40aeb_b3cd93f47b054321802b4aaacfad3faa.pdf. [Accessed 12 03 2022].
- [28] L. Clancy, Aerodynamics, London: Pitman Publishing Limited, 1975.
- [29] United States Military, “MIL-F-8785C,” U.S. Department of Defense, Washington D.C., 1980.
- [30] T. Kandasamy, S. Rakheja and A. K. Ahmed, “An Analysis of Baffles Designs for Limiting Fluid Slosh in Partly Filled Tank Trucks.,” *Open Transportation Journal*, vol. 4, pp. 23-32, 2010.
- [31] A. Dasgupta, “Effect of Tank Cross-Section and Longitudinal Baffles on Transient Liquid Slosh in Partly-Filled Road Tankers,” Concordia University, 2011.

- [32] D. Moss, Pressure Vessel Design Manual, Oxford: Gulf Professional Publishing, 2004.
- [33] C. C. (. Michael David Hutter, C. C. (. Steven Thomas Marine and C. C. (. Richard Lawnewce Ken Woodland, “PORTABLE AIRBORNE FIREFIGHTING AND SENSING SYSTEM”. US Patent 10/755,088, 23 November 2006.
- [34] G. Lovellette, “Safe Drop Height for Fixed-Wing Airtankers,” USDA Forest Service, Technology and Development , [Online]. Available: <https://www.fs.fed.us/rm/fire/pubs/htmlpubs/htm00572317/index.htm>. [Accessed 9 May 2022].
- [35] M. H. Sadraey, Aircraft Design: A Systems Engineering Approach, Wiley, 2012.
- [36] E. M. Greitzer, Z. S. Spakovský and I. A. Waitz, “16. Unified: Thermodynamics and Propulsion,” Massachusetts Institute of Technology, Cambridge, 2002.
- [37] P. Jackson, Jane's All the World's Aircraft 2006-2007, Surrey: Jane's Information Group, 2006.
- [38] B. P. Epps and R. W. Kimball, “OpenProp v3: Open-source software for the design and analysis of marine propellers and horizontal-axis turbines,” 2013. [Online]. Available: <http://engineering.dartmouth.edu/epps/openprop>.
- [39] M. A. R. Silvestre, J. Morgado and J. C. Pascoa, “JBLADE: a Propeller Design and Analysis Code,” in *2013 International Powered Lift Conference*, Los Angeles, California, 2013.
- [40] J. B. Delano and M. M. Carmel, “Tests of Two-Blade Propellers in the Langley 8-Foot High-Speed Tunnel to Determine the Effect on Propeller Performance of a Modification of Inboard Pitch Distribution,” National Advisory Committee for Aeronautics, Washington DC, 1951.
- [41] A. Brocklehurst and E. P. N. Duque, “Experimental and numerical study of the British Experimental Rotor Programme Blade,” in *AIAA Applied Aerodynamics Conference*, Portland, Oregon, 1990.
- [42] A. M. Aydin, C. Moler and R. Saputra, “Plate Type Heat Exchanger Design,” Department of Chemical Engineering, Middle East Technical University, Ankara, 2016.
- [43] R. Liebeck, Advanced subsonic airplane design & economic studies, Cleveland, Ohio: National Aeronautics and Space Administration, Lewis Research Centre.
- [44] A. Singh, “Firefighting Aircraft Market Size,” 2022.
- [45] Coulson Aviation, “COULSON AVIATION - Global Leaders in Aerial Firefighting,” 2022. [Online]. Available: <https://www.coulsonaviationusa.com/>.
- [46] USDA (U.S. Department of Agriculture), “FY 2022 - Budget Justification,” Washington D.C., 2022.

- [47] A. Gallagher, “Colorado firefighting: research and innovation in aerial firefighting equipment,” 1 April 2021. [Online]. Available: <https://www.airmedandrescue.com/latest/long-read/colorado-firefighting-research-and-innovation-aerial-firefighting-equipment>.
- [48] G. Readfearn, “Australian PM Scott Morrison agrees to permanently increase aerial firefighting funding,” 2020. [Online]. Available: <https://www.theguardian.com/australia-news/2020/jan/04/australian-pm-scott-morrison-agrees-to-permanently-increase-aerial-firefighting-funding>.
- [49] P. Pryce, “Canada's Fragmented Firefighting,” 2016. [Online]. Available: <https://natoassociation.ca/canadas-fragmented-firefighting/>.
- [50] M. Langfield, “Aerial firefighting in the Asia-Pacific Region,” 2021. [Online]. Available: <https://natoassociation.ca/canadas-fragmented-firefighting/>.
- [51] L. Clancy, Aerodynamics, London: Pitman Publishing Limited, 1975.
- [52] G. Lovellette, “Safe Drop Height for Fixed-Wing Airtankers,” 2000. [Online]. Available: <https://www.fs.fed.us/rm/fire/pubs/htmlpubs/htm00572317/index.htm>. [Accessed 11 November 2021].

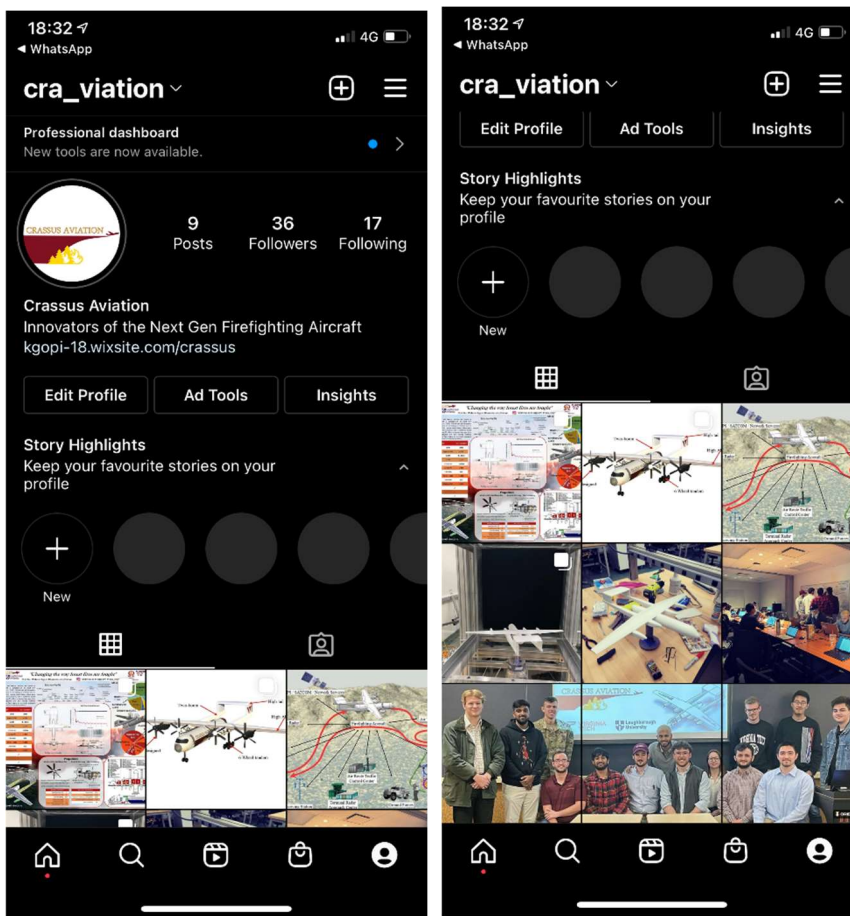
Appendix

Public Engagement

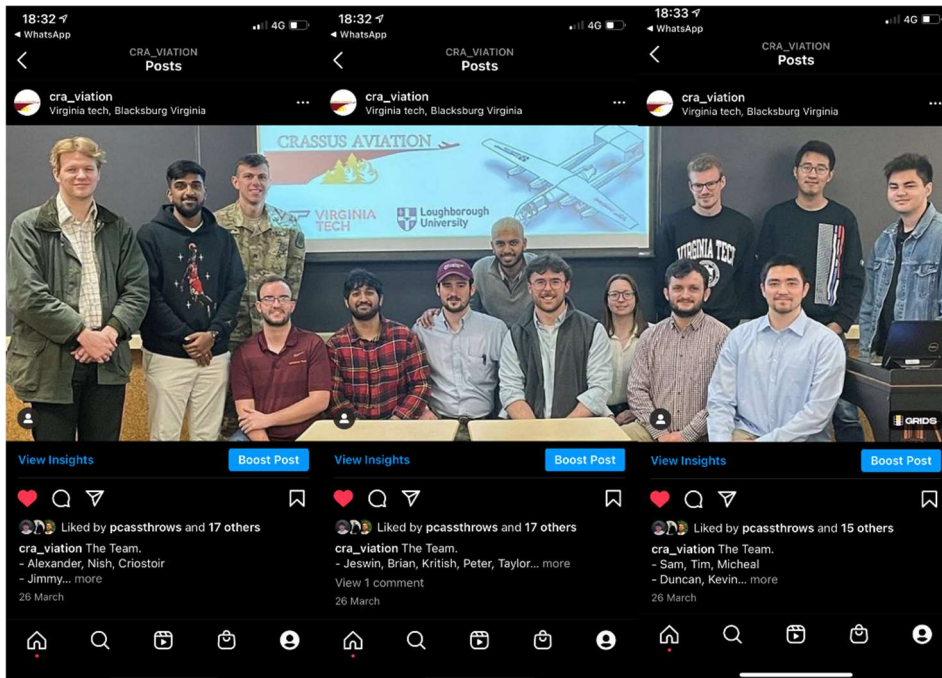
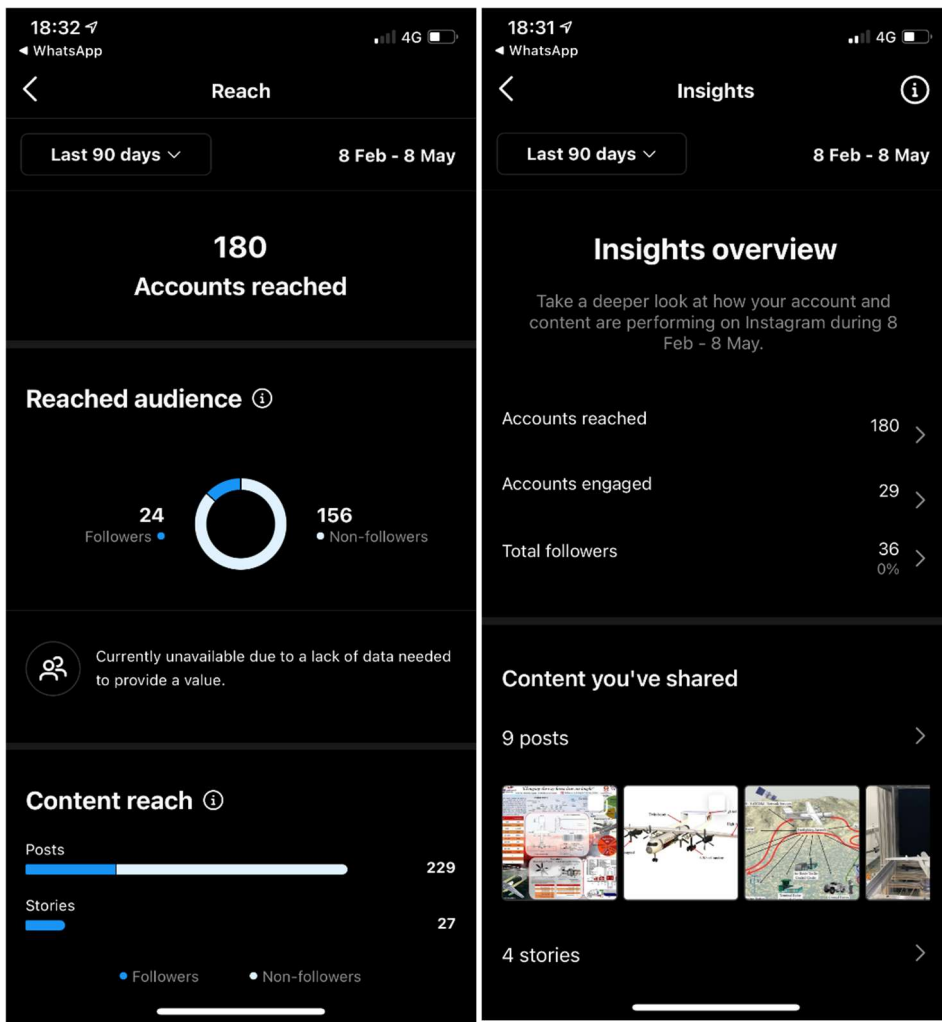
1. Social Media Engagement:

An Instagram account and a website is created to advertise our project. The Instagram account is primarily given the role of project updates. This allows the viewers to follow our project journey from the concept stages to the final post revealing our final product – Nerodia LV22.

Instagram Link: https://www.instagram.com/cra_viation/



Here is Crassus Aviation's Instagram profile page.



A total of 180 accounts visited Crassus Aviation's Instagram profile at least once.

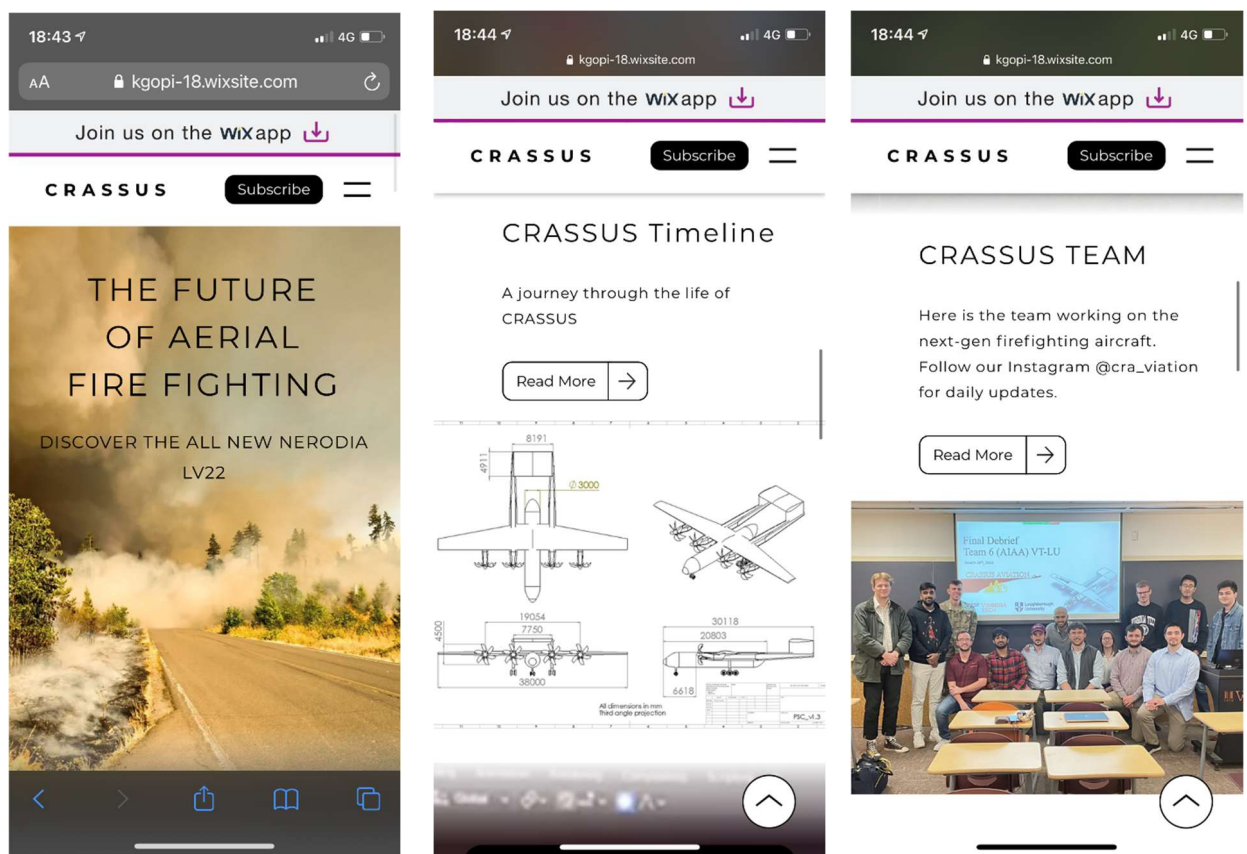
Clever photo editing allowed Crassus Aviation to post the entire team seamlessly across 3 posts.

2. Website

The website on the other hand is created to act as a method of public engagement. The website is interactive and reveals information about our product the more one scrolls through it. A newsletter subscription is available on the website to entice visitors to interact with Crassus Aviation. Furthermore, a Job Application page exists to act as a playful gesture, that Crassus Aviation encourages visitors to interact with.

Website Link: <https://kgopi-18.wixsite.com/crassus>

The website is made to be mobile friendly too.



3. Email

An email account is created in order to keep both website and social media within a business perspective. As well as that the email is used for public outreach whilst contacting businesses about our project.

crassusaviation@gmail.com

4. Business Outreach

America Trip:

A project-oriented trip to Virginia Tech proved beneficial for both the project as well as for team bonding. Upholding a strict 9-5 working day schedule allowed for effective work to be completed. Dinner was scheduled every night for 4 days promoting informal relationships between team members.

In order to aid with operating requirements, the Australian NAFC have been contacted through email, who replied very enthusiastically with a lengthy document of Australian firefighting specifications. This greatly aided CA's user requirements study.

Furthermore, upon completion of CA's detailed design, NAFC was contacted once more with Nerodia's final design details and requested for some feedback on the viability of the design. Once more the NAFC exceeded our expectations with their very informative response. The below figure displays their constructive feedback. Their comments regarding the payload tank insinuates they were unaware about our tank baffling and pressurisation system, hence we ensured to include this information in abundance throughout the report. Structures have been reinforced to reduce fatigue as much as possible.

AM

Andrew Matthews <andrew.matthews@nafc.org.au>

Wed 04/05/2022 01:32

To: (s) Kritish Gopi



** THIS MESSAGE ORIGINATED OUTSIDE LOUGHBOROUGH UNIVERSITY **

** Be wary of links or attachments, especially if the email is unsolicited or you don't recognise the sender's email address. **

Kritish,

Just a couple of points from me.

Retardant tanks need vertical height to accelerate the mass down through the drop doors at the start of the drop – so a tall triangular shape is going to outperform a cylinder.

Look at the shape of the Coulson RADS XL or AirTractor AT802 tanks for an example.

Controlling the drop characteristics is a key to getting an even pattern on the ground.

Tank shape and door design are a big part of this

If you look at air tanker accidents over the last 30 years, structural fatigue and low speed controllability have been common contributing factors

Make sure you overtly address these in your work

Are you sure you have the cost and weight of avionics right?

Airtanker operations are conducted visually (day VFR or NVIS) transit to and from site can be IFR

An off the shelf Garmin glass cockpit would meet the needs of a large airtanker and surpass the gear currently in us in most existing aircraft

Andrew Matthews

Manager Capability

National Aerial Firefighting Centre

Please note: I work Monday - Thursday.

Level 1 / 340 Albert Street | East Melbourne | 3002

m: 0418 310 743 | w: www.nafc.org.au



Meeting Minutes

Master Minutes tracker

RAG status	
	Action overdue/at risk
	Action in progress
	Action complete

GDP	Fire Fighting Aircraft			
Meeting date	Present (Discord)			
Item number	Discussion	Action	Action owner(s)	RAG status
17/01/2022	Duncan Livingstone (DL) Pip Thorpe-Morgan (PTM) Sam Markert (SM) Kritish Gopi (KG) Nish Selvakumar (NS)	Jeswin Roy (JR) Peter Cassidy (PC) Brian Kelly (BK) Taylor Ordile (TO) Letian Leng (LL)		
1	Need to make a decision as to which concept will be used, decision matrix comparing two concepts using actual values	Reformat Decision matrix and populate with both schools' concepts	PC	
2	Split up roles and partner up with VT members to enable project progression	Determine roles and assign Primary, support, and potentially assistant	All	
3	Lboro and VT must agree on requirements before further work can resume	Share RFP with each school (Lboro need to collate properly)		
4	Need to determine consistent file system	Middle ground, Discord for meetings, Teams for file storage	-	

Meeting date	Present (Teams)			
18/01/2022	Pip Thorpe-Morgan (PTM) Sam Markert (SM) Kritish Gopi (KG) Nish Selvakumar (NS)			
Item number	Discussion	Action	Action owner(s)	RAG status
5	Basic mission profile to evolve concept (help from VT MP)	Start on Mission profile	PTM	
6	Get access to VT interim report (google drive) to compare concepts in down-selection matrix	Get access to google drive, confer ratings during Thursday meeting	All	
7	Contact role counterparts to establish lines of communication	Send roles over to VT, contact counterparts in Thursday meeting	PC	

Meeting date		Present (Discord)			
20/01/2022		Duncan Livingstone (DL) Pip Thorpe-Morgan (PTM) Sam Markert (SM) Kritish Gopi (KG) Nish Selvakumar (NS)	Jeswin Roy (JR) Peter Cassidy (PC) Brian Kelly (BK) Michael Sharp (MS) Letian Leng (LL)	Kevin Yarnall (KY) Taylor Ordile (TO) Criostoir Neal (CN) Jimmy Murray (JM) Matt McCarney (MM)	
Item number	Discussion		Action	Action owner(s)	RAG status
8	VT to do majority of CAD work due to previous experience in first semester. Solidworks to be used as licenses accessible by everyone (NX not available at VT). Do not export from OpenVSP to Solidworks, CAD from scratch as much easier		No action	-	-
9	Recurring weekly meeting to be on Tuesdays (Thursdays are dedicated LU internal meetings to align with Formal reviews etc)		Determine reoccurring time slot that appeals the most members	PC	Green
10	Final concept to be mash-up of both concepts. Slightly decreased payload capacity of VT (for small airport requirement), and potentially twin boom of LU. VT calculation sheets to be used to assess combination.		Rerun sheets with amended values. Rejig concept.		Green
11	XFLR5 for preliminary stability and dynamics work, ANSYS Fluent or STAR-CCM+ for CFD work (depending on license availability at VT)		No action	-	-
12	Members to work predominantly in sub-groups, then report back to whole group at project review meetings. Cross-group communication vital for certain areas		Sub-groups to familiarise with each other - then receive macro work packages	ALL	-

Meeting date		Present (Discord)			
25/01/2022		Duncan Livingstone (DL) Pip Thorpe-Morgan (PTM) Sam Markert (SM) Kritish Gopi (KG) Nish Selvakumar (NS)	Jeswin Roy (JR) Peter Cassidy (PC) Brian Kelly (BK) Michael Sharp (MS) Letian Leng (LL)	Kevin Yarnall (KY) Taylor Ordile (TO) Criostoir Neal (CN) Jimmy Murray (JM) Matt McCarney (MM)	
Item number	Discussion		Action	Action owner(s)	RAG status
13	Use single excel sheet as sort of home for calculations (or summaries of calculations) which references other sheets. Add them as 'modules'. Stability module needs adding		Tidy up sheet so that it's of genuine use	BK, PC	
14	Pros and cons of conventional tail vs twin-boom. Whole group determined twin-boom as best opportunity. Allows for differing configurations, more interesting		-	-	-
15	Tail layout for twin-boom to be decided quantitatively. OpenVSP models to quickly generate tail layouts		OpenVSP analysis	?	Green
16	Delegate 1/2 deliverables to each subgroup, then leave micro-targets up to each subgroup as to how to achieve deliverable. Avoids micromanaging and allows for freedom of work		PM style moving forward	PC	Green

Meeting date	Present (Teams)			
27/01/2022	Duncan Livingstone (DL) Pip Thorpe-Morgan (PTM) Sam Markert (SM) Kritish Gopi (KG) Nish Selvakumar (NS)	Jeswin Roy (JR) Peter Cassidy (PC) Matt McCarney (MM)		
Item number	Discussion	Action	Action owner(s)	RAG status
17	Management style moving forward communicated to group - everyone happy with coming up with their own tasks to achieve deliverables	-	-	
18	CAD to be built by using wings from XFLRS, then exporting geometry to CAD for remainder of A/C	Familiarise with CAD process prior to formal review 1 / design freeze gateway review	?	
19	Preliminary XFLRS analysis using new wing (for adjusted payload) to be carried out within next week. Provides basic aero analysis and stability values	XFLRS analysis	SM, PTM	Green
20	Sub-systems amend systems block diagram to scope required subsys, liaise with Michael to build off VT current work	Sub-systems block diagram	MM	Green
21	Risk - determine scope of deliverables - do we have time for full fault trees and RCA? If work is dry then aid other subgroup	Scope determination	JR	Green
22	Structures - determine process moving forward for analysis - where does flight envelope fit in? (placed at start currently, is this correct?)	Structures process	DL	Green
23	Business Operations - start on branding/marketing for whole project. Work is less intense so resource to be shifted to other subgroups (structures)	Initial branding/marketing	KG	
24	Cost & Manufacturing - Formalise costing sheet to get headline figures - enable sheet to have A/C parameters fed in to update costs - account for materials?	Costing sheet	NS	Green
25	Performance - work with Aero group for XFLRS analysis. Rapid study of c.g. & stability for cylindrical tank and 4 spherical tanks (point masses in XFLRS)	XFLRS analysis	PTM	Green
26	VT Trip booked dates confirmed as March 19th - March 26th. Contact lecturers to confirm trip go/no-go	Email lecturers	PC	Green

Meeting date	Present (Discord)			
01/02/2022	Duncan Livingstone (DL) Pip Thorpe-Morgan (PTM) Sam Markert (SM) Kritish Gopi (KG) Nish Selvakumar (NS)	Jeswin Roy (JR) Peter Cassidy (PC) Brian Kelly (BK) Michael Sharp (MS) Letian Leng (LL)	Kevin Yarnall (KY) Taylor Ordile (TO) Criostoir Neal (CN) Jimmy Murray (JM) Matt McCarney (MM)	
Item number	Discussion	Action	Action owner(s)	RAG status
27	Decision made to go with 6000 usg payload to meet 150k lb small-airport requirement. This eases weight requirements aswell	-	-	-
28	Ensure subgroups make it known if input data required from other groups - to avoid fumbling around and waiting	-	-	-
29	Validation of XFLR5 using known A/C data, to justify use for stability	XFLR5 Validation exercise	BK / PTM	Green
30	Decision made to go with shorter TO distance requirement - to increase number of airports able to be operated out of. Adjustments to one area required (power or wing area or aerofoil)	-	-	-
31	Wing weight required for C.G. estimation. Sub-systems weight estimations also requires: final geometry, structural weight (fuselage, empennage, wing, control surfaces)	Weight estimations	TO / DL / MM / MS	Green
32	Structures group requires a large number of aero parameters to construct accurate V-n diagram. Struct to liaise with Aero	Formalisation of aero to be able to provide parameters	BK / SM / DL	Green
33	Materials tool available on Iboro lab PC's to be used for material selection - very useful	Familiarise with tool	DL	Green
34	Propeller decision: see if there's enough data to use an off-the-shelf prop, if not fill the gaps of data-sheets using Jblade/Qblade/Xrotor	Propeller investigation	PC / KY	Green
35	Risk analysis to be conducted for operational phase of flight (indirect fire attack - loiter, dump, loiter)	-	-	-

Meeting date	Present (Teams)			
03/02/2022	Duncan Livingstone (DL) Pip Thorpe-Morgan (PTM) Sam Markert (SM) Kritish Gopi (KG) Nish Selvakumar (NS)	Jeswin Roy (JR) Peter Cassidy (PC) Matt McCarney (MM)		
Item number	Discussion	Action	Action owner(s)	RAG status
36	Payload tank chat - if using 4 tanks can go with 2x2 layout (4 drops minimum for Australia regs). However AIAA RFP states 2000usg per drop minimum, which would mean 8000usg payload (higher than decided 6000usg)	Discuss with Brian our options	PC	Green
37	Twin-boom (two vert fins) vs conventional tail - very prelim stability analysis in XFLR5 ready for formal review 1	XFLR5 stability analysis (continued)	PTM / CN / SM	Amber
38	Ask lecturers in formal review 1 how far we should go with risk analysis (fault trees etc)	Ask lecturers in FR1	ALL	Green
39	Isograph risk software - will need to request access for 2 weeks or so	Enquire about software after FR1	JR	White
40	Get familiar with blender for A/C animations and renderings for further down the line	Practice Blender	PC	Green

Meeting date	Present (Discord)			
08/02/2022	Duncan Livingstone (DL) Pip Thorpe-Morgan (PTM) Sam Markert (SM) Kritish Gopi (KG) Nish Selvakumar (NS)	Jeswin Roy (JR) Peter Cassidy (PC) Brian Kelly (BK) Michael Sharp (MS) Letian Leng (LL)	Kevin Yarnall (KY) Taylor Ordile (TO) Criostoir Neal (CN) Jimmy Murray (JM) Matt McCarney (MM)	
Item number	Discussion	Action	Action owner(s)	RAG status
41	Once payload is dropped, there'll be too much lift on the wing - can negatively affect flying on return to base. Solution is to cruise at higher altitude to reduce lift (with slight nose down pitch and/or flare)	Analyse effects in XFLR5	SM / BK	Green
42	Two separate analyses required for wing surfaces and fuselage - also get drag breakdown for A/C (wings & body) for design freeze gateway review	Extend current analysis once fuselage modelled	SM / BK	Green
43	Might not be hitting margins for gust loads (TO) - so need to recheck V-n calculations. Lift curve slope affects this so potential to change airfoil shape (at this early stage) with aero group	Recheck V-n calculations, liaise with aero	DL / TO	Green
44	Propulsion - need to check bleed capacity for A/C power and payload pressurisation (liaise with sub-systems group)	Investigate engine bleed of PW150	PC / KY	Green
45	Payload pressurisation system - where does this fit into systems hierarchy? - how does this work for the modularity aspect?	Subsystems work on payload	MM / JM	Green
46	Systems positioning in A/C geometry for CG estimation - get rough positions but do not cement anything yet	Rough out systems positions in CAD	LL	Green
47	Determine ideal stability conditions - do we want our A/C to be statically/dynamically stable or unstable? Consider stability of competitor aircraft	Stability decision	CN / PTM	Green
48	Gantt chart timings and deliverables to be filled out prior to end of the week (Friday 11th February) - at least up to design freeze gateway review	Fill out Gantt timings	ALL	Green
49	Headshot images for VT PDR	Upload headshots to teams / send to PC	ALL (LU)	Green

Meeting date	Present (Teams)			
11/02/2022	Duncan Livingstone (DL) Pip Thorpe-Morgan (PTM) Sam Markert (SM) Kritish Gopi (KG) Nish Selvakumar (NS) Jeswin Roy (JR) Peter Cassidy (PC) Matt McCarney (MM)			
Item number	Discussion	Action	Action owner(s)	RAG status
50	Performance summary on small handout for design freeze gateway review. Three-view drawings need to be printed out	Create handout for review in week 3	PC	Green
51	Weight of main wing, vertical/horizontal stabilisers necessary for C.G. analysis	Find out how to accurately estimate weight of wings	NS	Green
52	Find out if Max Ramp Weight (Taxi weight) is to be assessed - is this already included in weight fractions. Adjust weight fraction and OEW target to account for 150k lb requirement	Investigate Max Ramp Weight. Adjust weight fractions.	BK / SM	Green
53	Start layout of internal systems ready for render for DFGR	Systems internal layout CAD	MM / LL	Green

Meeting date	Present (Discord)			
15/02/2022	Duncan Livingstone (DL) Pip Thorpe-Morgan (PTM) Sam Markert (SM) Kritish Gopi (KG) Jeswin Roy (JR) Peter Cassidy (PC) Brian Kelly (BK) Michael Sharp (MS) Letian Leng (LL) Kevin Yarnall (KY) Taylor Ordile (TO) Criostoir Neal (CN) Jimmy Murray (JM) Matt McCarney (MM)			
Item number	Discussion	Action	Action owner(s)	RAG status
54	Decision to optimise A/C performance and aero configuration for better full weight performance to be fully bespoke firebomber/heavy-lift transport. Loss in efficiency for dash and ferry scenarios (loss of effic in wing and turboprops at high alt)	Confirm A/C parameters for DFGR. Suggested 40kft 330kn	SM / BK / PC / DL / LL	Green
55	Would be good if some LU members could join VT weekly project review (with professors) on Mondays at 8pm UTC	Attend Monday 8pm UTC meetings	LU	Green
56	LU Apparently not to be involved with IPDR meeting (at VT) - contradicting information from LU lecturers	-	-	-

Meeting date	Present (Teams)			
17/02/2022	Duncan Livingstone (DL) Pip Thorpe-Morgan (PTM) Sam Markert (SM) Kritish Gopi (KG) Nish Selvakumar (NS) Jeswin Roy (JR) Peter Cassidy (PC) Matt McCarney (MM)			
Item number	Discussion	Action	Action owner(s)	RAG status
57	Project management update for design freeze gateway review. Required gantt activities and timings for each subgroup for detailed design phase (now till end of project)	Subgroups to update gantt chart	ALL	Green
58	LU travel plans. Traveller details to be sent to Rhian Watt (excel with 4 members sent as one, remaining members send individually). Room pairings to be confirmed.	Send Passport details. Determine room pairings	LU	Green
59	Product name and branding. Decided on Crassus Aviation for LU company name. List of aircraft names proposed, vote to decide	Vote on aircraft name in next meeting	ALL	Green
60	Further project deliverables to be decided to enable detailed design phase	Determine deliverables and next design steps	ALL	Green

Meeting date	Present (Discord)			
22/02/2022	Duncan Livingstone (DL) Pip Thorpe-Morgan (PTM) Sam Markert (SM) Kritish Gopi (KG) Nish Selvakumar (NS)	Jeswin Roy (JR) Peter Cassidy (PC) Brian Kelly (BK) Michael Sharp (MS)	Kevin Yarnall (KY) Taylor Ordile (TO) Criostoir Neal (CN) Jimmy Murray (JM) Letian Leng (LL)	
Item number	Discussion	Action	Action owner(s)	RAG status
61	Current horizontal tail area is roughly $10m^2$ too small. Can either increase in chord length or stretch booms (to move tail further rear). Combination of both (boom 2m further back and increase chord) as solution.	Finalise tail geometry. Check overturn angle with extended booms	BK / SM / MS	
62	Actual tail geometry not fixed yet, however values are close and should not particularly impact other areas (close enough for design freeze)	Finalise tail geometry	BK / SM / MS	
63	LU require internal layout by end of Wednesday (23rd) so that can model rough internals	Tim to provide layout	LL	
64	Mass breakdown finished and cg position now known with ability to easily adjust in excel sheet. Cg shift now known aswell - roughly 10%MAC max).	Formliase mass and cg breakdown for DFGR	PTM	
65	Finalise position of mass components and use to create envelope (consider doing y and z planes aswell)	Finalise mass positions and look at other A/C planes	PTM / CN	
66	Payload been overlooked somewhat, create new subgroup to cover design and analysis - take load off subsystems group	Create deliverables for payload subgroup	JR / NS	
67	Integration of landing gear into booms with engines - now sizing and location has been determined	Boom integration	LL	

Meeting date	Present (Discord)			
23/02/2022	Duncan Livingstone (DL) Pip Thorpe-Morgan (PTM) Sam Markert (SM) Kritish Gopi (KG) Nish Selvakumar (NS)	Jeswin Roy (JR) Peter Cassidy (PC) Brian Kelly (BK) Taylor Ordile (TO) Kevin Yarnall (KY)		
Item number	Discussion	Action	Action owner(s)	RAG status
68	Issue with spherical tanks clashing with wing inside fuselage - would not be able to sit on cg / clash with wing spar. Solutions suggested of lowering the fueslage, elliptical tanks, building spars around tanks. Solution in item 69	-	-	-
69	Decision to drop fuselage WRT wing (so is less submerged and more internal room), and move to single long cylindrical tank (with hemispherical ends). Massively decreases cg shift (30%MAC to ~5%MAC)	Amend geometry and cg calculations	LL / PTM / TO	
70	How to size cylindrical tank? 2.2m wide, 2m tall, 7.37m long. Allows for plumbing room and support structure below payload tank	Change internal systems layout to accommodate	LL / MS / PC	
71	Landing gear folding - how can we fit them into current booms without drastic design changes	Investigate landing gear stowage	LL	

Meeting date	Present (Design Freeze Gateway Review)			
24/02/2022	Duncan Livingstone (DL) Pip Thorpe-Morgan (PTM) Sam Markert (SM) Kritish Gopi (KG) Nish Selvakumar (NS)	Jeswin Roy (JR) Peter Cassidy (PC) James Knowles Paul Cunningham John Newton	Gary Page	
Item number	Discussion	Action	Action owner(s)	RAG status
72	Issue with payload when at half capacity - fluid will move to rear of container during climb - unfavourable cg shift. How can we prevent the bulk movement to the rear of the container? One-way valves to keep fluid in centre of tank	Explore unique solutions to tank internals	JR / NS / DL / BK	
73	Can the aircraft land with full payload? How can we build redundancies into payload system incase of inability to drop payload (mechanical backup release valve?)	Payload redundancy	JR / NS / DL / BK	
74	Costing, need more than 2 prototypes for R&D phase, also then consider selling prototypes on to other countries (think Indonesia or Australia)	Adjust costing plan	NS / JM	
75	Next steps in design to be determined to allow for detailed design phase	Detailed design phase scope	PC / BK / LL / DL	
76	Can we now start on a more accurate balanced field length calculation?	Balanced field length calc	BK	

Meeting date	Present (Discord)			
01/03/2022	Duncan Livingstone (DL) Pip Thorpe-Morgan (PTM) Sam Markert (SM) Kritish Gopi (KG) Nish Selvakumar (NS)	Jeswin Roy (JR) Peter Cassidy (PC) Brian Kelly (BK) Michael Sharp (MS) Letian Leng (LL)	Kevin Yarnall (KY) Taylor Ordile (TO) Criostoir Neal (CN) Jimmy Murray (JM) Matt McCarney (MM)	
Item number	Discussion	Action	Action owner(s)	RAG status
77	Required to define internally stored systems in tail/boom so can start on structural layout	Tail/boom internal systems	MS / MM / DL / TO	
78	Difficulty finding wing structural design references - inhibiting design of structures and subsequent FEA	Find wing structures references	DL	
79	Cement propeller diameter and key values (as other areas rely on this), and build values into integration sheet	Confirm values, extend prop box on sheet	PC / KY	
80	Make decision on hybrid combination of electric and hydraulic actuators for control surfaces (which surfaces will require more force?)	Control surfaces actuator decision	MS / MM	
81	Manufacturing values needed - amount of fuel burned per flight, and block time per flight (for operations and maintenance)	Get required values to costing & BusOps team	NS / JM	
82	Aircraft seems expensive - further research to find ways of mitigating costs (will become more accurate as detailed design carries on)	Reduce airframe costs	NS / JM	
83	Final name for A/C decided. Had the project not needed to be professional, 'Infamous Duck' (ID6000) would've been chosen. For sake of business case, 'Nerodia' chosen (common watersnake)	Build into marketing and branding	KG	

Meeting date	Present (Teams)			
03/03/2022	Duncan Livingstone (DL) Pip Thorpe-Morgan (PTM) Sam Markert (SM) Kritish Gopi (KG) Nish Selvakumar (NS)	Jeswin Roy (JR) Peter Cassidy (PC) Matt McCarney (MM)		
Item number	Discussion	Action	Action owner(s)	RAG status
84	Aero high-lift devices (slats & flaps) require design and analysis work	HLD design	BK / SM	Green
85	CFD - design is in mature enough state that simulations can be setup and started	CFD sim start	SM	Green
86	Can wing be made constant chord from fuselage out to booms? Massively simplify design for aero and structural analysis. Will either need to decrease chord at fuselage or increase chord at tips (likely combination of both)	Wing adjustment for aero and structures	BK / SM	Green
87	Branding and marketing update. Google sites or Wix to be used for website. Consider platforms for advertising (TikTok??) using renders and videos	Website start	KG	Green

Meeting date	Present (Discord)			
08/03/2022	Duncan Livingstone (DL) Pip Thorpe-Morgan (PTM) Sam Markert (SM) Kritish Gopi (KG) Nish Selvakumar (NS)	Jeswin Roy (JR) Peter Cassidy (PC) Brian Kelly (BK) Michael Sharp (MS) Letian Leng (LL)	Kevin Yarnall (KY) Taylor Ordile (TO) Criostoir Neal (CN) Jimmy Murray (JM) Matt McCarney (MM)	
Item number	Discussion	Action	Action owner(s)	RAG status
88	Feedback from iPDR - can we get weights during phases of flight to show cg throughout mission. What loads are experienced on A/C during each phase of flight? What are extreme manoeuvres?	Combine Vn and cg shift diagram in some way	DL / PTM	Green
89	Drop patterns revisit - how can we calculate/predict this with differing tank pressures and heights? Without turning into full FYP	Drop patterns revisit	JR / NS	Red
90	Actually determine how many airports have small airfield requirement. To quantifiably determine benefit of moving from 8000usg to 6000usg	Small airfield data analysis	BK	Green
91	Create graph to show how much larger the aircraft would have to be to meet 8000usg (multiple plotted points for range of payload values)	Create aircraft carpet plot	BK	Red

Meeting date	Present (Formal review 2)			
10/03/2022	Duncan Livingstone (DL) Pip Thorpe-Morgan (PTM) Sam Markert (SM) Kritish Gopi (KG) Nish Selvakumar (NS) Jeswin Roy (JR) Peter Cassidy (PC) Matt McCarney (MM) James Knowles John Newton			
Item number	Discussion	Action	Action owner(s)	RAG status
92	Are winglets necessary? Should we just make the wing longer (too much of a design change now) - check aerodynamic benefit against structural load - put case forward for each	Winglets design cases	BK / SM	Green
93	Are fore/aft trim tanks required? Reconsider need, especially dual rear trims - would we be able to pump between them quick enough	Reconsider trim tanks	MM / MS	Green
94	How valid is OpenProp? Validation exercise of simple A/C prop against XROTOR required. Reynolds number limitations? Prop optimised for cruise - check if actually able to perform at TO	Validation exercise + check set optimum conditions	PC / KY	Green
95	Spiral mode root just in positive real plane - if it was slightly more unstable then Dutch roll would be better (which is a higher concern than spiral mode)	Amend AC stability for favourable modes	PTM / CN	Green
96	How will the dynamic stability modes change with sloshing of the payload? How can this very nonlinear system be simplified for analysis?	Stability and payload coupling for analysis	PTM / DL / NS / JR / KG	Green
97	Operations and maintenance costs (per hour of flying) seem quite cheap - double check numbers (use civil and military numbers for ballpark figures)	Costing adjustment	NS / JM	Green
98	Payload baffling - determine number required to quash sloshing to suitable level. Simple MATLAB calculation first then extend to CFD	Payload baffling design	DL / NS / JR / KG	Green

Meeting date	Present (Final Debrief in Randolph Hall)			
24/03/2022	Duncan Livingstone (DL) Pip Thorpe-Morgan (PTM) Sam Markert (SM) Kritish Gopi (KG) Nish Selvakumar (NS)	Jeswin Roy (JR) Peter Cassidy (PC) Brian Kelly (BK) Michael Sharp (MS) Letian Leng (LL)	Kevin Yarnall (KY) Taylor Ordile (TO) Criostoir Neal (CN) Jimmy Murray (JM) Matt McCarney (MM)	James Knowles Paul Cunningham Pradeep Raj Michael Butler
Item number	Discussion	Action	Action owner(s)	RAG status
99	Ensure Payload split casing is of adequate size (flanges and fasteners) - and has adequate sealing (deformable or elastic type)	Payload design work	JR / NS	Green
100	Structures - wing structure looks discontinuous from initial diagram - adjust and use A400m internal structure as guide. Skin thickness at root seems a bit thick (9mm)	Structures refinement	DL / TO	Green
101	Stability - lecturers talked about AVL or Tornado for dynamic stability - but we already have these from XFLR5? Do we need to use them then?	Dynamic stability analysis	PTM / CN	Green
102	Straight leading edge and swept trailing edge - can we justify this given it's usually the other way round?	Design justification	SM / BK	Red
103	Characterist benefits of single payload tank rather than multiple spheres - make very clear	Design justification	PTM	Green
104	Confirm baffle gaps at top are large enough to allow for RFP fill rate (ideally as small as possible to minimise spill over)	Calculate fill rate	JR / NS / KG	Green
105	Rethink APU downselection matrix - not necessary to have more power than required - so shouldn't be a weighted value (same with pneumatic power). Make prel. selections based on req power, then use fuel cons. And weight to downselect	Rejig APU downselection	MS / MM	Green
106	Costing - breakdown 'manufacturing cost' a bit more discretely (labour, parts, etc). And change 'Airframe' to 'Aircraft'	Amend costing	JM / NS	Green

Meeting date	Present (Discord)			
29/03/2022	Duncan Livingstone (DL) Pip Thorpe-Morgan (PTM) Sam Markert (SM) Kritish Gopi (KG) Nish Selvakumar (NS)	Jeswin Roy (JR) Peter Cassidy (PC) Brian Kelly (BK) Michael Sharp (MS) Letian Leng (LL)	Kevin Yarnall (KY) Taylor Ordile (TO) Criostoir Neal (CN) Jimmy Murray (JM) Matt McCarney (MM)	
Item number	Discussion	Action	Action owner(s)	RAG status
107	CFD exploration of aero stall devices - probably a good end point for project (see item 114)	Stall devices	SM / BK / KY	Green
108	Get Blender animation of A/C ready for 24th April VT presentation	Blender work	PC	Yellow
109	Final report page count - liaise with both school lecturers. Try for happy medium of around 115 (100 for VT, 120 for LU)	Contact lecturers Re page count (LU formal review)	BK / PC	Green
110	Decided on full design freeze 2 weeks before handin (4th at internal deadline) - to allow time for quality presentation of analysis. Gives 20th April	-	-	
111	Pintle Nozzle CFD to check dispersion and nozzle parameters	Nozzle CFD / CAD	PTM / PC / JR / NS	Green

Meeting date	Present (Formal review 3)				
31/03/2022	Duncan Livingstone (DL) Pip Thorpe-Morgan (PTM) Sam Markert (SM) Kritish Gopi (KG) Nish Selvakumar (NS)	Jeswin Roy (JR) Peter Cassidy (PC) Matt McCarney (MM)			
Item number	Discussion	Action	Action owner(s)	RAG status	
112	Internal configuration - heat exchanger to be located in wing - can take cooling air from oversized engine air intake. Use dumped hot air for de-icing. How much cooling power needed for heat exchanger?	Heat exchanger calcs	PC	Green	
113	Check airfoil correlation between XFLR5 and Abbot Theory of Wing Sections	Recheck airfoil against theory	SM / BK	Green	
114	Preliminary CFD looks as if A/C is in deep stall - consider wing cuff/dogtooth/notched leading edge to better stall characteristics (see item 107)	Stall devices work	SM / BK	Green	
115	Subsystems - go for systems unique to our design - otherwise design exercise would be redundant. Automatic system to help with drop. Check for cutting edge (low TRL) with 2030 deployment in mind	Project-unique subsystems	MM / MS	Green	
116	Propulsion - Get data for whole range of pitch angles	Prop pitch angles	KY	Green	
117	One way valves need to be offset (in regular straight grid atm) for better packing efficiency and more material where hinges will be located	Baffle CAD update	NS / JR / KG / TO	Green	
118	Can create final report together with VT page limit, then for LU version add extra pages of busops and further analysis to fill out 120 pages. VT not required to split into 20 pages main 100 supporting - so consider separate report in next meeting	Group discussion about report	ALL	Green	

Meeting date	Present (Discord)			
29/03/2022	Duncan Livingstone (DL) Pip Thorpe-Morgan (PTM) Sam Markert (SM) Kritish Gopi (KG) Nish Selvakumar (NS)	Jeswin Roy (JR) Peter Cassidy (PC) Brian Kelly (BK) Michael Sharp (MS) Letian Leng (LL)	Kevin Yarnall (KY) Taylor Ordile (TO) Criostoir Neal (CN) Jimmy Murray (JM) Matt McCarney (MM)	
Item number	Discussion	Action	Action owner(s)	RAG status
107	CFD exploration of aero stall devices - probably a good end point for project (see item 114)	Stall devices	SM / BK / KY	Green
108	Get Blender animation of A/C ready for 24th April VT presentation	Blender work	PC	Yellow
109	Final report page count - liaise with both school lecturers. Try for happy medium of around 115 (100 for VT, 120 for LU)	Contact lecturers Re page count (LU formal review)	BK / PC	Green
110	Decided on full design freeze 2 weeks before handin (4th internal deadline) - to allow time for quality presentation of analysis. Gives 20th April	-	-	White
111	Pintle Nozzle CFD to check dispersion and nozzle parameters	Nozzle CFD / CAD	PTM / PC / JR / NS	Green

Meeting date	Present (Formal review 3)			
31/03/2022	Duncan Livingstone (DL) Pip Thorpe-Morgan (PTM) Sam Markert (SM) Kritish Gopi (KG) Nish Selvakumar (NS)	Jeswin Roy (JR) Peter Cassidy (PC) Matt McCarney (MM)		
Item number	Discussion	Action	Action owner(s)	RAG status
112	Internal configuration - heat exchanger to be located in wing - can take cooling air from oversized engine air intake. Use dumped hot air for de-icing. How much cooling power needed for heat exchanger?	Heat exchanger calcs	PC	Green
113	Check airfoil correlation between XFLR5 and Abbot Theory of Wing Sections	Recheck airfoil against theory	SM / BK	Green
114	Preliminary CFD looks as if A/C is in deep stall - consider wing cuff/dogtooth/notched leading edge to better stall characteristics (see item 107)	Stall devices work	SM / BK	Green
115	Subsystems - go for systems unique to our design - otherwise design exercise would be redundant. Automatic system to help with drop. Check for cutting edge (low TRL) with 2030 deployment in mind	Project-unique subsystems	MM / MS	Green
116	Propulsion - Get data for whole range of pitch angles	Prop pitch angles	KY	Green
117	One way valves need to be offset (in regular straight grid atm) for better packing efficiency and more material where hinges will be located	Baffle CAD update	NS / JR / KG / TO	Green
118	Can create final report together with VT page limit, then for LU version add extra pages of busops and further analysis to fill out 120 pages. VT not required to split into 20 pages main 100 supporting - so consider separate report in next meeting	Group discussion about report	ALL	Green

Meeting date	Present (Discord)			
05/04/2022	Pip Thorpe-Morgan (PTM) Sam Markert (SM) Kritish Gopi (KG) Nish Selvakumar (NS)	Jeswin Roy (JR) Peter Cassidy (PC) Brian Kelly (BK) Michael Sharp (MS) Letian Leng (LL)	Kevin Yarnall (KY) Taylor Ordile (TO) Criostoir Neal (CN) Jimmy Murray (JM) Matt McCarney (MM)	
Item number	Discussion	Action	Action owner(s)	RAG status
119	Each subgroup to mock up internals of what they want and where (using CAD screenshots). Hopefully will give CAD person a good idea of layout and take everyone's requirements into account	Subgroup internal layouts	ALL	Green
120	Too late for wing geometry changes for stall management (dogtooth/cuff) - will go with stall fences as much easier to design and integrate	Stall fences design & analysis	SM / BK	Green
121	Heat exchanger to dump hot air on inboard flaps (blown) to help with stall	Heat exchanger dump	PC / SM	Green
122	BusOps requires help with website - needs someone with good general overview of subgroups for information (there's many tabs to fill out)	Website fleshing out	KG / PC / BK	Green
123	Payload one-way-valve and bleed calculations need checking	Check calculations	JR / NS / PC / BK	Green

Meeting date	Present (Discord)			
26/04/2022	Duncan Livingstone (DL) Pip Thorpe-Morgan (PTM) Sam Markert (SM) Kritish Gopi (KG) Nish Selvakumar (NS)	Jeswin Roy (JR) Peter Cassidy (PC) Brian Kelly (BK) Michael Sharp (MS) Letian Leng (LL)	Kevin Yarnall (KY) Taylor Ordile (TO) Criostoir Neal (CN) Jimmy Murray (JM) Matt McCarney (MM)	
Item number	Discussion	Action	Action owner(s)	RAG status
124	Solidworks to Blender export issue - features used to model control surfaces, windscreen, doors, body panels, livery - all excluded from SW export. If we want to use blender for report/poster, will need to redraw entirety of what is excluded	Make SW render as good as can be - take the L	LL / PC / KG	Green
125	Effort not spent drawing rn is effort spent writing/formatting report and figure. LU to complete render for presentation but not report.	-		
126	More structure required than initially thought for inboard wing section (2million Nm stiffness required) and payload mounting. Final mass inc. updated structure still under initial estimate of 68tonnes	Create final mass breakdown	PTM	Green
127	VT poster due THIS week 28th April (with presentation) - LU to help with layout and content generation as will be very similar to LU poster	Help with VT poster	ALL	Green